AN ABSTRACT FOR THE THESIS OF

Fernando G. Ruiz for the degree of Master of Science in Physical Oceanography presented on March 1, 1993.

Title: Wind Estimates from Beneath the Ocean Surface Using Acoustic Doppler Current Profilers.

Redacted for Privacy

Abstract approved: _____
Michael Kosro, Ph.D.

Echoes from a moored Acoustic Doppler Current Profiler (ADCP) returning from the ocean's surface are usually discarded for the analysis of surface currents profiles, since they are highly contaminated by sidelobe signals. Nevertheless it was found that the near surface Doppler data contained useful information for estimating surface winds.

Three separated ADCP data sets with corresponding meteorological information were analyzed with two purposes: to find the relationship between the active backscatter energy from an ADCP acoustic pulse and the wind speed; and to find, if any, a relationship between the Doppler direction from the ADCP surface data and the wind direction. These correlations were compared in order to find a universal equation. Assessing both purposes would allow the prediction of wind velocity by moored ADCP, without additional expensive and vulnerable surface instrumentation any where.

There is a well-established relationship between passive ambient noise and wind speed; Piggott (1965) found it to be 7.2 dB (decibel) per wind speed double, or approximately proportional to the wind speed squared. However the initial assumption in the development of this thesis was that a relationship between active backscatter energy and the wind speed should exist as well. On the basis of the analysis done to these three data sets, this relationship was found to be on average 9.7 ± 0.8 dB per wind speed double, or that the active backscatter energy is approximately proportional to the wind speed cubed (actually to the power of 3.2 ± 0.3). However this relationship was found to be frequency dependent.

Wind data were collected by meteorological buoys at the three experiments, and additional wind data were provided by a research vessel (*RV Wecoma*) present in the

vicinity of two of three experiments. Ship based wind data were used only when the vessel was within 10 km of each ADCP. Whenever meteorological sensors were over 10 km from the ADCP under analysis, a 13 hour moving average scheme was applied to both data sets, *i.e.*, meteorological and acoustical. Hourly averaged wind speeds, and surface active backscatter energy recorded at a moored ADCP were compared. This backscatter energy was normalized to a 100 m reference depth by the transmission losses, which account for acoustic spreading and absorption, and wind speeds were normalized to 10 m reference height. The combination of these two corrections produced a good overlap of measurements from different locations.

About six months of data were obtained from a single ADCP moored in shallow water, about 12 nm (nautical miles) off the coast of Coos Bay Oregon; wind data were obtained from a C-MAN station at Cape Arago. A strong relationship was found at this site between smoothed active backscatter energy and smoothed wind speed. The ratio of acoustic direction's dynamic range (signal) to the residuals' standard deviation (noise) was high, which produced a good relationship between the smoothed acoustic direction and the wind direction.

Results of Brown *et al.* (1992) were re-analyzed here. About a week and a half of data were obtained from three ADCPs moored in deep water beneath three meteorological buoys, about 120 to 170 nm off shore at the Gulf of Tehuantepec, Mexico. Additional meteorological measurements were provided by the research vessel. Since ADCPs were almost beneath the meteorological buoys, the 13 hour smoothing scheme was not needed at these stations. A strong relationship was found between active backscatter energy and wind speed from all meteorological data sources; the best fit was obtained from a combined (buoy and ship) data set. A low signal to noise ratio produced a weak relationship between Doppler direction and wind direction.

About a month of data were obtained from three ADCPs moored in deep water during the coastal transition zone (CTZ) experiment, about 90 nm off Point Arena, northern California. Two National Data Buoy Center (NDBC) buoys located 10 and 20 nm off shore provided meteorological data. The research vessel provided additional wind measurements. A strong relationship was found between smoothed active backscatter energy and smoothed wind speed with the ship data. Buoy data were probably too contaminated by the influence of coastal processes, and a combined data set produced a noisy time series due to large offsets between coastal buoy winds and high sea ship winds. Again a low signal to noise ratio produced a weak relationship between smoothed ship wind direction and smoothed acoustic direction, and no relationship was found between smoothed buoy wind direction and smoothed acoustic direction.

To determine if the relationships found above were the same, no mater where the instrument was placed, comparisons between regression results were performed. These comparisons are appropriate only when the same instrument is used in a different location. Therefore, only two sets of comparisons were possible: the results using instrument 197 at Coos Bay and CTZ, and the results using instrument 201 at CTZ and Mexico. The slope coefficients of intensities' regressions from the 197 results were similar (0.031 ± 0.001 in Coos Bay and 0.029 ± 0.003 in CTZ), as were the 201 results (0.030 ± 0.003 in Mexico and 0.035 ± 0.002 in CTZ). At all sites except Coos Bay, variability in wind direction was limited, and only low correlations between wind direction and acoustic direction were found; rms (root mean square) error in wind direction estimated from acoustical direction in the surface bins was 30° to 40°.

In conclusion a strong relationship was found between the active backscatter energy (BE) and wind speed at 10 m height (U_{10}). This relationship has the form $BE \approx U_{10}^{\mu}$, where on average, at the ADCP's operation frequency (300 kHz), $\mu \approx 3.2$. However, Schott's (1989) experiments showed a frequency dependence of this power exponent. ADCP backscatter energy provides some skill in predicting wind speeds, however it was not possible to find a single equation that would be valid at every site. A weak relationship was found between the acoustic direction and the wind direction. To obtain a reliable direction relationship, it is necessary to have a large dynamic range (signal) to residuals' standard deviation (noise) ratio; to obtain a regression slope coefficient, for the directions data set, greater than 0.95, a S/N ratio greater than 4.5 is necessary. There is a clear spreading of LOG10(WS) at wind speeds lower than 3.5 m/s. We do not know what the ADCP is actually measuring at the surface bin. Wind measurements must be taken close to the ADCP in order to build a prediction model, or to use it. Coastal influences on meteorological data are strong enough to destroy the relationship with acoustic measurements; specially when both sensors are apart from each other.

Wind Estimates from Beneath the Ocean Surface
Using Acoustic Doppler Current Profilers.

by

Fernando G. Ruiz

A THESIS

submitted to

Oregon State University

in partial fulfillment of
the requirements for the
degree of

Master of Science

Completed March 1, 1993
Commencement June 1993

APPROVED:

Redacted for Privacy

_____

Associate Professor of Oceanography in charge of major

Redacted for Privacy

_____

Dean of the College of Oceanic and Atmospheric Science

Redacted for Privacy

_____

Dean of Graduate School

Date thesis is presented _____ March 1, 1993

Typed by Fernando G. Ruiz for: _____ Fernando G. Ruiz.

Acknowledgement

TABLE OF CONTENTS

LIST OF FIGURES

LIST OF TABLES

Wind Estimates from Beneath the Ocean Surface Using Acoustic Doppler Current Profilers.

Chapter 1

Introduction

An Acoustic Doppler Current Profiler (ADCP) is an instrument used by oceanographers to measure water velocity profile. This instrument measures the Doppler shift of the backscatter energy produced by free moving particles in the water column, such as small bubbles, zooplankton, and phytoplankton. These particles are called scatterers, and are assumed to move at the water velocity (RD Instruments *et al.*, 1989).

Moored ADCPs provide a versatile technique to measure current profiles in a variety of marine situations, Pettigrew and Irish (1983). There is one drawback: when the echo returns from a hard surface such as the sea surface or bottom, it is much stronger than the echo from scatterers in the water. This high energy echo may get into the ADCP receiver via a secondary lobe, and hence overcome the sidelobe suppression of the transducer array (See Appendix B). Data from distances close to the surface should normally be rejected, therefore a shadow zone is created (RD Instruments *et al.*, 1989). The vertical extent of this shadow zone is defined by:

$$z = D(1 - \cos \phi)$$

where D = depth of the ADCP transducer, ϕ = angle of the transmitted pulse to the vertical and z = depth of the shadow zone.

The ADCP data acquisition device breaks the water column into equal depth intervals called bins (See Appendix B). Hence, for upward looking ADCPs, a shadow zone is expected in the bins at the surface. For downward looking ADCPs, the shadow zone is close to the ocean bottom. All of the ADCPs in the present study are upward looking.

The ADCP provides a measurement proportional to the backscatter energy versus bin number, which is called an amplitude profile. Each profile has a strong peak at the ocean's surface. To obtain the data to be analyzed in this thesis, the bin number at which the surface peak occurs is identified. Once the surface bin is found, all data from this bin are extracted. This is done to every amplitude profile.

There is a well-established relationship between the wind speed and the ambient acoustic noise detected by passive receivers (Urick, 1983; Evans *et al.*, 1984). Recently, Vagle *et al.* (1990) confirmed this relationship of inferring oceanic winds from underwater

ambient sound. In fact, Piggott (1965) demonstrated (by one year measurements on the Scotian shelve in water depth of about 150 ft), that the increase of ambient acoustic noise with wind speed was found to be 7.2 dB per wind speed double, or an increase of intensity slightly greater than the square of the wind speed. However the process by which the ocean does this is still unknown.

On the basis of the assumption that the ADCP measures backscatter energy - proportional to the scatterer's density - of an active acoustic pulse, and that the bubbles' (scatterers) density in the surface bin depends on the wind speed to the power of 3.5 (Wu, 1988), a relationship between the wind speed and echo energy of the upper most bin should exist.

Schott (1989) found in the Gulf of Lions in the Mediterranean that the ADCP acoustical direction (the direction of the apparent current in the surface bin) was highly correlated to the wind direction measured by a ship when closer than 100 km from the ADCP. Since two ADCPs of different frequency were used, a frequency dependent slope coefficient was found. He also found a strong relationship between the wind speed and the active backscatter energy in the ADCP's surface bin.

Brown et al. (1992) found in the Gulf of Tehuantepec, Mexico a weak relationship between the acoustic direction and wind direction, but also confirmed the strong correlation between the wind speed and the active backscatter energy. These data were re-analyzed in this study in Chapter 3.

Therefore, as Schott (1989) and Brown et al. (1992) did, a relationship between the echo strength (ES) and wind speed (WS), as well as a relationship between the acoustic (Doppler) direction (AD) and the wind direction (WD) was investigated in this thesis.

In fact, the results of this study show enough evidence to conclude that there is a strong correlation between the wind speed and the backscatter energy produced by an active acoustic pulse. However it was not found a single equation valid at every site. The increase of backscatter energy with wind speed was found to be 2.5 dB higher than for the passive ambient noise (See Chapter 5). Also, in agreement with Brown et al. (1992), a weak correlation between wind direction and acoustic direction was found.

In principle upward looking ADCPs offer the potential to determine local surface wind stress without additional expensive and vulnerable surface instrumentation. They also offer the potential to collect synchronized meteorological and oceanographical data sets, instead of ship-board or land-based data that often fail to truly represent the in situ conditions.

Data Sets

The first and longest data set was obtained over the continental shelf near Coos Bay, Oregon, U.S.A. (Figure 2.1). This experiment had one ADCP (serial number 197) to collect oceanographic data. The ADCP was moored 12 nm off shore at 84 m depth in water 95 m deep. Meteorological data were collected by a Coastal-Marine Automated Network (C-MAN) station, which was situated on the coast at Cape Arago (Figure 2.1). The record length of this site is about six months. Meteorological and oceanographic averaged data were collected every 15 minutes.

The second data set was obtained at the Gulf of Tehuantepec, Mexico (Figure 3.1). This experiment had three ADCP moorings (serial numbers 197, 201 and 209) to collect oceanographic data. The moorings were situated 120 to 170 nm off shore in water depths of 4000 m. Meteorological data were collected by buoys mounted on surface moorings near the ADCP moorings (Figure 3.1). The RV Wecoma, equipped with standard meteorological sensors, was also present in the vicinity providing additional measurements of wind direction and intensity. The meteorological buoy at the mooring with the ADCP serial number 197 did not operate. The meteorological buoy at the mooring with the ADCP serial number 201 collected only 74 hours of data and then sank during a strong wind event. The meteorological buoy at the mooring with the ADCP serial number 209 collected 260 hours of data, but the direction sensor malfunctioned, so only wind speed data are available. Meteorological averaged data from the buoys were collected every 6 minutes. Oceanographic averaged data from the ADCPs were collected every 30 minutes, and meteorological averaged data from the RV Wecoma were collected every minute (Brown et al., 1992). Since the meteorological buoy near mooring 197 did not operate, and the RV Wecoma was closer than 10 km to this site only three times, no further analysis will be done with this mooring.

The third data set was obtained during the Coastal Transition Zone (CTZ) experiment off the coast of northern California, U.S.A., north of San Francisco (Figure 4.1). This experiment had three ADCPs (serial numbers 197, 201 and 209) to collect oceanographic data. The ADCPs were situated about 91 nm off Point Arena, California (Figure 4.1). Meteorological data came from two buoys, maintained by the National Data Buoy Center (NDBC), at 10 nm off Mendocino, and 20 nm off Bodega Head, California (Figure 4.1). The RV Wecoma, equipped with standard meteorological sensors, was also present in the vicinity providing additional measurements of wind direction and intensity. The ocean's surface was not in view of ADCP 209, hence this data set will not be used. ADCP 197 collected data for 765 hours (32 days), and ADCP 201 collected for 846 hours

(35 days). Meteorological averaged data from the *RV Wecoma* and buoys were collected every 1 and 5 minutes respectively. Oceanographic averaged data from the ADCPs were collected every 5 minutes.

Data Pre-processing

When meteorological data are taken from a buoy and compared with the ADCP data, they will be called "buoy data". When meteorological data are taken from ship measurements and compared to ADCP data, they will be called "ship data". When both data sets are combined, they will be called "combined data". Also, the echo strength (ES) and wind speed (WS) data sets will be referred to as the intensities, and the acoustic direction (AD) and wind direction (WD) as the directions. All data sets used in this study will be averaged to an hourly basis in order to have equally time spaced measurements.

Ship data will be used for the regression calculations only when closer than 10 km (5.4 nm) to each ADCP mooring. Greater distances were tried out and discarded, since those data sets produced larger errors and weaker fits to the regression model.

For data analysis purposes the ADCP's backscatter energy is transformed into echo strength (ES). The ES is obtained indirectly from the automatic gain circuit (AGC) in the ADCP's electronic receiver (RD Instruments *et al.*, 1989). The AGC provides a measure of the backscatter energy in the form of counts. The counts multiplied by a conversion factor gives the echo strength in decibels. (See Appendix B for detailed discussion)

$$ES = 0.46(counts(0.9966)^{(22^\circ - T^\circ)})$$

where

ES	:	echo strength measured in dB
0.46	:	conversion factor in dB/counts
counts	:	output of the AGC circuit
$(0.9966)^{(22^\circ - T^\circ)}$	:	temperature correction factor
T°	:	ADCP electronics temperature in °C

The conversion factor is a nominal value from the RD Instruments design specifications. There was no calibration of any ADCP in the water, and inter-comparisons between different instruments would therefore be inappropriate. The intention is however to compare the same instruments in different locations, *i.e.*, the regression results from instrument 197 in Coos Bay might be compared with the results of instrument 197 in the CTZ experiment.

Wind speed collected by buoys with the wind sensor at a height other than 10 m will be converted to a 10 m reference. This will be done by a wind logarithmic profile scheme, using an aerodynamic roughness length, $z_0 = 2x10^{-4}$ m (Kinsman 1965, and Stull 1988), of the form: (See Appendix B)

$$\overline{U_r} = \overline{U_b}\{\frac{\ln(z_r/z_0)}{\ln(z_b/z_0)}\}$$

where:

$\overline{U_r}$: wind speed at the reference height, 10 m

$\overline{U_b}$: wind speed at the buoy height in m/s

z_r : reference height, 10 m

z_b : buoy height in m

z_0 : aerodynamic roughness length, $2x10^{-4}$ m

A wind measurement below the 10 m reference height, due to the nature of the log-wind profile, will be strongly attenuated by surface drag. Hence it will be more amplified by the correction factor. On the other hand winds measured above the 10 m reference are less affected by the surface boundary layer, hence less affected by the profile.

The C-MAN buoy at Cape Arago is located at a height of 18 m above sea level, and the structure that holds the wind sensor is 15 m high. Since both heights, *i.e.*, 15 or 33 meters, are above the 10 m reference, either correction factor has a similar value. (See Chapter 1). Supposing that the mean wind roughly follows the land surface, the wind speed sensor at Coos Bay will be assumed to be at the 15 m height of the structure above the site. In the Mexican experiment, the sensors were at 1.3 m height, and in the CTZ experiment they were at 3 m height.

When wind sensors was located far from the ADCP, e.g., at Coos Bay and CTZ, a 13 hr moving average was applied to the involved data sets. A 13 hour moving average was chosen, instead of a 12 hour, in order to be symmetric and therefore keep the time reference unchanged with respect to the unsmoothed data. Afterwards the wind speed and direction, as well as the acoustic direction were trigonometrically reconstructed from the new filtered orthogonal components. This filtering process was not required for the Mexican experiment, since the meteorological buoys were nearly on top of the ADCPs.

Based on early studies in this matter, *i.e.*, Schott (1989) and Brown (1992), to analyze these hourly averaged data sets (and smoothed in Coos Bay and CTZ), a simple linear regression model was selected (See Appendix A). This model will relate the intensities, *i.e.*, echo strength to predict wind speed, and the directions, *i.e.*, the acoustic direction to predict wind direction.

The functional relationship between the backscatter energy and the wind speed is well described by a logarithmic law (Schott 1989), hence wind speeds were log-transformed, since the backscatter energy has been converted to echo strength, which is a log-transformation too.

At very low wind speeds the anemometer directional sensor becomes unreliable; consequently wind direction (WD), and hence acoustic direction (AD), were screened out when wind speed was less than 1.5 m/s (approximately 3 knots). In the case of the CTZ experiment, due to the great distance between the meteorological buoy and the ADCP - compared to the distance where WD changes near the coast - wind directions were screened out when wind speed was less than 3.0 m/s (approximately 6 knots). In order to keep the scope of the model as wide as possible, and to be able to predict the absence of wind by an ADCP echo strength measurement, there was no screening of wind speed (WS) and echo strength (ES), because of low wind speeds (with the sole exception of zero wind speeds, which were screened to allow the base ten logarithms to be computed).

To make comparisons between same instruments deployed at different locations, and possibly at different depths, all acoustical data were converted to a 100 m reference depth. Therefore, to account for spreading and absorption, the Transmission Losses (TL) were calculated by the equation (See Appendix B):

$$TL = 2 * \{20 \log(\frac{r_2}{r_1}) + e(r_2 - r_1)\} \text{ dB}$$

where:

TL : transmission losses in dB
r_1 : ADCP's depth in m
r_2 : reference depth equal to 100 m
e : absorption coefficient in dB/m

The factor of two is included to take into account the upward and downward transit of the acoustic energy from and to the reference depth. Hence, the echo strength (ES) is obtained as a summation of the ES (without TL correction) plus the transmission losses, formally:

$$ES = ES_{without\_TL} + TL$$

The acoustic direction (AD) was obtained trigonometrically from the hourly averaged North-South (v) and the East-West (u) velocity components of the surface bin, formally: $AD = \tan^{-1}(\frac{u}{v})$. Notice that in order to measure angles, the oceanographic convention was adopted to measure the wind directions, i.e., the angles are measured from the true north, denoting the particle's direction of motion.

Chapter 2

The Coos Bay Experiment

During the Spring and Summer of 1989, an ADCP mooring was deployed about 12 nautical miles off the coast of Coos Bay, Oregon, where acoustical data were measured for a period of six months (Figure 2.1). Meteorological data (wind speed and direction) were also obtained by a Coastal-Marine Automated Network (C-MAN) station at Cape Arago for the same period (Figure 2.1).

A simple linear regression model will be applied to the intensities, ES and WS, as well as to the directions, AD and WD, to predict wind velocity.

Oceanographic Background

On a large scale, the North Pacific weather is affected by two major atmospheric pressure cells: the North Pacific high and the Aleutian low. They produce the so called "Summer" and "Winter" conditions. In winter, the large Aleutian low dominates the weather of the Northern Pacific. Storms move counterclockwise around the low, slide off the north side of the North Pacific high, and blow onshore from the Southwest. In Summer, the North Pacific high moves northward off Oregon and northern California. Winds circulate clockwise around the high and blow from north to south along the coast. The coastal circulation in the North Pacific reflects large-scale air movements. (Parmenter and Bailey 1985).

The Observations

The ADCP mooring was situated at 43° 10.8' N latitude and 124° 33.9' W longitude with an upward looking 307.2 kHz ADCP configured for a 30° acoustic beam angle at a depth of 84 m. See Table 2.1 for details of the ADCP setup.

Meteorological information was measured by a Coastal-Marine Automated Network (C-MAN) station at 43° 20.4' N latitude and 124° 22.2' W longitude (Figure 2.1) which is on a site at 18 m height (59 feet) over the sea level at Cape Arago. The wind sensor was mounted on a 15 m (49 feet) structure above the site height (NDBC *et al* 1992). The scale factor required to correct the 15 m height of the wind speed sensor to 10 m is 0.964, assuming a logarithmic wind profile.

Table 2.1: Setup of ADCP Serial Number 197 off the coast of Coos Bay for the 1989 Spring and Summer experiment. The variability on the instrument depth is a standard deviation.

Mooring name	**Coos Bay 197**
Location	043°10.8' N 124°33.9' W
Distance off shore	12 nm
Instrument depth	84 ±0.34 m
Water depth	95 m
Serial number	**197**
Frequency	307.2 kHz
Beam angle	30°
Number of bins	30
Bin length	4.0 m
Pulse length	4.0 m
Pings per ensemble	100
Ensemble time avg.	900 sec
Deployed	May 01, 1989
Recovered	October 31, 1989

Wind Speed Estimates

Figure 2.2 shows both time series of intensities, where ES and WS have been smoothed with the 13 hour moving average. Notice the correspondence between the time series of ES and WS. Figure 2.3 shows the histograms of the wind speed (WS), echo strength (ES) and log-transformed wind speed (LOG10(WS)). It can be seen that taking the logarithm improved the wind speed histogram distribution compared to the untransformed wind speed histogram, in the sense of becoming more like the echo strength histogram.

The integral time scale calculation of the time between effectively independent samples (Appendix A) yields $\tau = 0.824$ days using ±500 hourly lags in the autocorrelation computation. With this integral time scale, 205 effective degrees of freedom were obtained (from 4058 correlated data points by the method explained in Appendix A).

A simple linear regression model $\log(WS) = b_0 + b_1 ES$ of echo strength against the log-transformed wind speed, both smoothed with a 13 hr moving average, yields the following coefficients at the 95% significance level with 205 effective degrees of freedom (Figure 2.4):

$$b_0 = -1.792 \pm 0.063$$
$$b_1 = 0.031 \pm 0.0009$$

with a correlation coefficient $r = 0.730$, where WS is measured in m/s, and ES in dB.

The 99% significance levels for b_0 and b_1 are ± 0.084 and ± 0.0012 respectively. The variance analysis (Appendix A) yields:

$$s_e^2 = MSE = 0.061$$
$$s_{b_1}^2 = 2.105 x 10^{-7}$$
$$s_{b_0}^2 = 1.031 x 10^{-3}$$

where:

s_e^2: Sample error variance or mean square error, MSE

$s_{b_1}^2$: Sample variance of the slope b_1

$s_{b_0}^2$: Sample variance of the intercept b_0

The correlation coefficient $r = 0.730$ suggests that almost 50% of the variance is explained by a simple linear regression. The other 50% belongs to some other *predictors* (measurements) that were not taken into account by this model. Perhaps a multiple linear regression including the ocean currents, atmospheric pressure, sea water temperature, sea water density, ADCP's pitch and roll, or some other predictor might produce a better coefficient of determination R^2 (or hindcast skill), hence a better fit to a multiple linear regression model. One must keep in mind that adding predictors may increase the artificial skill (predictability) of the model (Chelton 1983).

In theory, for each level of the independent variable ES, there is a normal population of responses, *i.e.*, a normal distribution of the LOG10(WS), where each distribution's mean falls on a straight line and all variances are the same (See Appendix A). Since this is rarely observed, the confidence interval theory is used instead (Ostle and Malone 1988, and Neter *et al*. 1989). The confidence interval predicts, with a known probability, a range where all the normal population means are expected to fall. The very small confidence interval in Figure 2.4 is due to the fact that most of the LOG10(WS) means, for a given level of ES, fall almost along a straight line, so that the slope of the regression model is very well determined.

There is an assumption that has been violated. The residuals, the difference between the predicted and measured LOG10(WS), do not have constant variance (which

is obvious from the triangular shape of the scatter plot, Figure 2.4). This assumption violation may alter slightly the results from the inference theory (See Appendix A).

Wind Direction Estimates

The direction measurements were plotted (Figure 2.5) and two main data clusters were observed, one at the origin of the coordinate system and the other at about 180°. This is not surprising, since Oregon's summer winds are polarized along the coast.

There were two minor clusters: around the left-upper and right-lower corners of the plot. This occurred due to the circularity of the wind directional type of measurement, e.g., a wind direction of 001° and 359° are very close, but when plotted in a XY scatter graph, they look very spread out. This poses a problem, since the normal average of two northward directions, 001° and 359°, is southward (180°). This effect also damages the analysis of variance, and biases the regression function. To correct this error, two alternatives were tried out.

The first alternative is to calculate the principal axes of wind and acoustic data sets (Kundu and Allen 1976, and Fofonoff 1969). Principal axes were calculated for the buoy wind direction, and for the ADCP current direction in the surface bin. If both sets are rotated to their correspondent principal axes, the regression analysis results do not improve by much. So this alternative was discarded in favor of the next one.

The second alternative is to compute a difference series by subtracting the wind direction (WD) from the matching acoustic direction (AD), $AD - WD$. If the difference is greater than +300°, WD is incremented by 360°. If the difference is less than -300°, WD is decreased by 360°. Doing this, a new wind direction series was created which had a larger scope than the original one, since the new WD series goes from -60° to 420°. This new data series will be called the folded wind data set. The generation of the folded data set can be visualized as folding the lower-right corner to the upper-right corner of the plot in Figure 2.5. This applies similarly to the left side of the graph, but it folds the upper-left corner to the lower-left corner.

Figure 2.6 shows the time series of directions, where AD and the folded WD have been hourly averaged and then smoothed with a 13 hour moving average. Figure 2.7 shows the histograms of the acoustic direction (AD), C-MAN folded wind direction (WD), and the difference $AD - WD$. Notice in the third histogram that the majority of the differences are shifted roughly toward +5° to +10°. This means that the water parcels in the upper most bin are moving to the right of the wind direction.

The integral time scale calculation of the time between effectively independent samples, yields $\tau = 0.504$ days using ± 500 hourly lags in the autocorrelation computation. With this integral time scale, 256 effective degrees of freedom were obtained (from 3094 correlated data points by the method explained in Appendix A).

A simple linear regression model $WD = b_0 + b_1 AD$ of acoustic direction (AD) against the folded wind direction (WD), both smoothed with a 13 hr moving average, yields the following coefficients at the 95% significance level with 256 effective degrees of freedom (Figure 2.8):

$$b_0 = -7.493 \pm 2.740$$
$$b_1 = 1.005 \pm 0.0149$$

with a correlation coefficient $r = 0.923$, where AD and WD are measured in degrees.

The 99% significance levels for b_0 and b_1 are ± 3.616 and ± 0.0196 respectively.

The variance analysis (Appendix A) yields:

$$s_e^2 = MSE = 1250.3$$
$$s_{b_1}^2 = 5.696 x 10^{-5}$$
$$s_{b_0}^2 = 1.934$$

The correlation coefficient $r = 0.923$ implies that almost 85% of the variance is explained by a simple linear regression model. The other 15% belongs to some other predictors (measurements) that were not taken into account by this model.

As with the intensities, the very small confidence interval in Figure 2.8 is due to the fact that most of the folded WD means for a given level of AD fall into almost a straight line. The outliers in Figure 2.8 can not bias the distribution of folded WD by much, since they are very few compared to the full record length. Notice again that the residuals have a non-equal variance.

Even though the slope of the regression function is slightly greater than one, the negative coefficient of the intercept (b_0) inhibits the value of WD from growing greater than the traditional 360°. For an AD = 0° the WD predicted by the model is $\approx -7.5°$, in which case 360° must be added to the result to get 352.5°; for the case of $AD = 360°$ the WD predicted by the model is $\approx 354.4°$, and it will never exceed the 360° value.

Special attention was given to the spread of ADCP direction that occurs when the wind is blowing towards the North (Figure 2.8). At first it was thought that this branch could be related to unreliable measurements due to low wind speeds, so the data points outside the prediction interval were identified and the wind speed checked at that instant. No relationship was found. Then it was analyzed if this branch could occur due to disturbances introduced by moderately long period waves, such as inertial oscillations

(period of 17.45 hr at this latitude) and diurnal tide. To test this, wider filters were applied to the direction data sets, namely a 25 and a 49 hour moving average schemes were examined. The number of data points outside the prediction interval were reduced, however the branch still was clearly distinguishable.
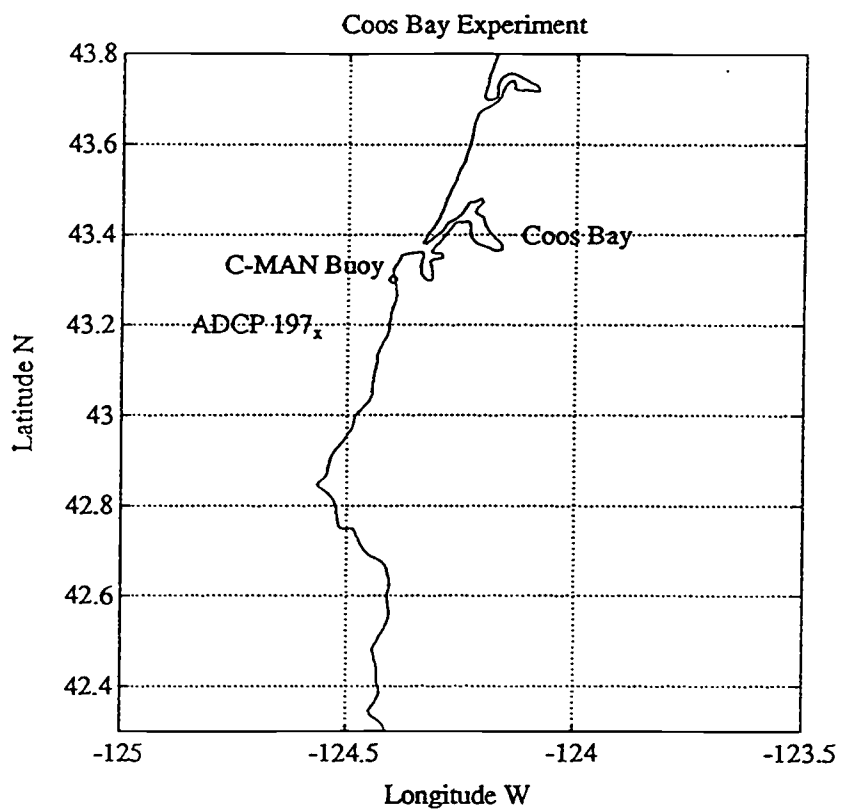
Figure 2.1 Location of the ADCP, about 12 nm off the coast of Coos Bay, and location of the C-MAN station at Cape Arago, Oregon, U.S.A.

14
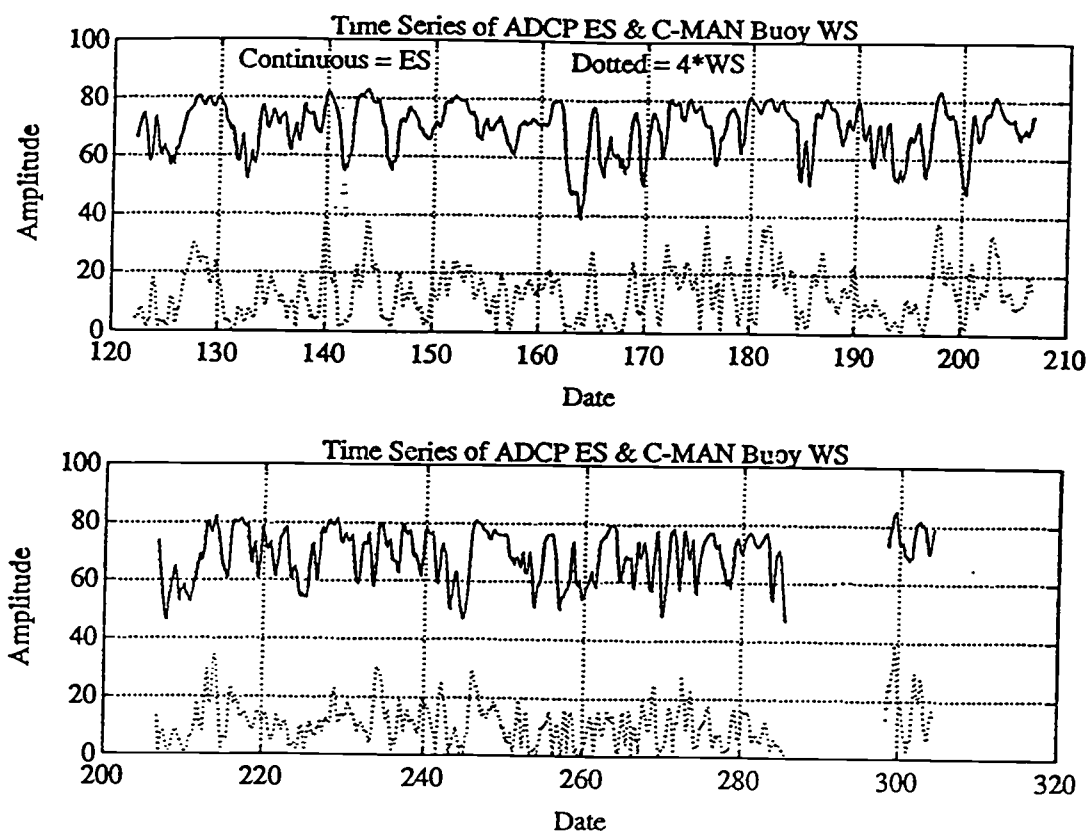
Figure 2.2   Time series of smoothed echo strength (ES) in the surface bin of the ADCP, and C-MAN buoy wind speed (WS), where ES and WS have been smoothed with a 13 hr moving average. The continuous line is the ES and the dotted line is four times the WS. At the end of the record there is a gap from date 285.5 to 298.7 in the data set due to a lack of measurements from the C-MAN buoy. Dates are in 1989 Julian days (May to October).
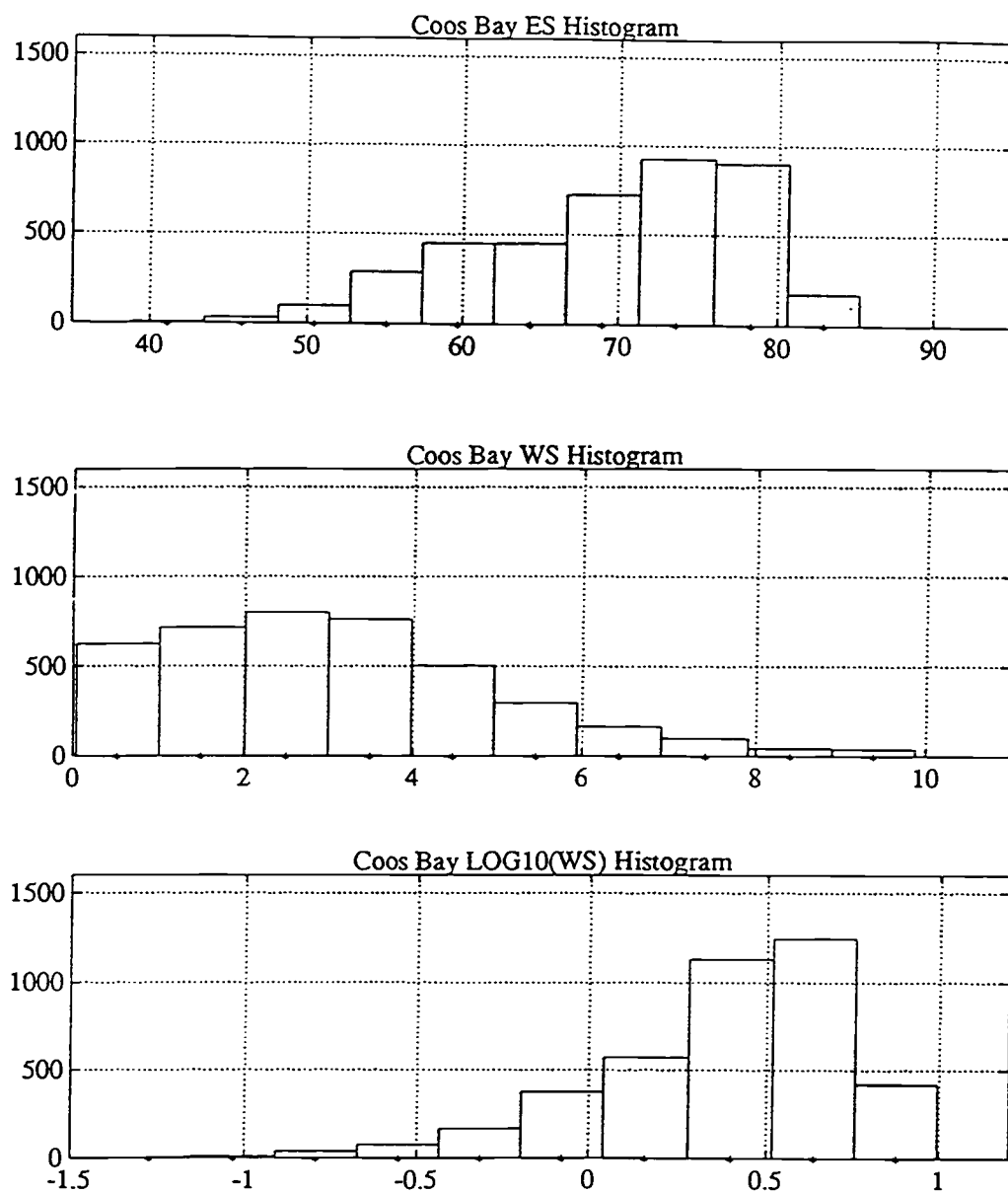
Figure 2.3 Histograms of echo strength (ES), wind speed (WS), and log-transformed wind speed (LOG10(WS)). Taking logarithm of the WS improved the distribution, making it more like the ES distribution.
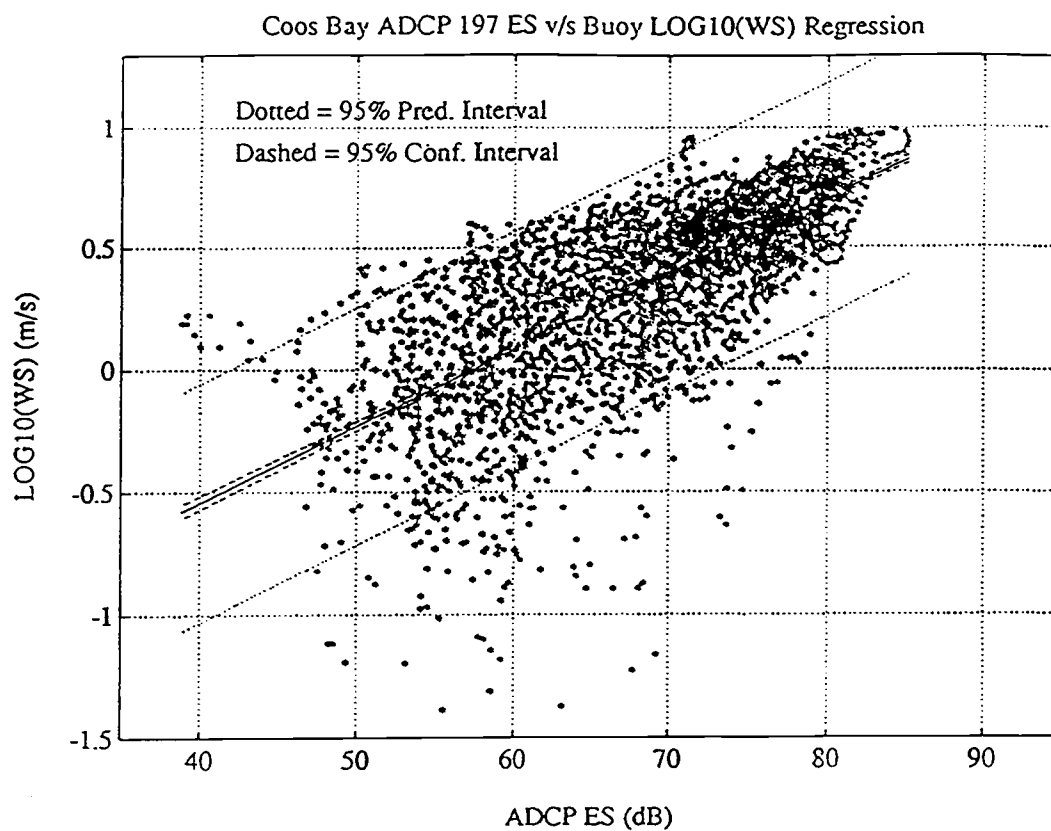
Figure 2.4   Scatter plot of ES and LOG10(WS) with the regression function, showing the 95% confidence and prediction intervals.
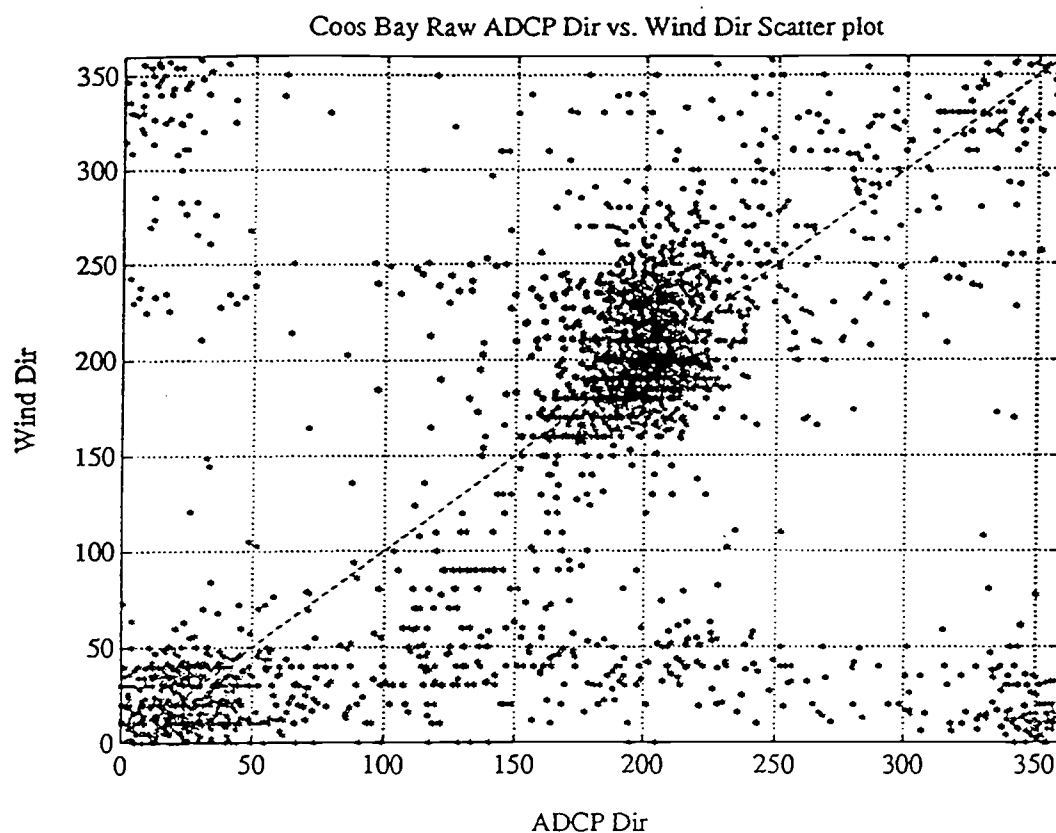
Figure 2.5 Scatter plot of acoustic and wind direction with no smoothing. When the buoy wind speed was zero its direction was ambiguous, and data were not used in this plot.
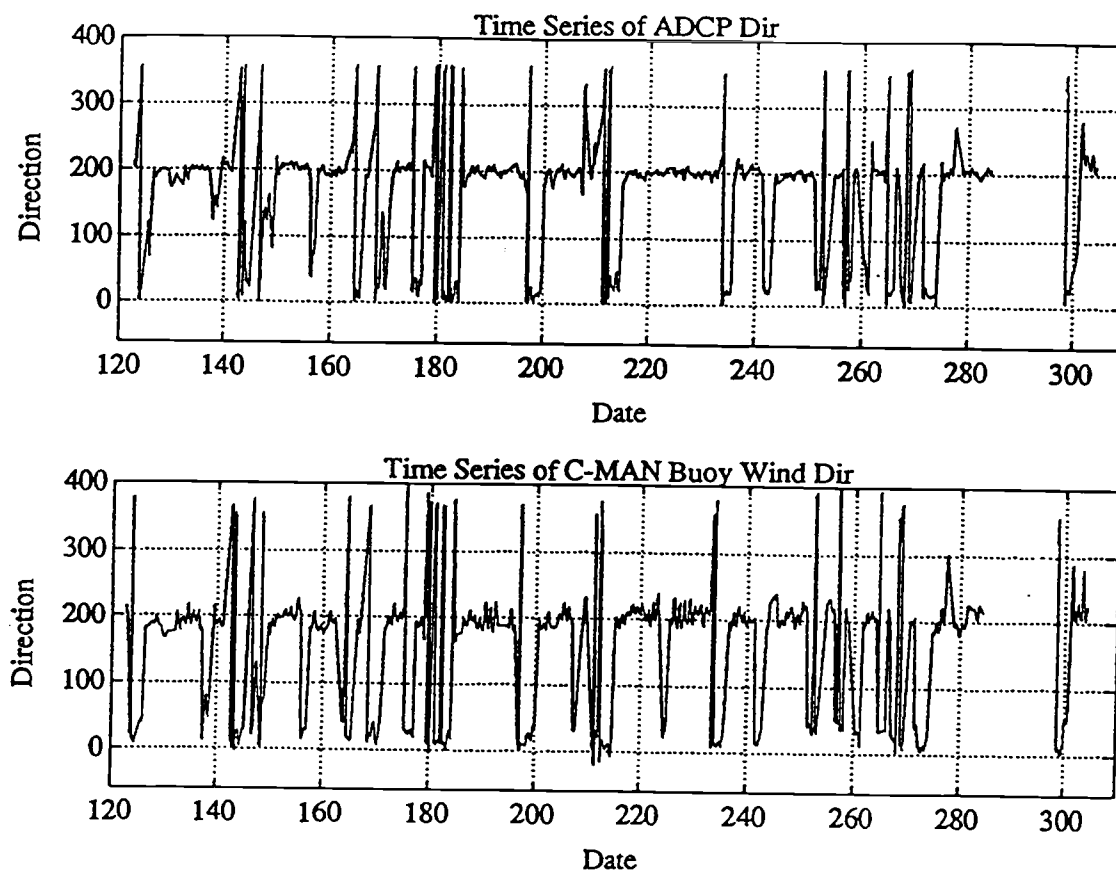
Figure 2.6   Time series of smoothed ADCP direction (AD) from the "current" measurement in the surface bin of the ADCP and folded C-MAN buoy wind direction (WD). Notice that the *y* axis of the wind direction plot goes from -40° to 400°. At the end of the record there is a gap from date 285.5 to 298.7 in the data set due to a lack of measurements from the C-MAN buoy. Dates are in 1989 Julian days (May to October).
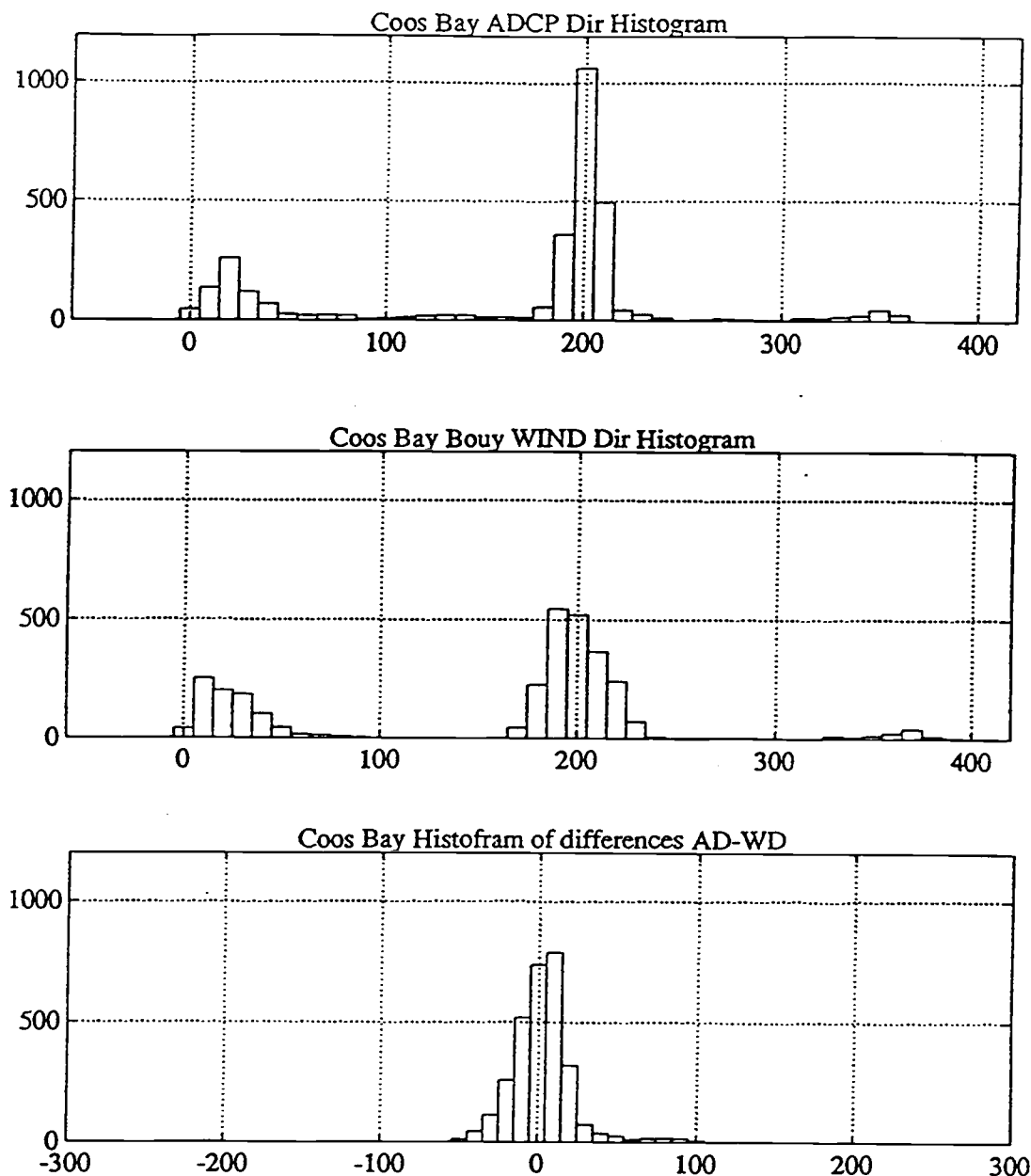
Figure 2.7   Histograms of ADCP direction (AD), folded C-MAN buoy wind direction (WD), and differences AD-WD. Notice that the majority of the differences are shifted roughly towards +5° to +10°, meaning that the ADCP velocity measurements show motion to the right of the wind direction. Where the histogram bin width is 10°.
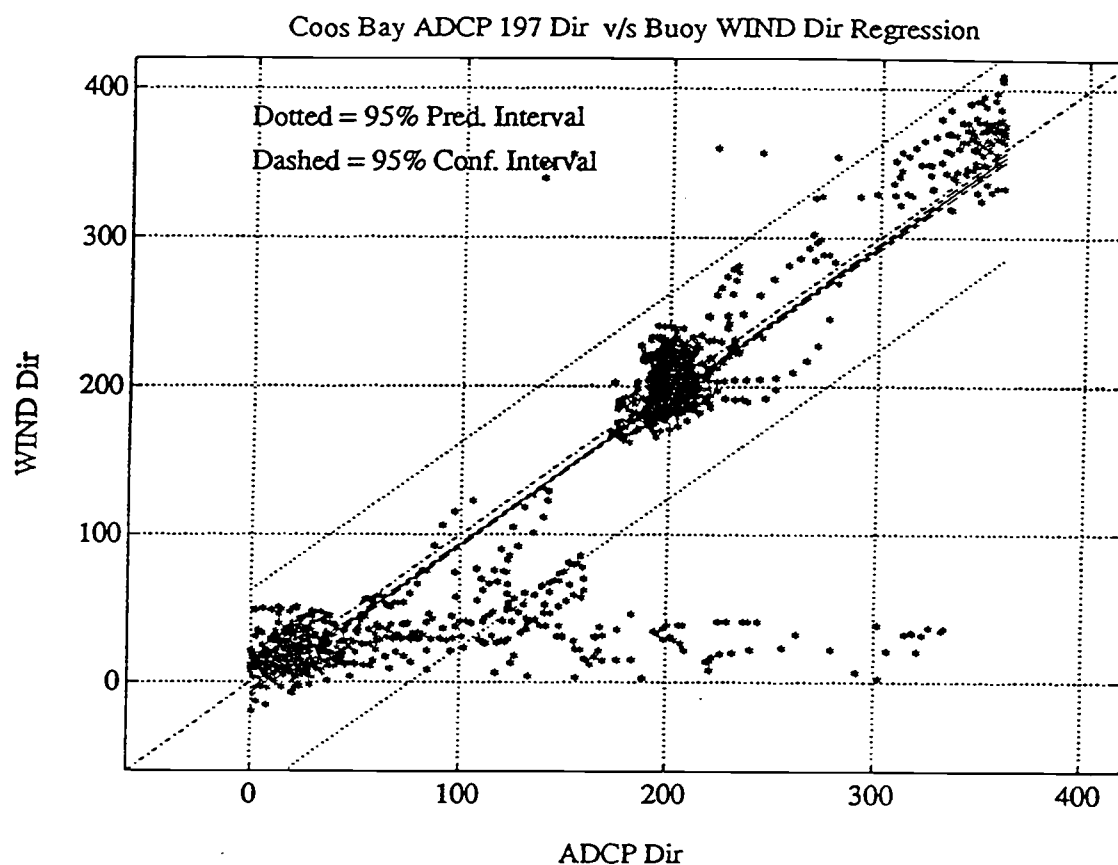
Figure 2.8 Scatter plot of AD and folded WD with regression function showing the 95% confidence and prediction intervals. When current and WD have the same general direction, the model is applicable. When WD is opposite to the current a wide spread of ADCP directions are generated.

Chapter 3

The Mexico Experiment

During the Winter of 1989, an experiment was carried out off the south west Pacific coast of Mexico. Three Acoustic Doppler Current Profiler (ADCP) moorings were deployed from 120 to 170 nautical miles from Tehuantepec city, off the coast of the Gulf of Tehuantepec, Mexico (Figure 3.1).

Acoustical data were measured for a period of two weeks. Meteorological data were collected at buoys mounted on surface moorings close to the ADCP moorings. The western buoy (associated to ADCP 197) did not operate (Figure 3.1). The central buoy (close to ADCP 201) collected data for 74 hours and sank during a strong wind event. The eastern meteorological buoy at the mooring with ADCP 209 collected 260 hours (11 days) of data, but the direction sensor malfunctioned, so there is only wind speed data available. The RV Wecoma, equipped with standard meteorological sensors, was also present in the vicinity providing additional measurements of wind direction and speed. The wind information from RV Wecoma will be used only when the ship was within 10 km of each buoy mooring. Since the meteorological buoy near mooring 197 did not operate, and the RV Wecoma was closer than 10 km to this site only three times, no further analysis will be done to this mooring.

A simple linear regression model will be applied to the intensities, i.e., ES and WS, as well as to the directions, i.e., AD and WD, with the purpose to predict wind velocity.

Oceanographic Background

During the months of October to March strong winds usually develop as a result of high-pressure incursions of polar air into the Gulf of Mexico, north of the Gulf of Tehuantepec. These incursions drive a series of fierce wind jets through the Chivela Pass, the low point of the northwest-southeast mountain range in Central America that separates both golfs, i.e., Gulf of Mexico from Tehuantepec. These strong winds are known locally as the Northers. (Hurd 1929). These jets are driven many hundreds of kilometers into the lower pressure regime over the Pacific. The typical duration of a wind pulse is 2 to 5 days with velocities 10 to 30 m/s. In the central Gulf, strong surface circulation, of the order 1.2 m/s, and intense cooling, by as much as 15°C with respect to the surrounding Pacific, are induced. The wind jet fans out over the Gulf as it exits the Chivela Pass, so that mean directions recorded within 50 km differed by 69°. (Brown et al. 1992).

The Observations

Each buoy/ADCP mooring was situated as indicated in Table 3.1 with upward looking 307.2 kHz ADCP configured for 30° acoustic beam angle.

Buoy wind speeds measured at a height of 1.3 m were converted to a 10 m reference height. The scale factor required to correct the 1.3 m height of the wind speed sensor to 10 m is 1.233, assuming a logarithmic wind profile (see Appendix B). Wind data from the ship were measured at 10 m.

For intensities as well as for directions, the integral time scale (τ) will be calculated using the full record length as the number of hourly lags in the autocorrelation computation (See Appendix A).

Table 3.1: Setup of both ADCP serial numbers 201 & 209 off the coast of the Gulf of Tehuantepec, Mexico for the 1989 Winter experiment. The off shore distances are measured from Tehuantepec city. The variability on the instruments' depth is a standard deviation.

Mooring Name	Tehuantepec 201	Tehuantepec 209
Location	14°18.0' N 95°18.8' W	13°42.3' N 94°18.4' W
Off shore distance	123.1 nm	167.8 nm
Inst. depth	121.98 ± 2.58 m	144.54 ± 1.37 m
Water depth	4000 m	4000 m
Serial Number	**201**	**209**
Frequency	307.2 kHz	307.2 kHz
Beam Angle	30°	30°
Number of Bins	60	60
Bin Length	4.0 m	4.0 m
Pulse Length	6.0 m	6.0 m
Pings per ensemble	135	135
Ensemble time avg.	300 sec	300 sec
Deployed	January 18, 1989	January 21, 1989
Recovered	February 2, 1989	February 5, 1989

Wind Speed Estimates

As shown in chapter one, a log-transformed wind speed improved the wind speed distribution, making it more like the echo strength histogram. Hence this transformation was also used in this chapter.

Mexico station 201:

Figure 3.2 shows the 74 hour time series of buoy intensities and directions. Notice that the direction differences increase at low wind speeds. Figure 3.3 shows time series of ship intensities and directions; there were only 14 observations when the ship was within 10 km from ADCP 201. Figure 3.4 shows the combined intensity data set, and Figure 3.5 shows the combined direction data set. At the onset of the Northers (day 21), it can be noticed that fluctuations in the echo strength time series closely imitate those of wind speed on time scales as short as an hour. Notice that when ship measurements are merged with buoy data they overlap quite well (Figure 3.4), specially at high WS.

Buoy Data:

The integral time scale calculation of the time between effectively independent samples, yields $\tau = 0.49$ days. With this integral time scale, 6 effective degrees of freedom were obtained (from 73 correlated data points by the method explained in Appendix A).

A simple linear regression model $\log(WS) = b_0 + b_1 ES$ of echo strength against the log-transformed wind speed, yields the following coefficients at the 95% significance level with 6 effective degrees of freedom (Figure 3.6):

$$b_0 = -1.558 \pm 0.286$$

$$b_1 = 0.032 \pm 0.004$$

with a correlation coefficient $r = 0.935$, where WS is measured in m/s, and ES in dB.

The 99% significance levels for b_0 and b_1 are ± 0.483 and ± 0.0066 respectively.

The variance analysis (Appendix A) yields:

$$s_e^2 = MSE = 0.018$$

$$s_{b_1}^2 = 2.040x10^{-6}$$

$$s_{b_0}^2 = 0.011$$

where:

s_e^2:   Sample error variance or mean square error, MSE

$s_{b_1}^2$:   Sample variance of the slope b_1

$s_{b_0}^2$:   Sample variance of the intercept b_0

Ship Data:

This data set has only 14 observations in a period of 16 days distributed into 5 clearly distinguishable events (Figure 3.3). The integral time scale of the buoy intensity data set was almost half a day, and assuming that both data sets have similar time scale variability, each approach of the ship to within 10 km of the ADCP 201, may be accounted for a degree of freedom. Actually the ship data set, compared to the buoy data, should have slightly shorter time scale variability, since it is uncorrelating the data measurements by moving in and out of the sampling region. However by choosing the integral time scale of half a day, we are being more conservative. Hence 5 effective degrees of freedom were obtained.

A simple linear regression model $\log(WS) = b_0 + b_1 ES$ of echo strength against the log-transformed wind speed, yields the following coefficients at the 95% significance level with 5 effective degrees of freedom (Figure 3.7):

$$b_0 = -1.052 \pm 0.293$$
$$b_1 = 0.025 \pm 0.004$$

with a correlation coefficient $r = 0.985$.

The 99% significance levels for b_0 and b_1 are ± 0.539 and ± 0.0074 respectively.

The variance analysis (Appendix A) yields:

$$s_e^2 = MSE = 0.0032$$
$$s_{b_1}^2 = 1.611 \times 10^{-6}$$
$$s_{b_0}^2 = 0.0085$$

Combined Data:

Since this data set has large gaps (Figure 3.4), the effective degrees of freedom are going to be calculated as the sum of the buoy's effective degrees of freedom plus the ship's, only when a ship measurement is not closer than half a day from any buoy measurement. This procedure yields 10 effective degrees of freedom, i.e., 6 from buoy's and only 4 from ship's degrees of freedom.

A simple linear regression model $\log(WS) = b_0 + b_1 ES$ of echo strength against the log-transformed wind speed, yields the following coefficients at the 95% significance level with 10 effective degrees of freedom (Figure 3.8):

$$b_0 = -1.466 \pm 0.206$$
$$b_1 = 0.030 \pm 0.0029$$

with a correlation coefficient $r = 0.936$.

The 99% significance levels for b_0 and b_1 are ± 0.300 and ± 0.0042 respectively.

The variance analysis (Appendix A) yields:

$$s_e^2 = MSE = 0.017$$

$$s_{b_1}^2 = 1.575x10^{-6}$$

$$s_{b_0}^2 = 0.008$$

Mexico station 209:

Figure 3.9 shows the time series of buoy intensities. Figure 3.10 shows the time series of ship intensities and directions. Figure 3.11 shows the combined intensity data set. Again as in station 201, fluctuations in the echo strength time series closely imitate those of wind speed on time scales as short as an hour. Notice again that when put together, ship and buoy intensity data merge quite well (Figure 3.11).

Buoy Data:

The integral time scale calculation of the time between effectively independent samples, yields $\tau = 0.51$ days. With this integral time scale, 21 effective degrees of freedom were obtained (from 259 correlated data points by the method explained in Appendix A).

A simple linear regression model $\log(WS) = b_0 + b_1 ES$ of echo strength against the log-transformed wind speed, yields the following coefficients at the 95% significance level with 21 effective degrees of freedom (Figure 3.12):

$$b_0 = -2.671 \pm 0.296$$

$$b_1 = 0.043 \pm 0.0037$$

with a correlation coefficient $r = 0.834$.

The 99% significance levels for b_0 and b_1 are ± 0.405 and ± 0.0051 respectively.

The variance analysis (Appendix A) yields:

$$s_e^2 = MSE = 0.044$$

$$s_{b_1}^2 = 3.164x10^{-6}$$

$$s_{b_0}^2 = 0.020$$

Ship Data:

This data set has only 15 observations in a period of 13 days distributed into 5 clearly distinguishable events. The integral time scale of the buoy intensities' data set was

about half a day, and assuming that both data sets have similar time scales variability, each approach of the ship to within 10 km of the ADCP 209, may be accounted for a degree of freedom. Hence 5 effective degrees of freedom were obtained.

A simple linear regression model $\log(WS) = b_0 + b_1 ES$ of echo strength against the log-transformed wind speed, yields the following coefficients at the 95% significance level with 5 effective degrees of freedom (Figure 3.13):

$$b_0 = -3.507 \pm 4.019$$

$$b_1 = 0.052 \pm 0.0537$$

with a correlation coefficient $r = 0.648$.

The 99% significance levels for b_0 and b_1 are ± 7.377 and ± 0.0986 respectively.

The variance analysis (Appendix A) yields:

$$s_e^2 = MSE = 0.075$$

$$s_{b_1}^2 = 285.106x10^{-6}$$

$$s_{b_0}^2 = 1.595$$

Combined Data:

Since this data set has large gaps (Figure 3.11), the effective degrees of freedom are going to be calculated as the sum of the buoy's effective degrees of freedom plus the ship's, only when a ship measurement is not closer than half a day from any buoy measurement. This procedure yields 24 effective degrees of freedom, i.e., 21 from buoy's and only 3 from ship's degrees of freedom.

A simple linear regression model $\log(WS) = b_0 + b_1 ES$ of echo strength against the log-transformed wind speed, yields the following coefficients at the 95% significance level with 24 effective degrees of freedom (Figure 3.14):

$$b_0 = -2.753 \pm 0.293$$

$$b_1 = 0.044 \pm 0.0038$$

with a correlation coefficient $r = 0.828$.

The 99% significance levels for b_0 and b_1 are ± 0.399 and ± 0.0051 respectively.

The variance analysis (Appendix A) yields:

$$s_e^2 = MSE = 0.047$$

$$s_{b_1}^2 = 3.297x10^{-6}$$

$$s_{b_0}^2 = 0.020$$

Comments on the results of Mexico intensities

At station 201, a simple linear model explains 87% of the variance when the buoy data is used. The ship data explains 97%, and when combined explains 88% of the variance. The same model at station 209, explains 70%, 42% and 68% of the variance for the buoy, ship and combined data respectively. One must keep in mind that, in both stations, the ship regressions were obtained from very few observations.

When buoy and ship data are put together to form the combined data set, they merge quite well, and from the regression analysis we get a good fit, small variances, and it provides more effective degrees of freedom, *i.e.*, better statistical inferences. Hence for further analysis the combined data set, from both stations, will be used.

The onset of the Northers is often dramatic (Figure 3.2 and 3.9). On February 21st wind speeds increased by 10 m/s in 90 minutes.

Wind Direction Estimates

Mexico station 201:

Figure 3.2 shows the time series of buoy directions. Figure 3.3 shows the time series of ship directions, and Figure 3.5 shows the combined direction data set. Notice that generally AD and WD agree quite well when WS is high (roughly when WS is greater than 5 m/s).

Buoy Data:

The integral time scale calculation of the time between effectively independent samples, yields $\tau = 0.19$ days. With this integral time scale, 14 effective degrees of freedom were obtained (from 64 correlated data points by the method explained in Appendix A).

A simple linear regression model $WD = b_0 + b_1 AD$ of acoustic direction (AD) against the wind direction (WD), yields the following coefficients at the 95% significance level with 14 effective degrees of freedom (Figure 3.15):

$$b_0 = -44.631 \pm 96.084$$

$$b_1 = 1.181 \pm 0.4673$$

with a correlation coefficient $r = 0.575$, where AD and WD are measured in degrees.

The 99% significance levels for b_0 and b_1 are ±134.712 and ±0.6552 respectively. The variance analysis (Appendix A) yields:

$$s_e^{\,2} = MSE = 164.090$$

$$s_{b_1}^{\,2} = 0.046$$

$$s_{b_0}^{\,2} = 1944.420$$

Ship Data:

This data set has only 14 observations in a period of 16 days distributed into 5 clearly distinguishable events. The integral time scale of the buoy directions' data set was about 5 hours, and assuming that both data sets have similar time scales variability, each approach of the ship to within 10 km of the ADCP 201, may be accounted for a degree of freedom. Hence 5 effective degrees of freedom were obtained.

A simple linear regression model $WD = b_0 + b_1 AD$ of acoustic direction (AD) against the wind direction (WD), yields the following coefficients at the 95% significance level with 5 effective degrees of freedom (Figure 3.16):

$$b_0 = -77.045 \pm 469.57$$

$$b_1 = 1.153 \pm 2.2251$$

with a correlation coefficient $r = 0.430$.

The true coefficient β_1 is not statistically different from zero, even with a 80% confidence. The variance analysis (Appendix A) yields:

$$s_e^{\,2} = MSE = 3316.569$$

$$s_{b_1}^{\,2} = 0.489$$

$$s_{b_0}^{\,2} = 21777.1$$

Combined Data:

Since this data set has large gaps (Figure 3.5), the effective degrees of freedom are going to be calculated as the sum of the buoy's effective degrees of freedom plus the ship's, only when a ship measurement is not closer than five hours from any buoy measurement. This procedure yields 18 effective degrees of freedom, i.e., 14 from buoy's and only 4 from ship's degrees of freedom.

A simple linear regression model $WD = b_0 + b_1 AD$ of acoustic direction (AD) against the wind direction (WD), yields the following coefficients at the 95% significance level with 18 effective degrees of freedom (Figure 3.17):

$$b_0 = -19.485 \pm 127.789$$

$$b_1 = 1.027 \pm 0.6181$$

with a correlation coefficient $r = 0.378$.

The 99% significance levels for b_0 and b_1 are ± 176.071 and ± 0.8516 respectively.

The variance analysis (Appendix A) yields:

$$s_e^2 = MSE = 888.686$$
$$s_{b_1}^2 = 0.085$$
$$s_{b_0}^2 = 3633.390$$

Comments on the results of Mexico directions

At station 201, a simple linear model explains 33% of the variance when the buoy data is used. The ship data explains 18%, and when combined explains 14% of the variance.

It is clear that a simple linear regression model does not explain the variability of this data set. Hence there is very limited predictability capacity.
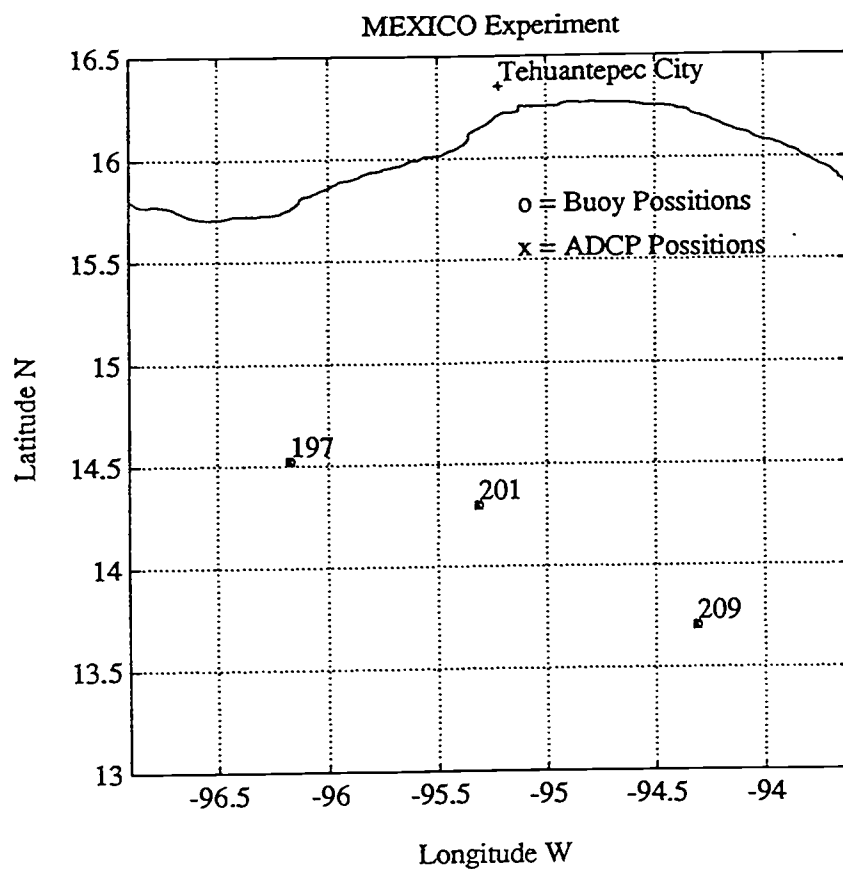
Figure 3.1 Location of the three buoy/ADCP moorings, 120 to 170 nm off the coast of the Gulf of Tehuantepec, Mexico. Off shore distances are measured from Tehuantepec city.
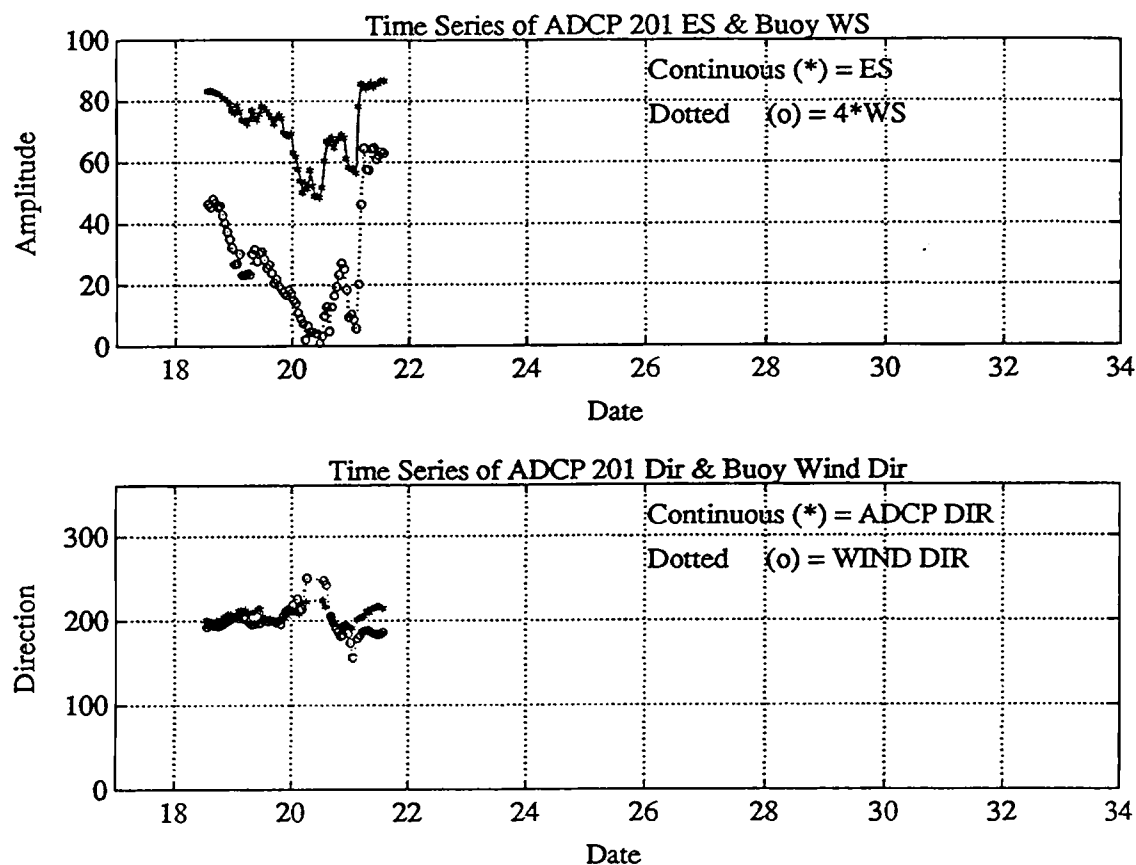
Figure 3.2 Station 201 buoy data time series of echo strength (ES) & wind speed (WS) (higher), ADCP and buoy wind direction (lower). The continuous line is the ES (higher) or ADCP direction (lower), and the dotted line is four times the WS (higher) or wind direction (lower). Dates are in 1989 Julian days (January and February).
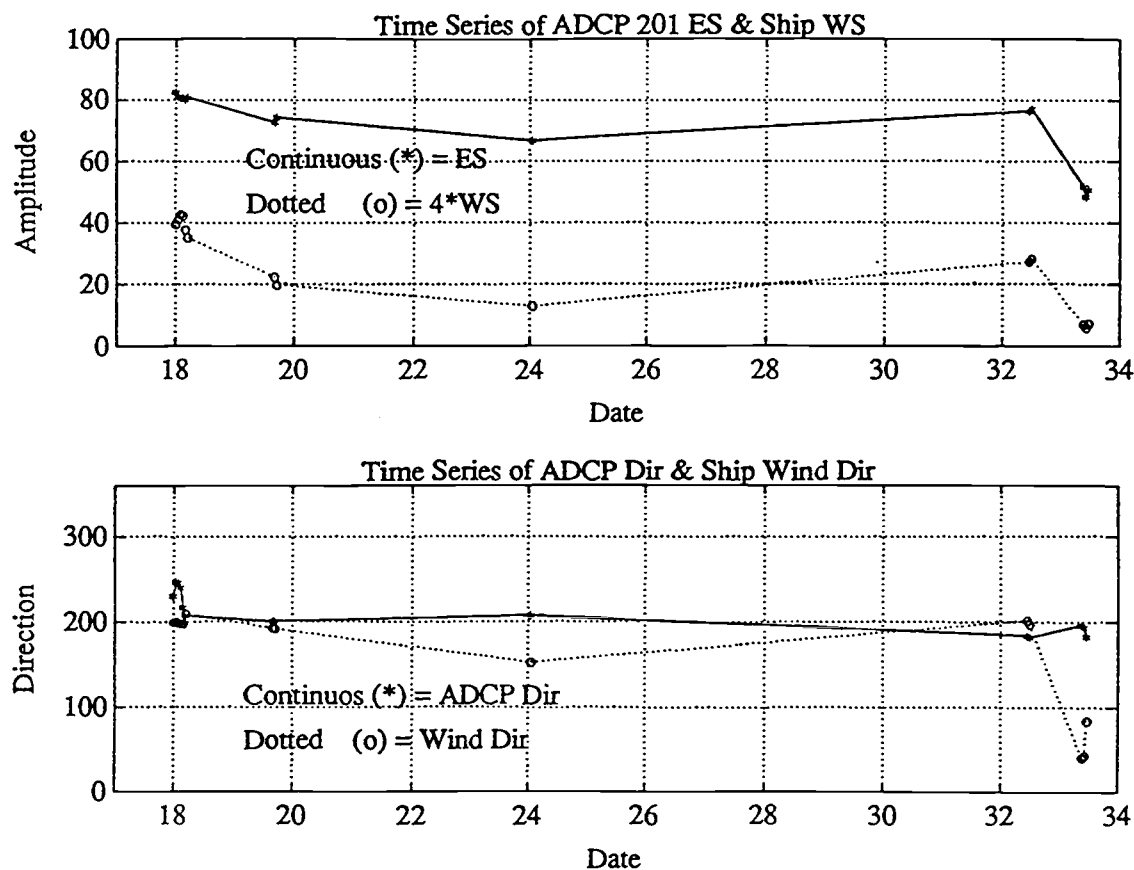
Figure 3.3   Station 201 ship data time series of echo strength (ES) & wind speed (WS) (higher), ADCP and ship wind direction (lower). The continuous line is the ES (higher) or ADCP direction (lower), and the dotted line is four times the WS (higher) or wind direction (lower). There were only 14 observations. Dates are in 1989 Julian days (January and February).

Time Series of Buoy & Ship 201 ES Data

* = ES when BUOY was used

o = ES when SHIP was used

Date

Time Series of Buoy & Ship 201 WS data

* = WS when BUOY was used

o = WS when SHIP was used
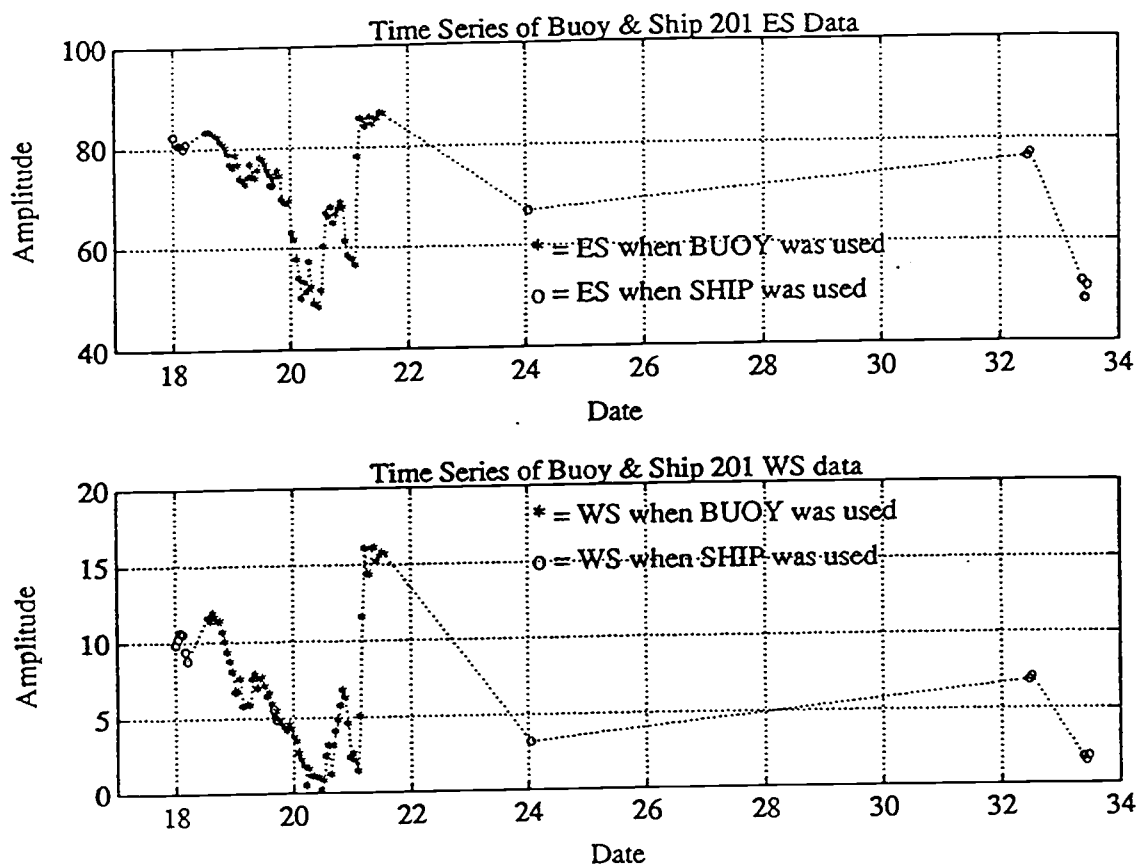
Date

Figure 3.4   Station 201 combined data time series of echo strength (ES) (higher) & wind speed (WS) (lower). Notice the good overlap of both time series. Dates are in 1989 Julian days (January and February).
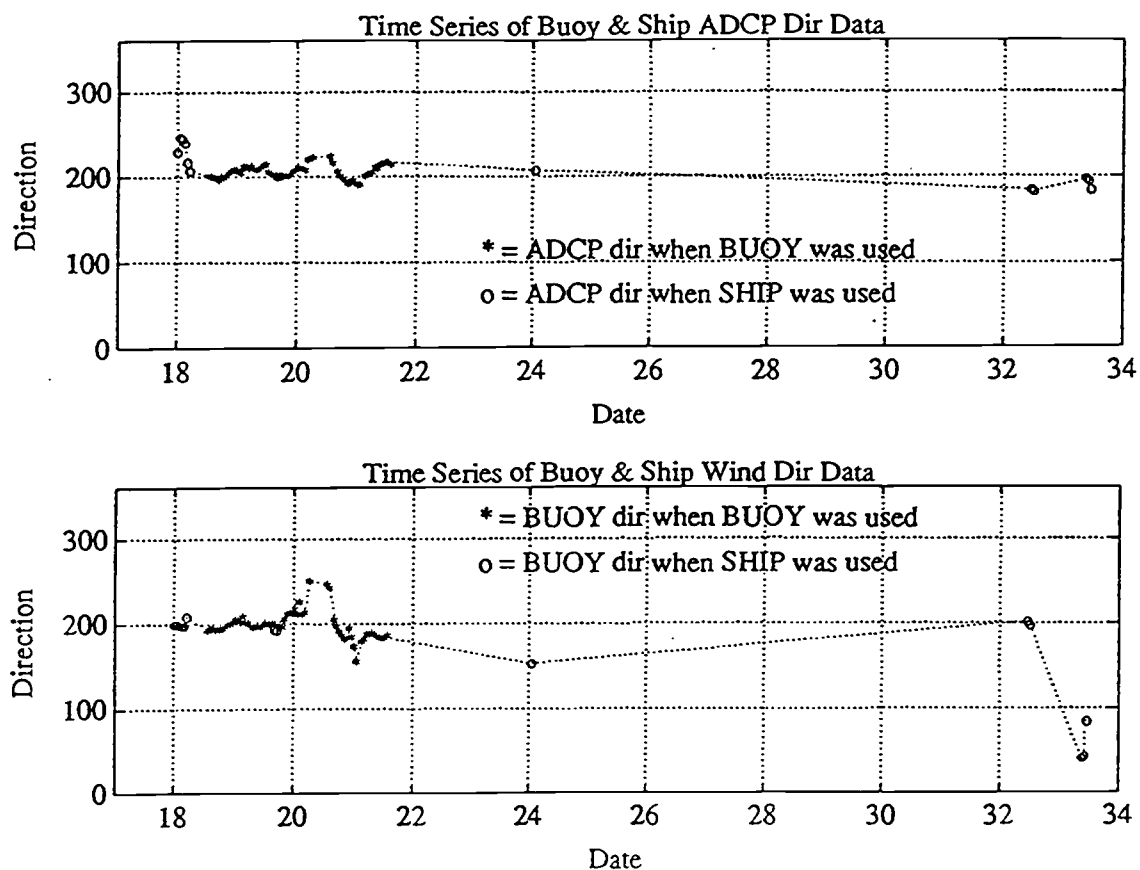
Figure 3.5 Station 201 combined data time series of ADCP direction (higher) & wind direction (lower). Dates are in 1989 Julian days (January and February).
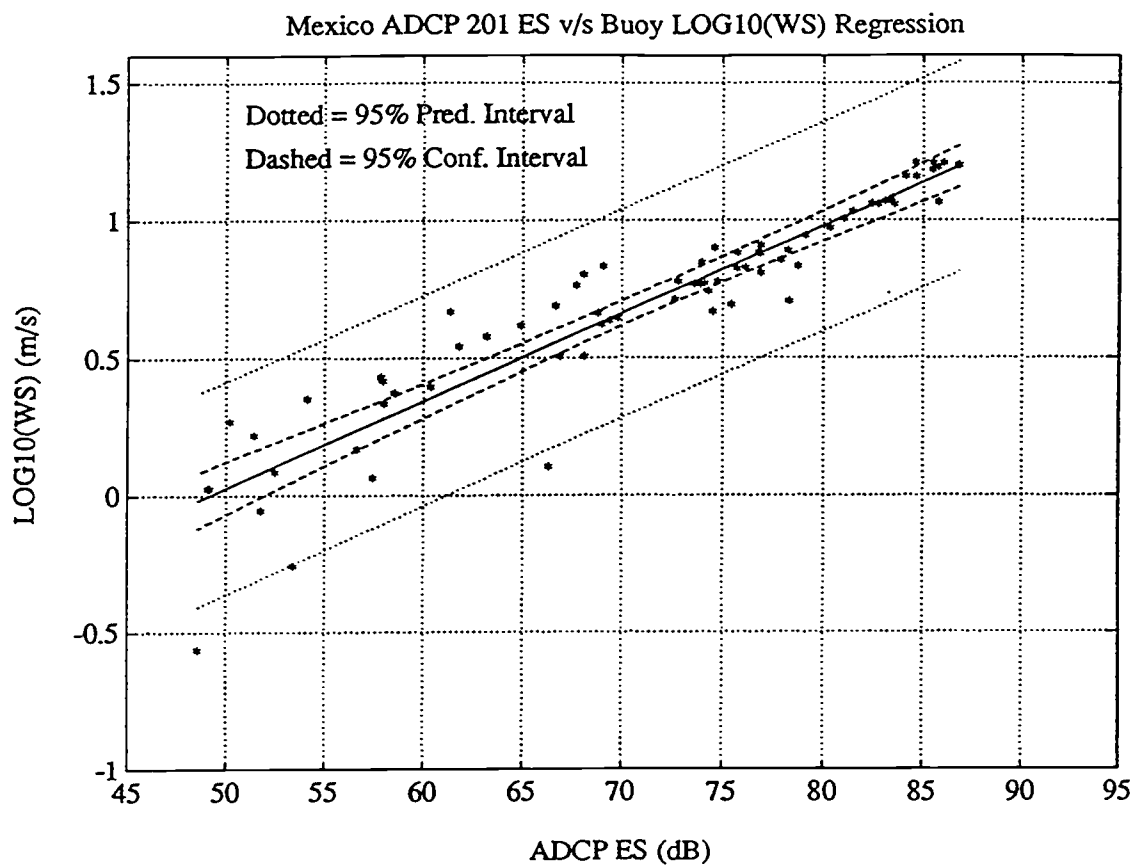
Figure 3.6 Station 201 buoy data scatter plot with the buoy-regression function, showing the 95% confidence and prediction intervals. Notice that the log of the wind speed slightly spreads out at ESs lower than 70 dB.

Mexico ADCP 201 ES v/s Ship LOG10(WS) Regression
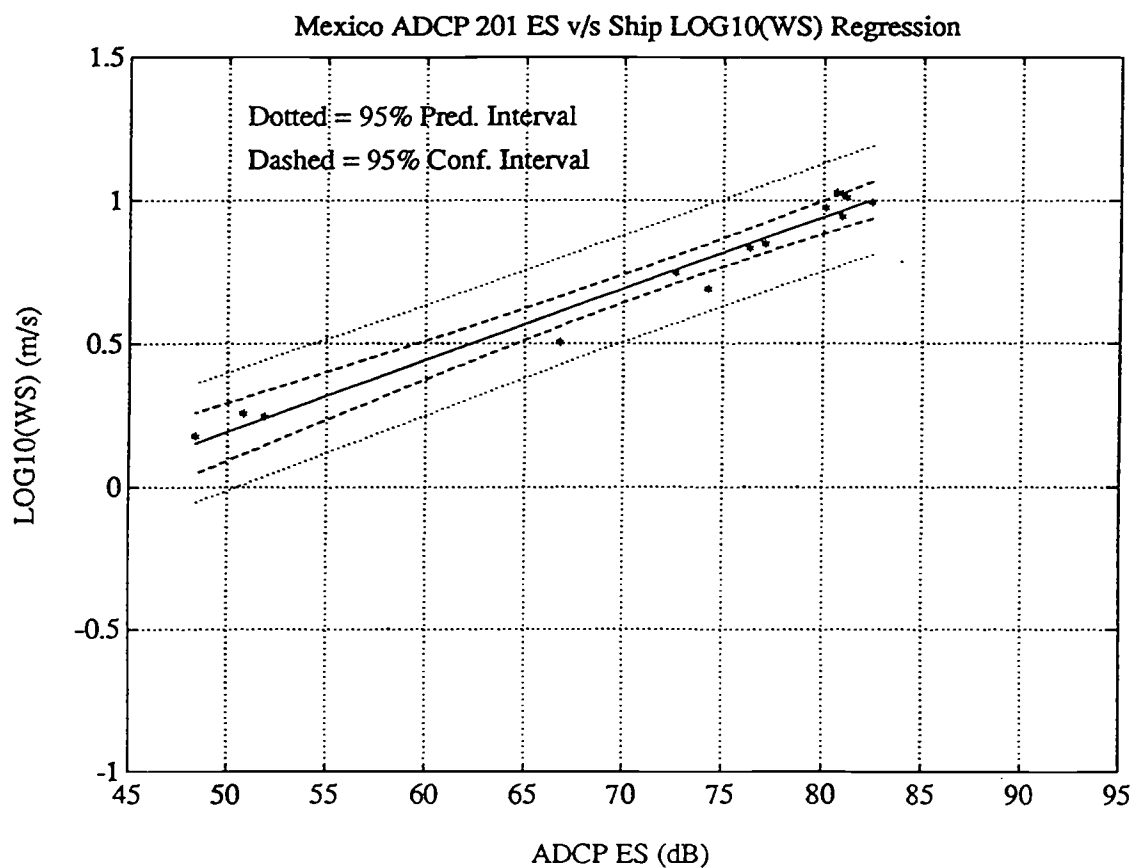
Figure 3.7   Station 201 ship data scatter plot with the ship-regression function, showing the 95% confidence and prediction intervals. The regression is done only over 14 data points.

Mexico ADCP 201 ES v/s Buoy & Ship LOG10(WS) Regression
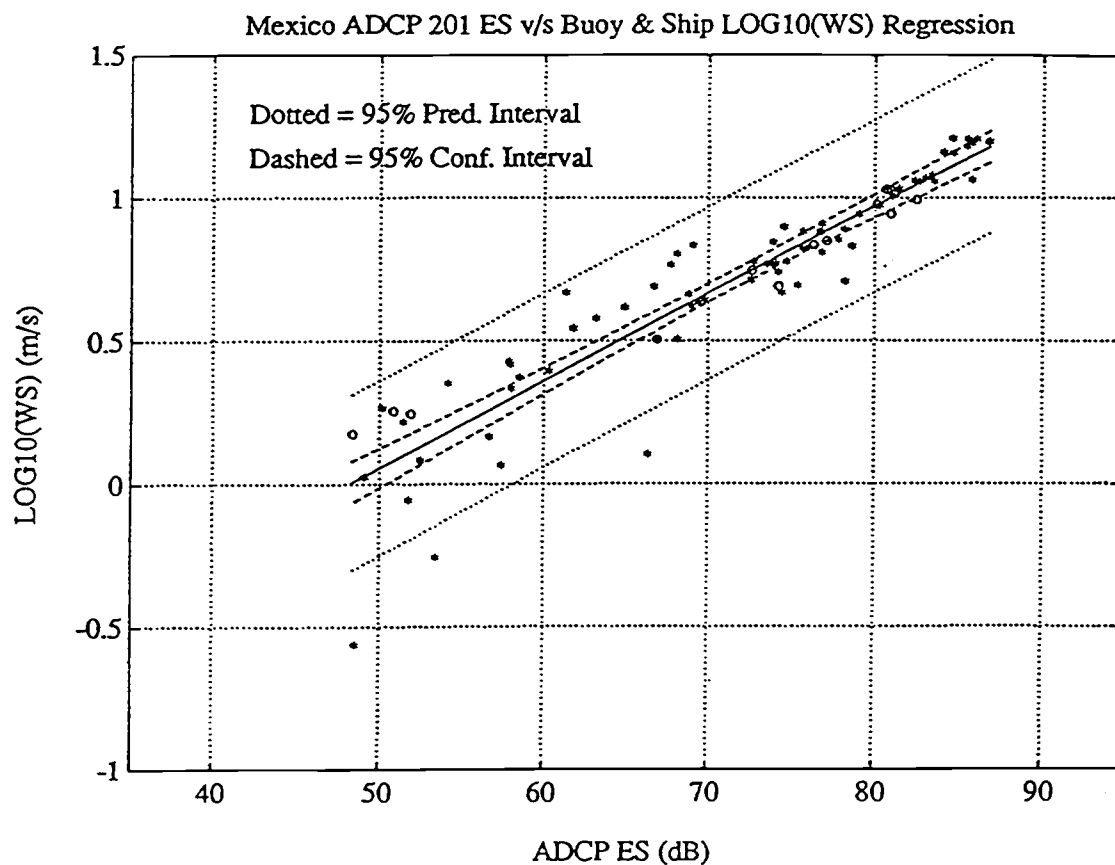
Figure 3.8 Station 201 combined data scatter plot with the combined-regression function, showing the 95% confidence and prediction intervals. Ship data (denoted by circles) lies over the buoy data (denoted by stars) smoothly. There is a slight spread of the log of the WS at ESs lower than 70 dB.
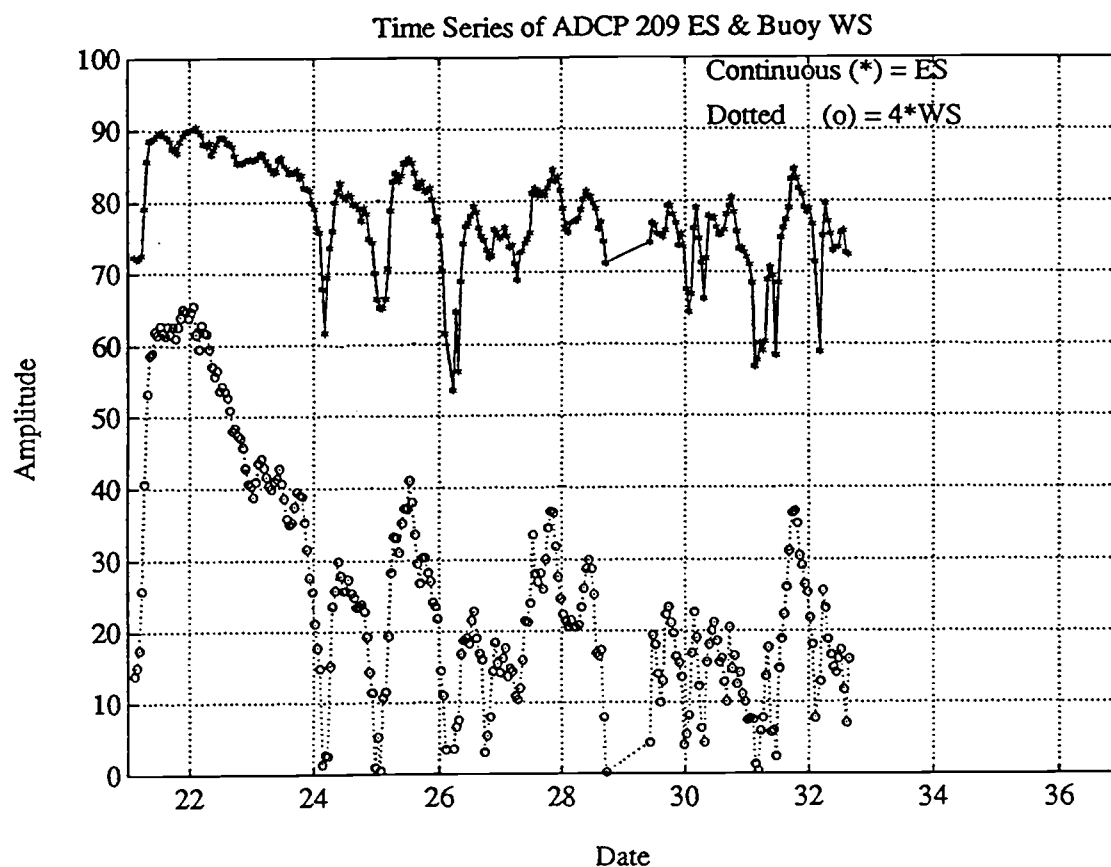
Figure 3.9 Station 209 buoy data time series of echo strength (ES) & wind
speed (WS). There is no wind direction data available. The
continuous line is the ES, and the dotted line is four times the
WS. Dates are in 1989 Julian days (January and February).
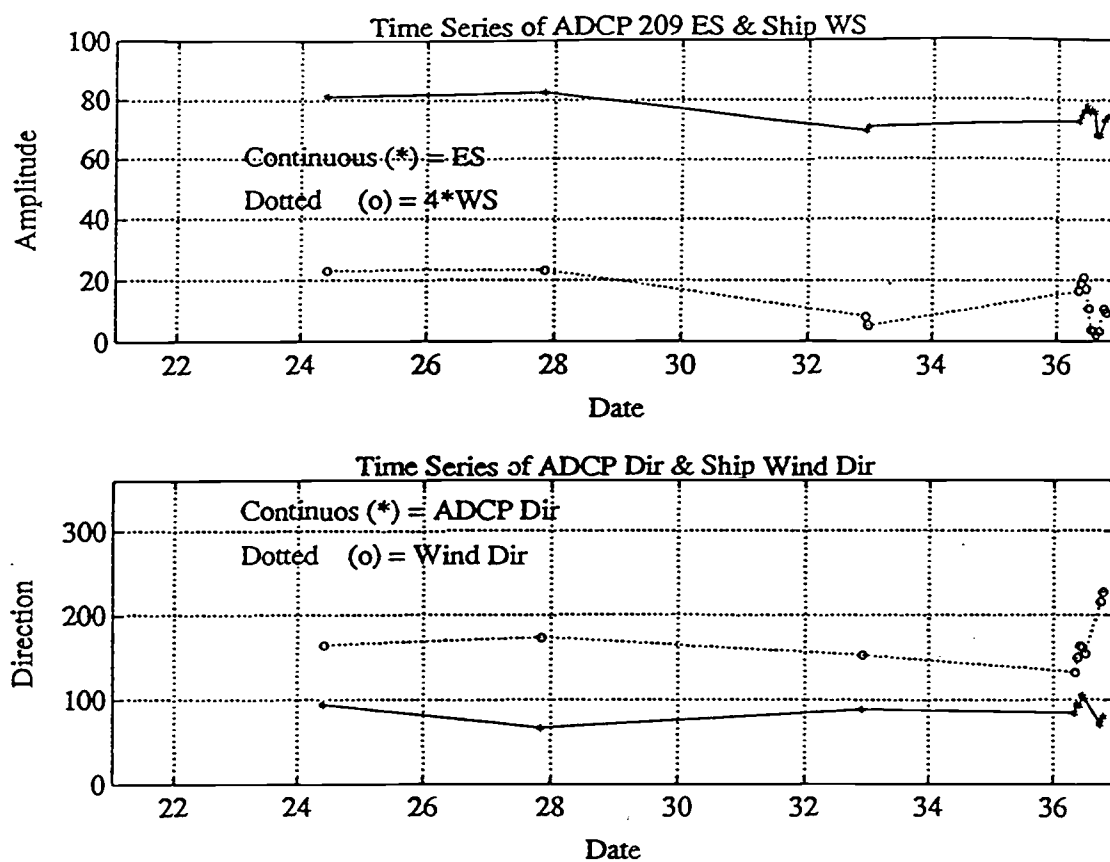
Figure 3.10   Station 209 ship data time series of echo strength (ES) & wind speed (WS) (higher), ADCP direction and wind direction (lower). The continuous line is the ES or ADCP direction, and the dotted line is four times the WS or wind direction respectively. There were only 15 observations. Dates are in 1989 Julian days (January and February).
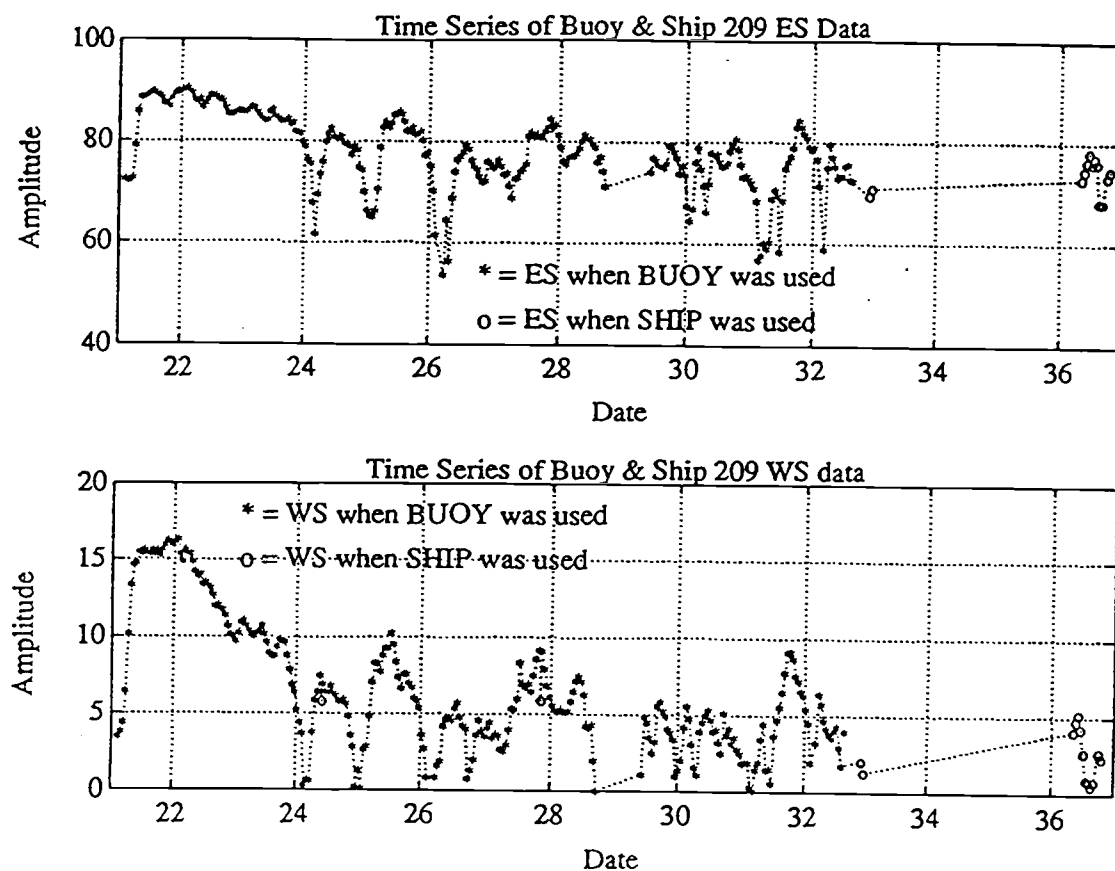
Figure 3.11 Station 209 combined data time series of echo strength (ES) (higher) & wind speed (WS) (lower). Dates are in 1989 Julian days (January and February).
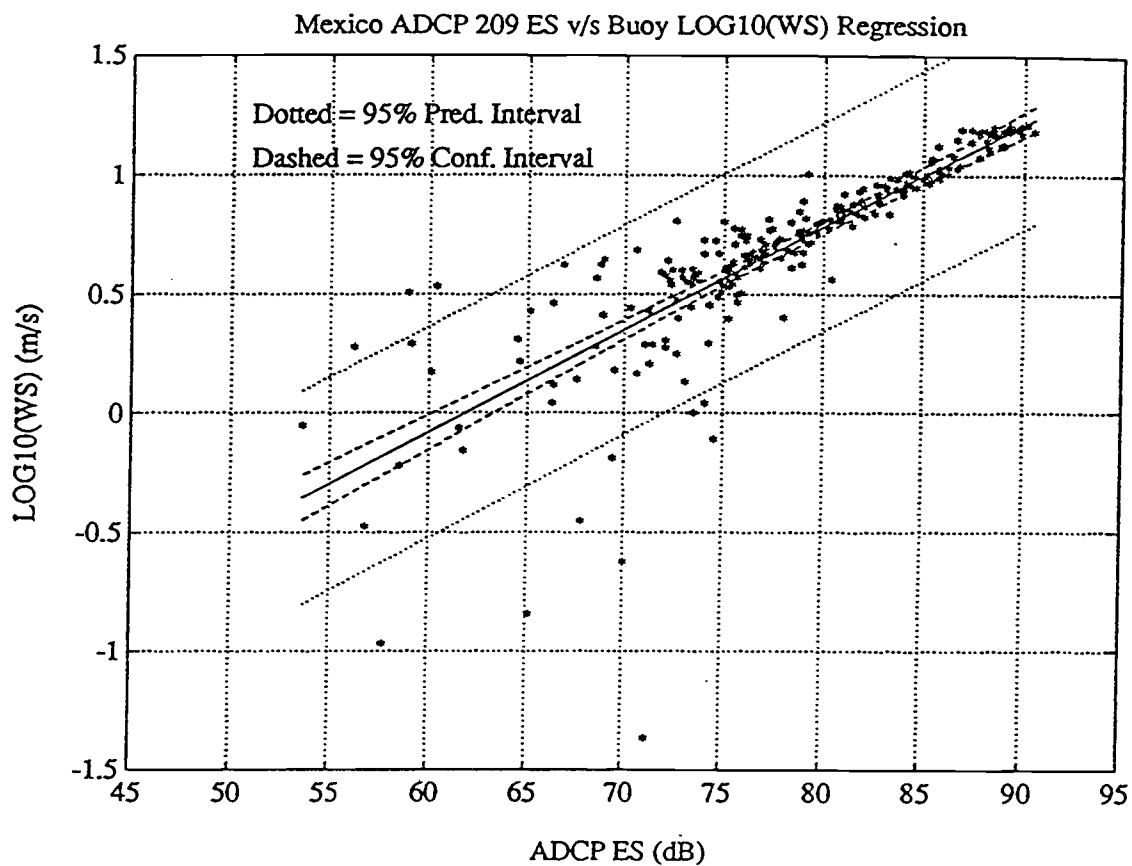
Figure 3.12 Station 209 buoy data scatter plot with the buoy-regression function, showing the 95% confidence and prediction intervals. Notice that the log of the wind speed strongly spreads out at ESs lower than 75 dB.
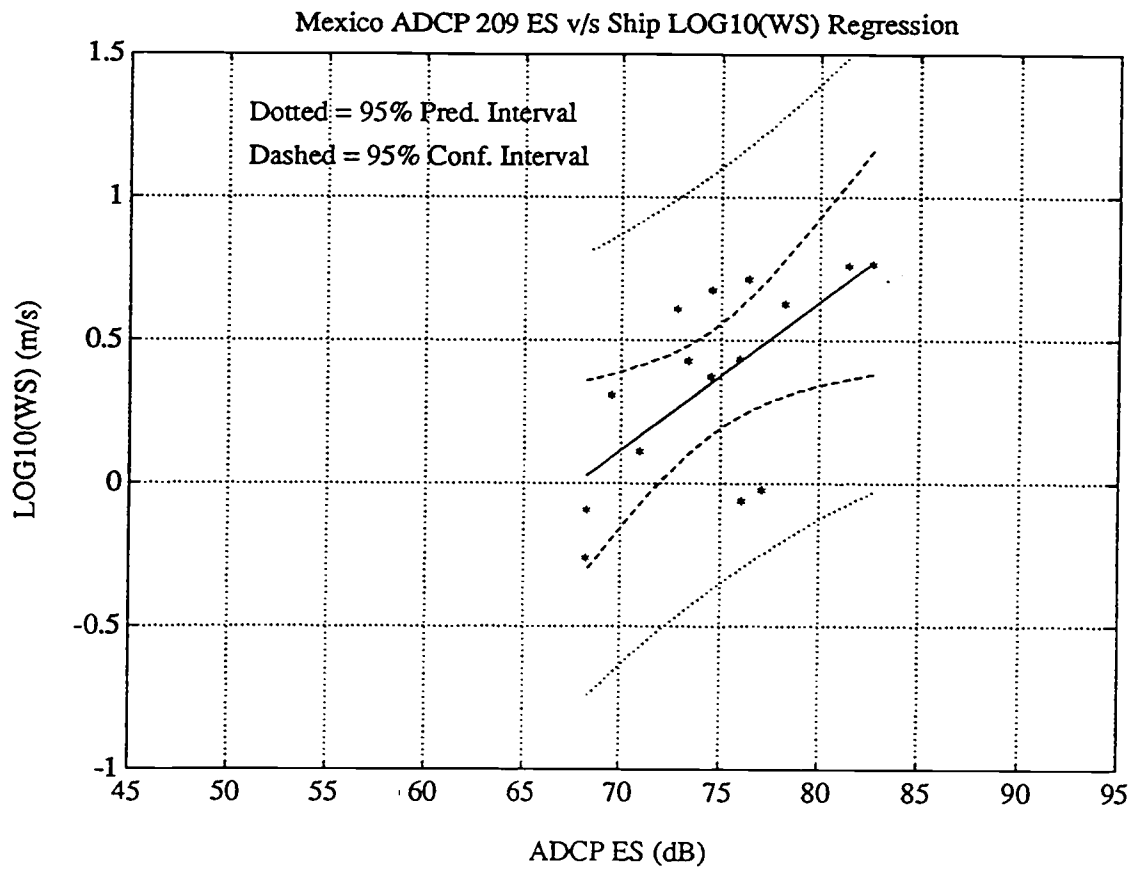
Figure 3.13   Station 209 ship data scatter plot with the ship-regression function, showing the 95% confidence and prediction intervals. Notice the short scope of this model. The regression is done only over 15 data points.
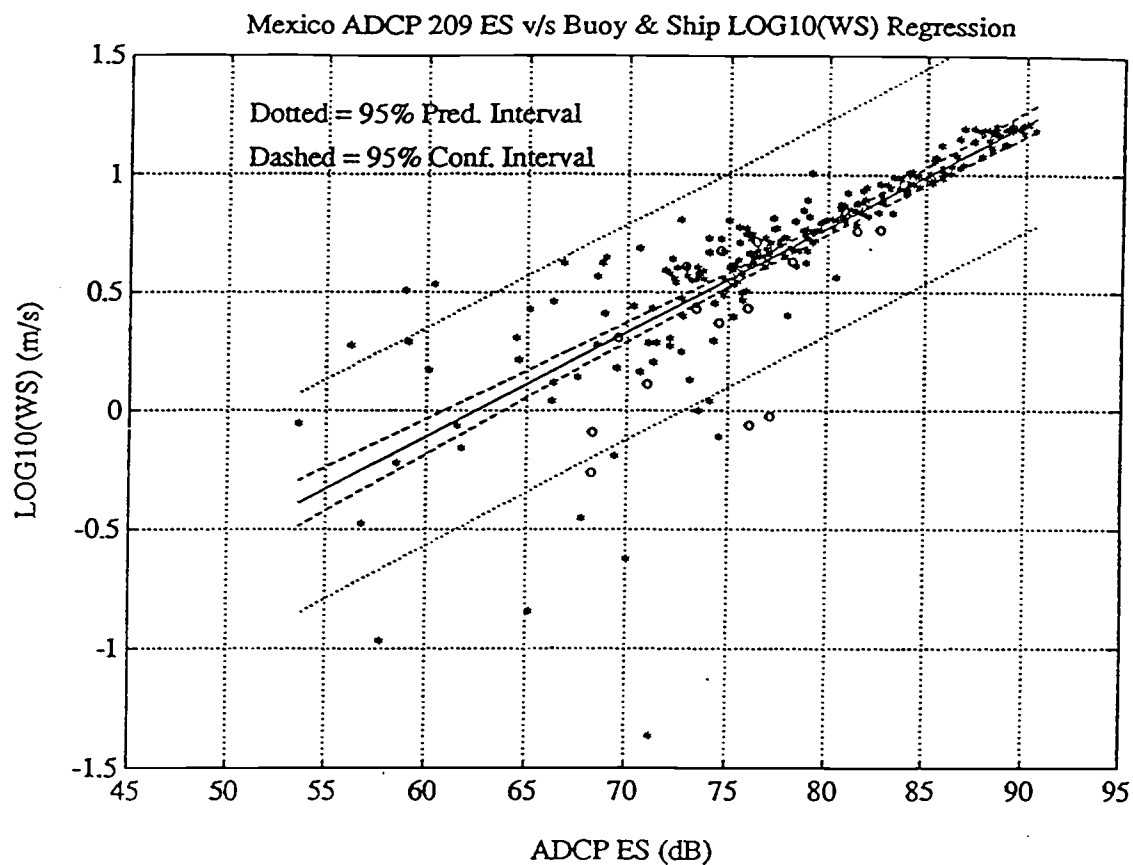
Figure 3.14 Station 209 combined data scatter plot with the combined-regression function, showing the 95% confidence and prediction intervals. Ship data (denoted by circles) lies shifted towards low wind speeds compared to the buoy data (denoted by stars). There is a strong spread of the log of the WS at ESs lower than 75 dB.

Mexico ADCP 201 Dir v/s Buoy Wind Dir Regression
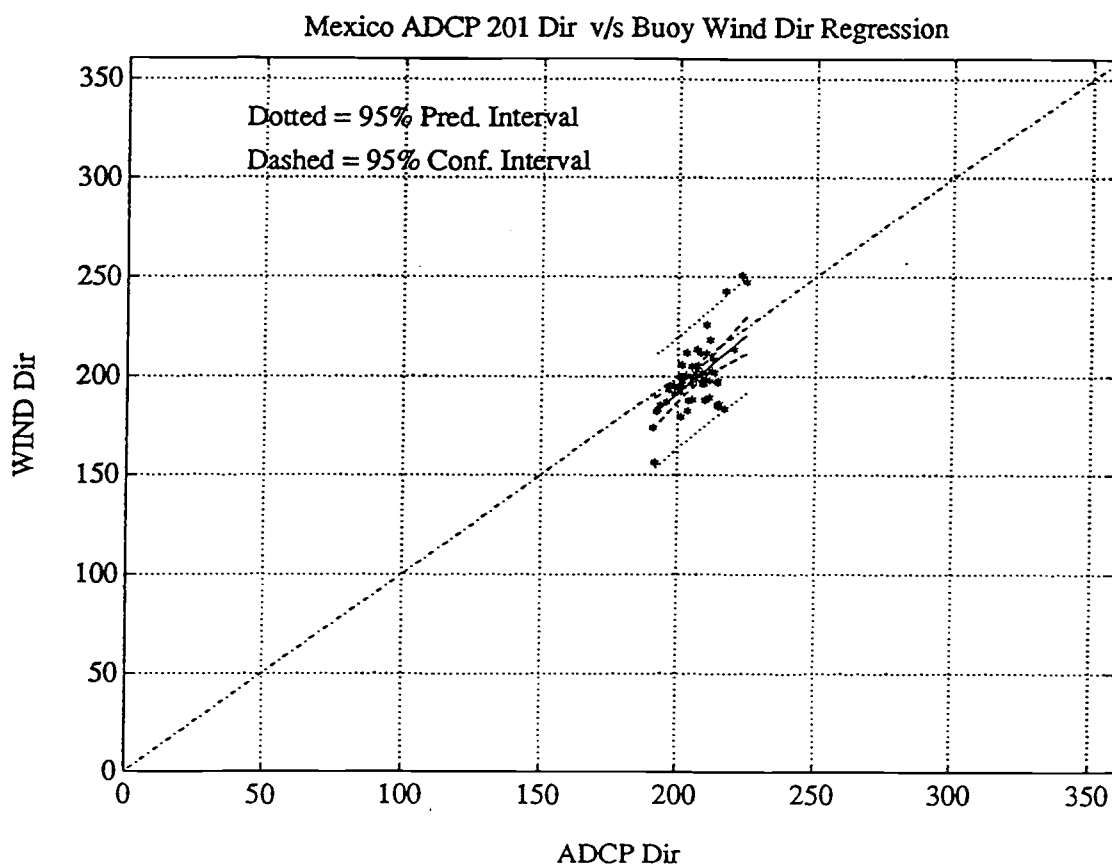
Figure 3.15 Station 201 buoy data scatter plot with the buoy-regression function, showing the 95% confidence and prediction intervals.
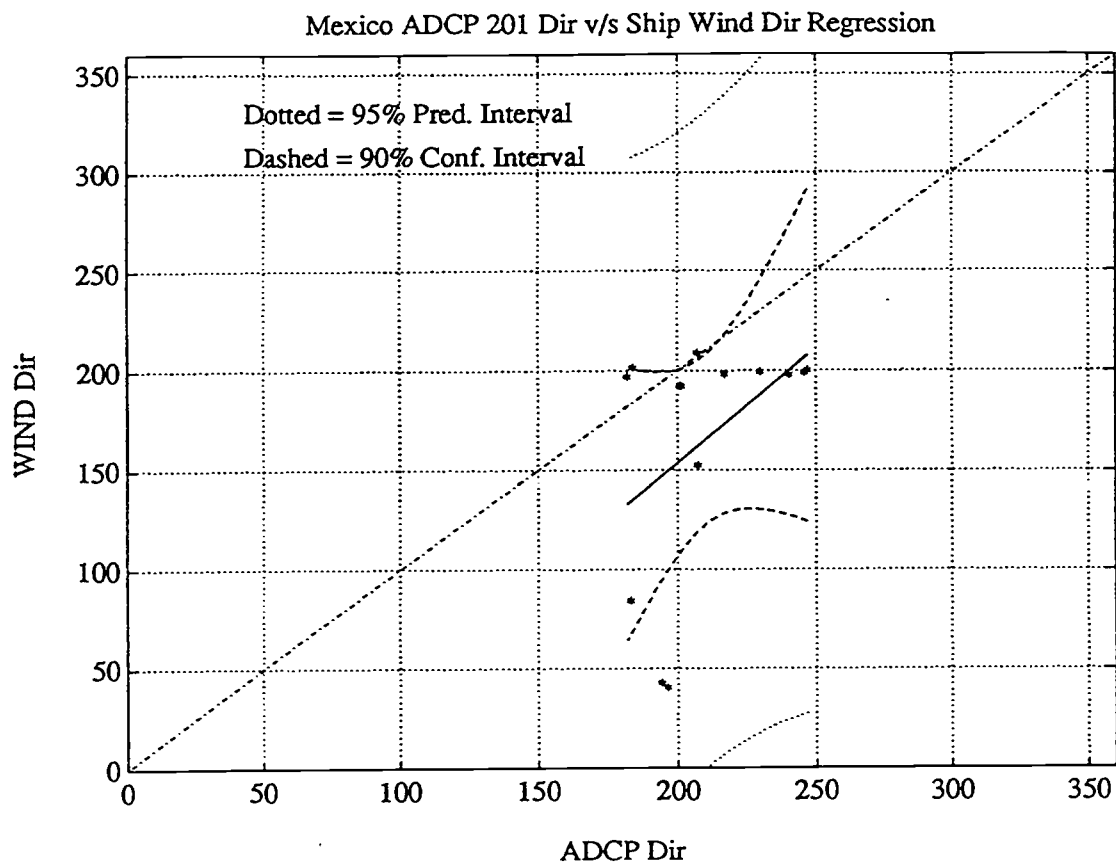
Figure 3.16 Station 201 ship data scatter plot with the ship-regression function, showing large 95% confidence and prediction intervals.

Mexico ADCP 201 Dir v/s Buoy & Ship Wind Dir Regression
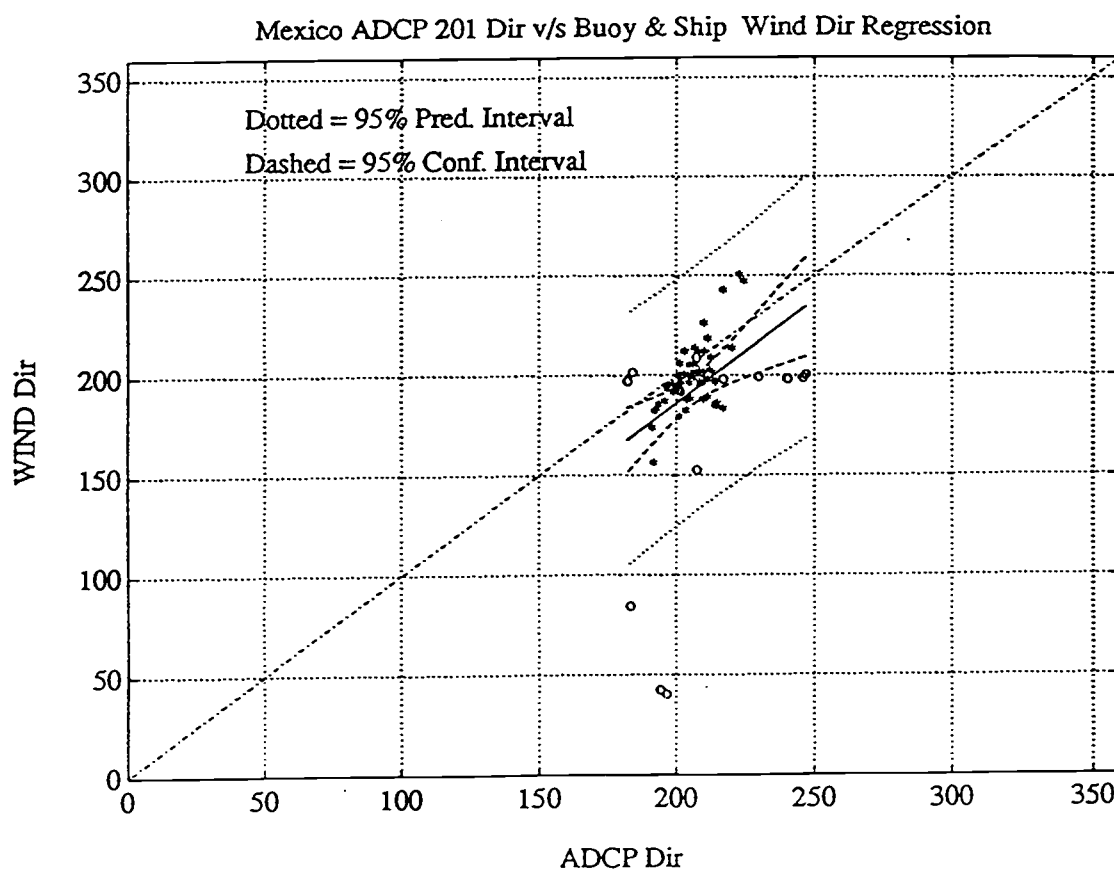
Figure 3.17 Station 201 Combined data scatter plot with the combined-regression function, showing the 95% confidence and prediction intervals.

Chapter 4

The Coastal Transition Zone
(CTZ) Experiment

During the Summer of 1988, an experiment was carried out on the Coastal Transition Zone (CTZ) off the coast of California, U.S.A. (Huger *et al.*, 1991). Three ADCPs moorings were deployed about 91 nautical miles off the coast of Point Arena, California (Figure 4.1). As stated in the introduction, only two of three ADCPs are going to be used, since the third (ADCP 209) was moored too deep to collect data from the surface. Acoustical data were measured in both ADCPs for a period slightly longer than one month. Meteorological data (wind speed and direction) were also obtained by two meteorological buoys about 20 nm off the coast for the same period (Figure 4.1). The *RV Wecoma*, equipped with standard meteorological sensors, was also present in the vicinity providing additional measurements of wind direction and speed. The wind information from the *RV Wecoma* will be used only when the ship was within 10 km of each ADCP. The large scale oceanographic background of northern California is similar to that of the Coos Bay experiments (Chapter 1).

A simple linear regression model will be applied to the intensities, ES and WS, as well as to the directions, AD and WD, to predict wind velocity.

The Observations

The ADCP moorings were situated 26 nm apart from each other with upward-looking 307.2 kHz ADCPs configured for 30° acoustic beam angle (Table 4.1).

Wind measurements were available from the National Data Buoy Center (NDBC) buoys, buoy 46014 located 10 nm off the coast of Mendocino, and buoy 46013 located 20 nm off Bodega Head (Figure 4.1). Buoy wind speeds measured at a height of 3 m were converted to a 10 m reference height. The scale factor required to correct the 3 m height of the wind speed sensor to 10 m is 1.125, assuming a logarithmic wind profile (see Appendix B). Wind data from the ship were measured at 10 m.

The computation of the integral time scale (τ) was made from the ship's leg 2, and then got effective degrees of freedom for the data sets.

Table 4.1: Setup of both ADCP serial numbers 197 & 201 off the coast of the Point Arena, California, U.S.A. for the 1988 Summer CTZ experiment. The off shore distances are measured from Point Arena. The variability on the instruments' depth is a standard deviation.

Mooring Name	CTZ 197	CTZ 201
Location	037°55.0' N 124°44.5' W	038°16.2' N 125°00.0' W
Off shore distance	90.6 nm	92.7 nm
Inst. depth	120.5 ±1.95 m	108.90 ± 2.38 m
Water depth	3992 m	3898 m
Serial number	**197**	**201**
Frequency	307.2 kHz	307.2 kHz
Beam Angle	30°	30°
Number of Bins	40	40
Bin Length	4.0 m	4.0 m
Pulse Length	6.0 m	6.0 m
Ensemble time avg.	150 sec	150 sec
Pings per ensemble	60	60
Deployed	June 25, 1988	June 21, 1988
Recovered	July 30, 1988	July 29, 1988

Wind Speed Estimates

As shown in chapter one, a log-transformed wind speed improved the wind speed distribution, making it more like the echo strength histogram. Hence this transformation was also used in this chapter.

To compute the regression model at station 197, meteorological data from both buoys were examined, since they were at comparable distances from ADCP 197 - buoy 46014 was at 92.8 nm and buoy 46013 at 88.5 nm. As expected a priori, buoy 46013 produced a slightly better fit to the ADCP data compared to buoy 46014. For station 201, buoy 46014 was at 86.7 nm and buoy 46013 at 101.9 nm. Again a slightly better fit was obtained from the closer buoy. Therefore station 201 regressions will be calculated with meteorological data from buoy 46014.

Recall that all hourly averaged data sets in this chapter were smoothed with the same 13 hr moving average filter as in Chapter 2.

CTZ station 197:

Figure 4.2 shows the time series of the smoothed echo strength (ES), buoy 46013 wind speed (WS), ADCP acoustic direction (AD), and buoy wind direction (WD). Figure 4.3 shows the same ADCP time series but with the ship data. Figure 4.4 shows the combined intensities and Figure 4.5 the combined directions. From these two last plots, it is learned that a combined scheme introduces large offsets between the ADCP and buoy data, probably due to the great distance between both instruments. Therefore it was not addressed in this study.

Ship Data:

The integral time scale calculation of the time between effectively independent samples, yields $\tau = 1.82$ days. With this integral time scale, 17 effective degrees of freedom were obtained (from 519 correlated data points by the method explained above and Appendix A).

A simple linear regression model $\log(WS) = b_0 + b_1 ES$ of echo strength against the log-transformed wind speed, both smoothed with a 13 hr moving average, yields the following coefficients at the 95% significance level with 17 effective degrees of freedom (Figure 4.6):

$$b_0 = -1.469 \pm 0.088$$
$$b_1 = 0.029 \pm 0.0034$$

with a correlation coefficient $r = 0.930$, where WS is measured in m/s, and ES in dB.

The 99% significance levels for b_0 and b_1 are ± 0.122 and ± 0.0047 respectively. The variance analysis (Appendix A) yields:

$$s_e^2 = MSE = 0.0045$$
$$s_{b_1}^2 = 2.585 x 10^{-6}$$
$$s_{b_0}^2 = 0.0017$$

where:

s_e^2:   Sample error variance or mean square error MSE

$s_{b_1}^2$:   Sample variance of the slope b_1

$s_{b_0}^2$:   Sample variance of the intercept b_0

Buoy 46013 Data:

The integral time scale calculation of the time between effectively independent samples, yields $\tau = 2.52$ days. With this integral time scale, 12 effective degrees of freedom were obtained (from 767 correlated data points by the method explained above and in Appendix A).

A simple linear regression model $\log(WS) = b_0 + b_1 ES$ of echo strength against the log-transformed wind speed, both smoothed with a 13 hr moving average, yields the following coefficients at the 95% significance level with 12 effective degrees of freedom (Figure 4.7):

$$b_0 = -1.068 \pm 0.282$$
$$b_1 = 0.024 \pm 0.0035$$

with a correlation coefficient $r = 0.485$.

The 99% significance levels for b_0 and b_1 are ± 0.401 and ± 0.0049 respectively. The variance analysis (Appendix A) yields:

$$s_e^2 = MSE = 0.107$$
$$s_{b_1}^2 = 2.435x10^{-6}$$
$$s_{b_0}^2 = 0.016$$

CTZ station 201:

Figure 4.8 shows the time series of the smoothed echo strength (ES), buoy 46014 wind speed (WS), ADCP 201 acoustical direction (AD), and buoy wind direction (WD). Figure 4.9 shows the same ADCP time series but with the ship data. Figure 4.10 shows the combined intensities and Figure 4.11 the combined directions. From these two last plots, again it was concluded that a combined scheme was not going to be addressed in this study.

Ship Data:

The integral time scale calculation of the time between effectively independent samples, yields $\tau = 1.82$ days. With this integral time scale, 18 effective degrees of freedom were obtained (from 545 correlated data points by the method explained above and in Appendix A).

A simple linear regression model $\log(WS) = b_0 + b_1 ES$ of echo strength against the log-transformed wind speed, both smoothed with a 13 hr moving average, yields the

following coefficients at the 95% significance level with 18 effective degrees of freedom (Figure 4.12):

$$b_0 = -1.937 \pm 0.164$$
$$b_1 = 0.035 \pm 0.002$$

with a correlation coefficient $r = 0.848$.

The 99% significance levels for b_0 and b_1 are ± 0.226 and ± 0.0028 respectively. The variance analysis (Appendix A) yields:

$$s_e^2 = MSE = 0.007$$
$$s_{b_1}^2 = 0.908x10^{-6}$$
$$s_{b_0}^2 = 0.006$$

Buoy 46014 Data:

The integral time scale calculation of the time between effectively independent samples, yields $\tau = 3.33$ days. With this integral time scale, 10 effective degrees of freedom were obtained (from 860 correlated data points by the method explained above and in Appendix A).

A simple linear regression model $\log(WS) = b_0 + b_1 ES$ of echo strength against the log-transformed wind speed, both smoothed with a 13 hr moving average, yields the following coefficients at the 95% significance level with 10 effective degrees of freedom (Figure 4.13):

$$b_0 = -1.900 \pm 0.216$$
$$b_1 = 0.033 \pm 0.0027$$

with a correlation coefficient $r = 0.695$.

The 99% significance levels for b_0 and b_1 are ± 0.315 and ± 0.0039 respectively. The variance analysis (Appendix A) yields:

$$s_e^2 = MSE = 0.0739$$
$$s_{b_1}^2 = 1.354x10^{-6}$$
$$s_{b_0}^2 = 0.0088$$

Comments on the results of CTZ intensities

Combined data were not used since it is clear from a comparison of Figures 4.8 and 4.9 that the coastal buoy winds differ from the ship winds, and that the ship winds provide a more local measurement for the ADCP. This is probably due to the great distance between both instruments. Recall that ship data were used only when the ship was closer than 10 km to each ADCP, in contrast to the buoys that were on average 90

nm apart from the ADCP. Notice that buoys were under the effects of coastal wind patterns, which is not the case of both ADCPs. (Figure 4.1)

At station 197 a simple linear regression model explains 86% and 24% of the variance when the ship and buoy 46013 data are used respectively. The same model at station 201 explains 72% and 48% of the variance for the ship and buoy 46014 data respectively. For further analysis the ship data set will be used.

Wind Direction Estimates

Since only ship data is going to be used for further analysis, the examination of buoy directions data will be dropped. As explained earlier combined data sets will not be used.

CTZ station 197:

Acoustical direction, and ship wind direction time series are showed in Figure 4.3. Figure 4.5 shows the combined direction time series that will not be used.

Ship Data:

The integral time scale calculation of the time between effectively independent samples, yields $\tau = 2.26$ days. With this integral time scale, 13 effective degrees of freedom were obtained (from 514 correlated data points by the method explained above and in Appendix A).

A simple linear regression model $WD = b_0 + b_1 AD$ of acoustic direction (AD) against the wind direction (WD), both smoothed with a 13 hr moving average, yields the following coefficients at the 95% significance level with 13 effective degrees of freedom (Figure 4.14):

$$b_0 = 70.605 \pm 16.547$$
$$b_1 = 0.477 \pm 0.0907$$

with a correlation coefficient $r = 0.452$.

The 99% significance levels for b_0 and b_1 are ± 23.35 and ± 0.1281 respectively. The variance analysis (Appendix A) yields:

$$s_e^2 = MSE = 314.491$$
$$s_{b_1}^2 = 0.0017$$
$$s_{b_0}^2 = 56.516$$

CTZ station 201:

Acoustical direction, and ship wind direction time series are showed in Figure 4.9. Figure 4.11 shows the combined direction time series that will not be used.

Ship Data:

The integral time calculation of the time between effectively independent samples, yields $\tau = 2.26$ days. With this integral time scale 14 effective degrees of freedom were obtained (from 545 correlated data points by the method explained above and in Appendix A).

A simple linear regression model $WD = b_0 + b_1 AD$ of acoustic direction (AD) against the wind direction (WD), both smoothed with a 13 hr moving average, yields the following coefficients at the 95% significance level with 14 effective degrees of freedom (Figure 4.15):

$$b_0 = 94.753 \pm 16.518$$
$$b_1 = 0.317 \pm 0.0872$$

with a correlation coefficient $r = 0.322$.

The 99% significance levels for b_0 and b_1 are ± 23.158 and ± 0.1222 respectively. The variance analysis (Appendix A) yields:

$$s_e^2 = MSE = 318.587$$
$$s_{b_1}^2 = 0.0016$$
$$s_{b_0}^2 = 57.462$$

Comments on the results of CTZ directions

From the extremely low correlation coefficients in all stations, it can be seen that a simple linear regression model does not explain the variability of this experiment. Hence there is no predictability capacity of the simple linear regression model in these two experiments.

At station 201, a simple linear regression model applied to the buoy data, yield a negative correlation, as well as a negative slope. At least the samples distribute close to the line of slope one (Figure 4.17).

Again it can be seen that the buoy information was not good for a simple linear regression model, probably due to the separation from the ADCP, and the proximity to the coast line. For further analysis the ship data set will be used.
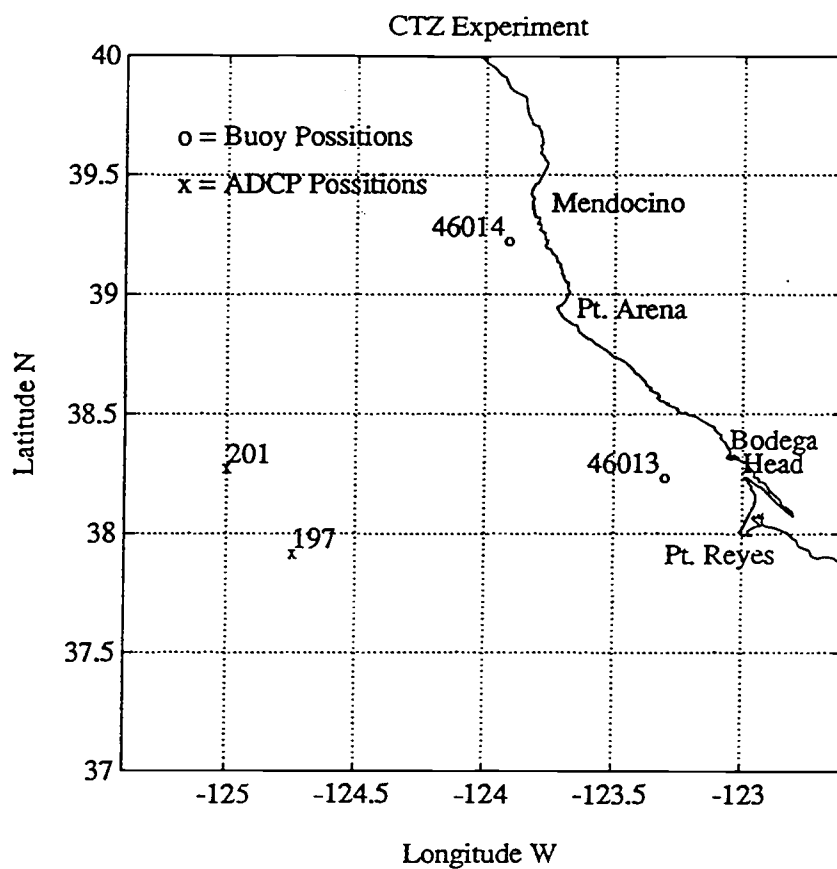
Figure 4.1   Location of ADCP serial numbers 197 and 201, about 91 nm off the coast of California. Map also shows the location of buoys 46014 at 10 nm off Mendocino, and 46014 at 20 nm off Bodega Head.
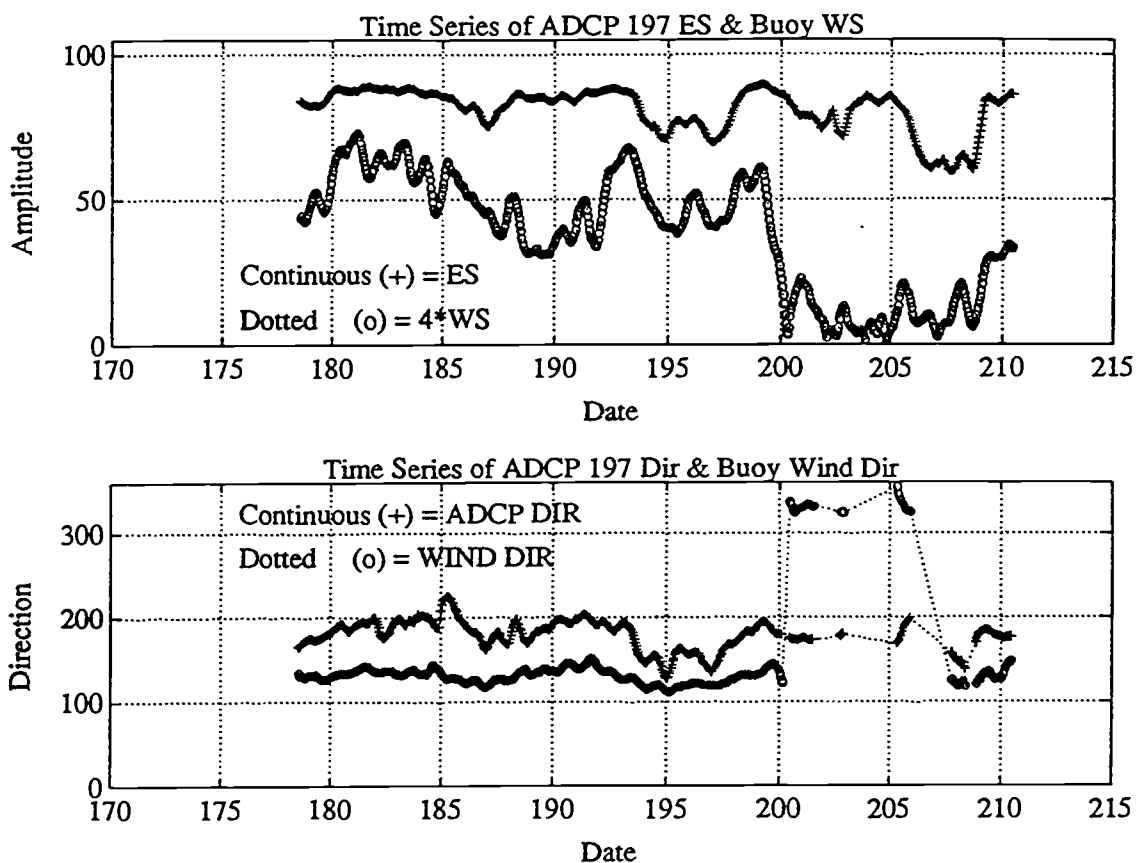
Figure 4.2   Station 197 time series of smoothed echo strength (ES), buoy
46013 wind speed (WS), acoustical direction (AD), and buoy
wind direction (WD), where ES, WS, AD, and WD have been
smoothed with a 13 hr moving average. Dates are in 1988 Julian
days. (late June and July)
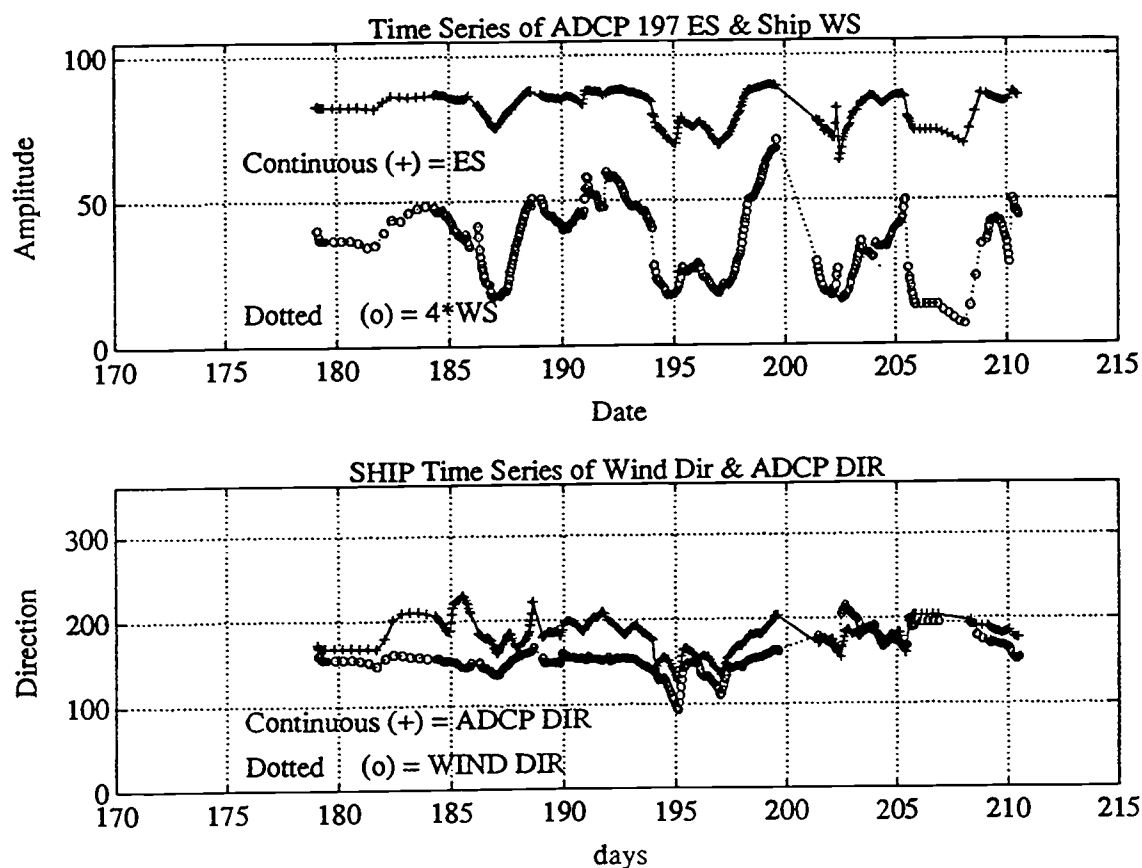
Figure 4.3   Station 197 time series of smoothed echo strength (ES), ship wind speed (WS), acoustical direction (AD), and ship wind direction (WD), where ES, WS, AD, and WD have been smoothed with a 13 hr moving average. Dates are in 1988 Julian days. (late June and July)
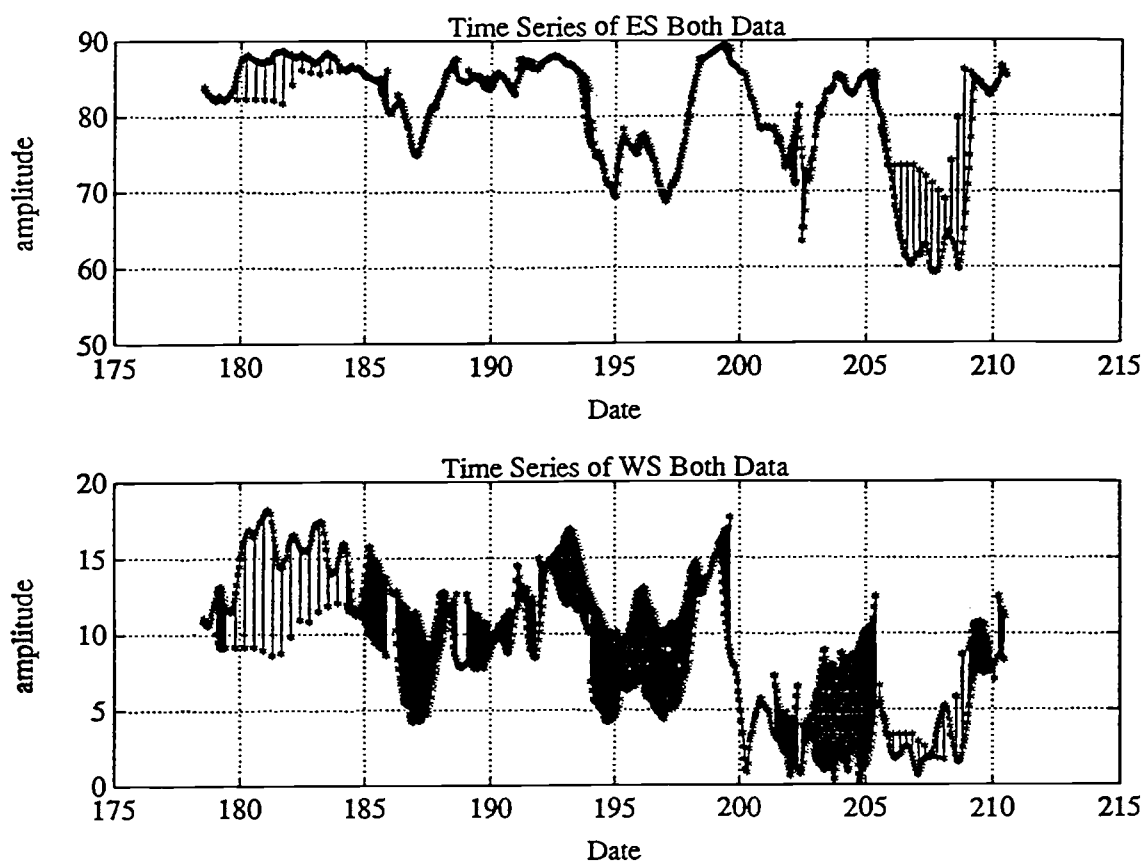
Figure 4.4   Station 197 time series of smoothed combined echo strength (ES) and wind speed (WS), where ES and WS have been smoothed with a 13 hr moving average. Notice the large off-set between both wind series, probably due to the great distance between ship and ADCP. Dates are in 1988 Julian days (late June and July).
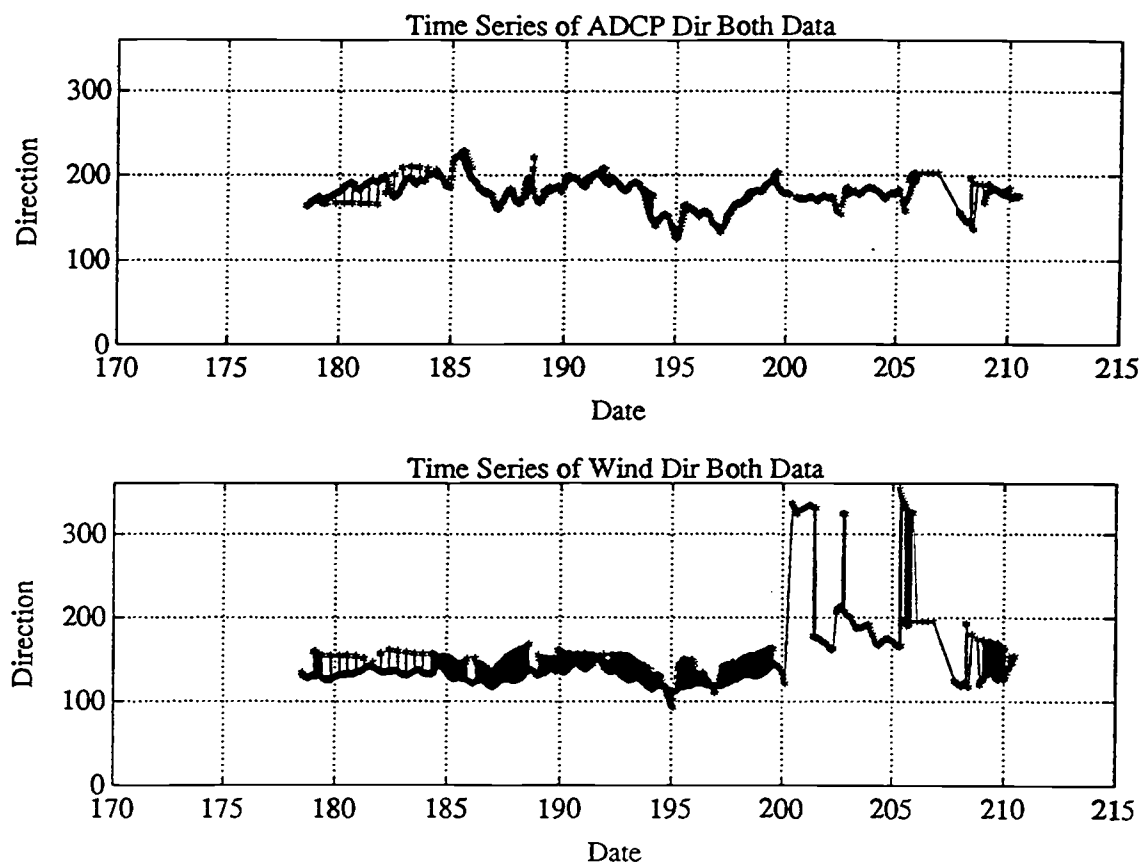
Figure 4.5   Station 197 time series of smoothed combined acoustical direction (AD) and wind direction (WD), where AD and WD have been smoothed with a 13 hr moving average. Notice the off-set between both wind series, probably due to the great distance between ship and ADCP. Dates are in 1988 Julian days (late June and July).

CTZ ADCP 197 ES v/s Ship LOG10(WS) Regression
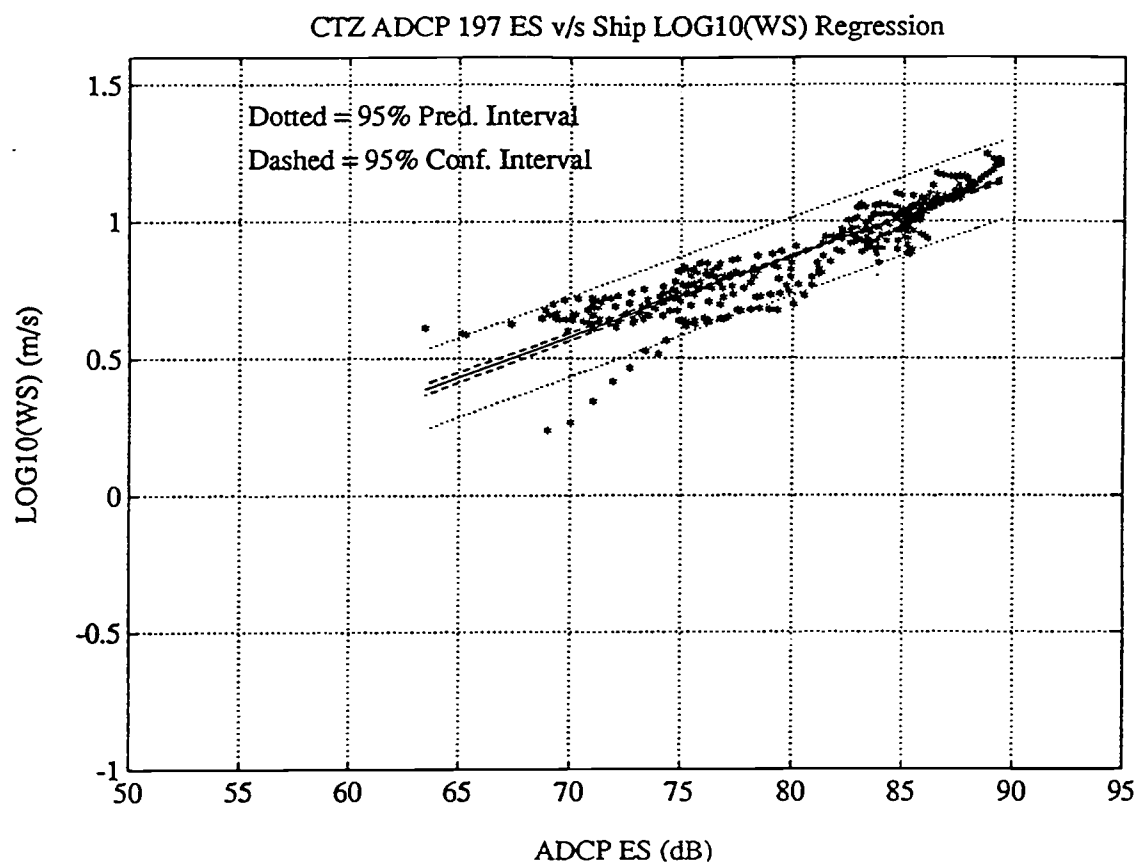
Figure 4.6 Station 197 ship data scatter plot of ES and LOG10(WS) with the ship-regression function, showing the 95% confidence and prediction intervals.
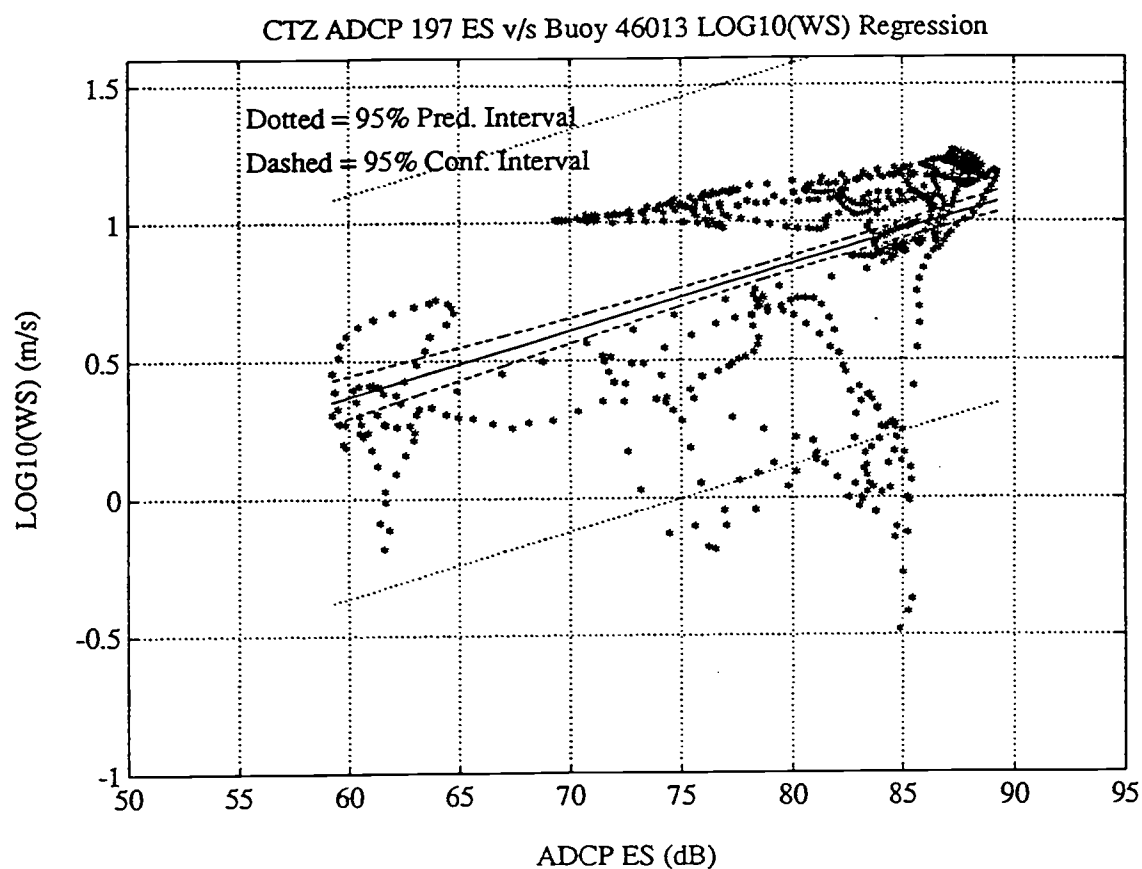
Figure 4.7   Station 197 buoy 46013 data scatter plot of ES and LOG10(WS) with the buoy-regression function, showing the 95% confidence and prediction intervals.
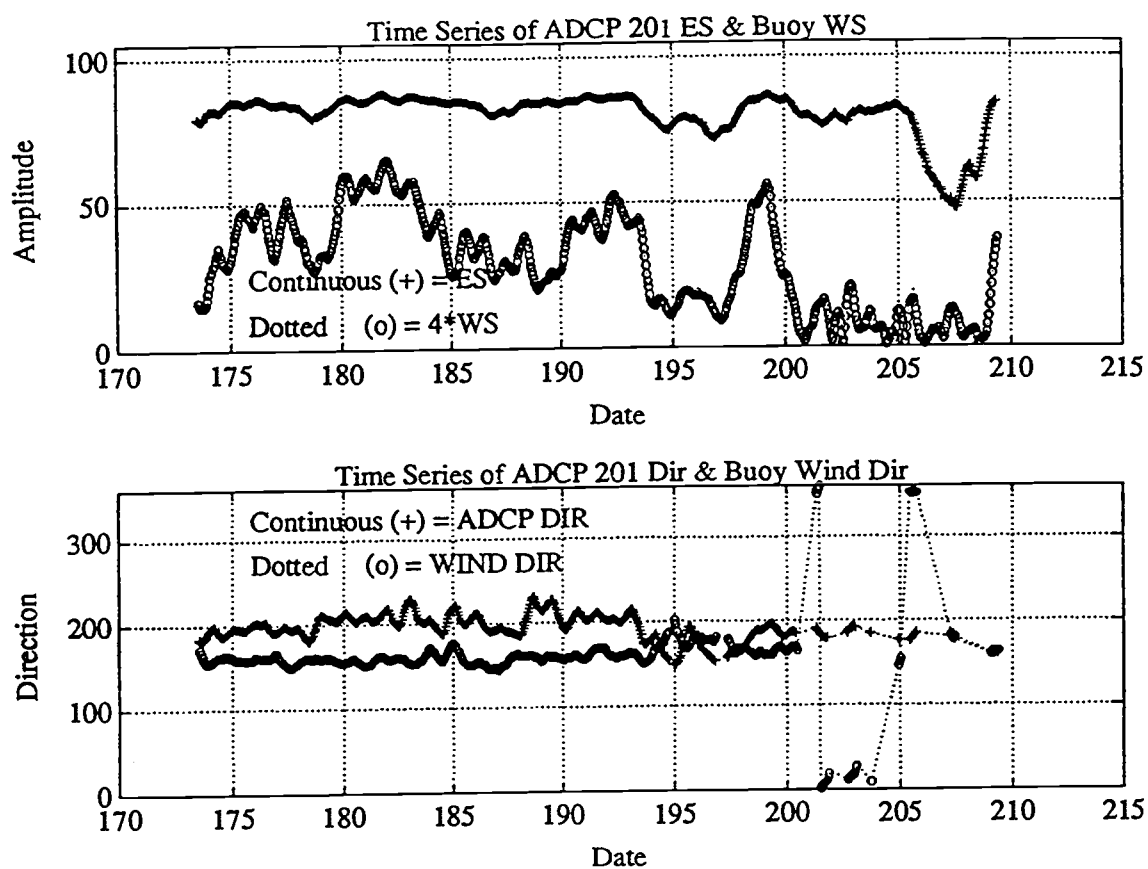
Figure 4.8   Station 201 time series of smoothed echo strength (ES), buoy 46014 wind speed (WS), acoustical direction (AD), and buoy wind direction (WD), where ES, WS, AD, and WD have been smoothed with a 13 hr moving average. Dates are in 1988 Julian days (late June and July).
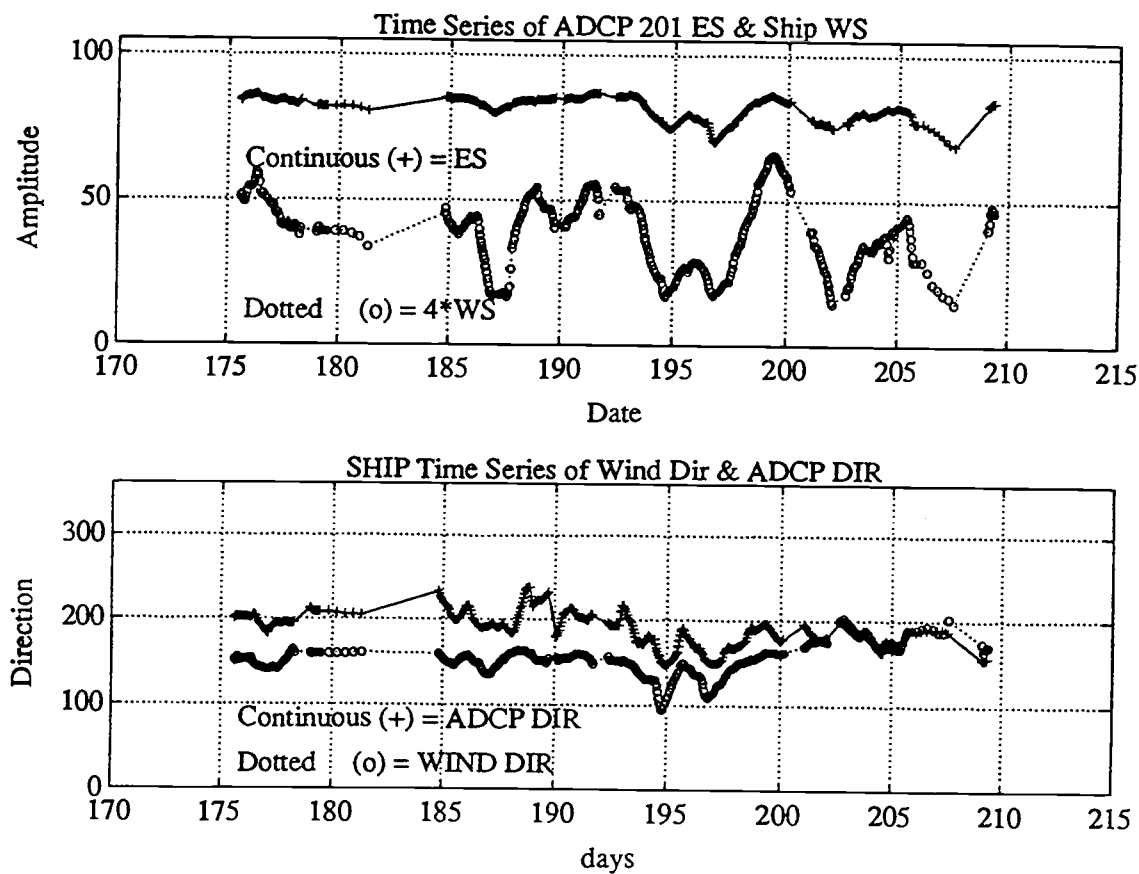
Figure 4.9   Station 201 time series of smoothed echo strength (ES), ship wind speed (WS), acoustical direction (AD), and ship wind direction (WD), where ES, WS, AD, and WD have been smoothed with a 13 hr moving average. Dates are in 1988 Julian days (late June and July).
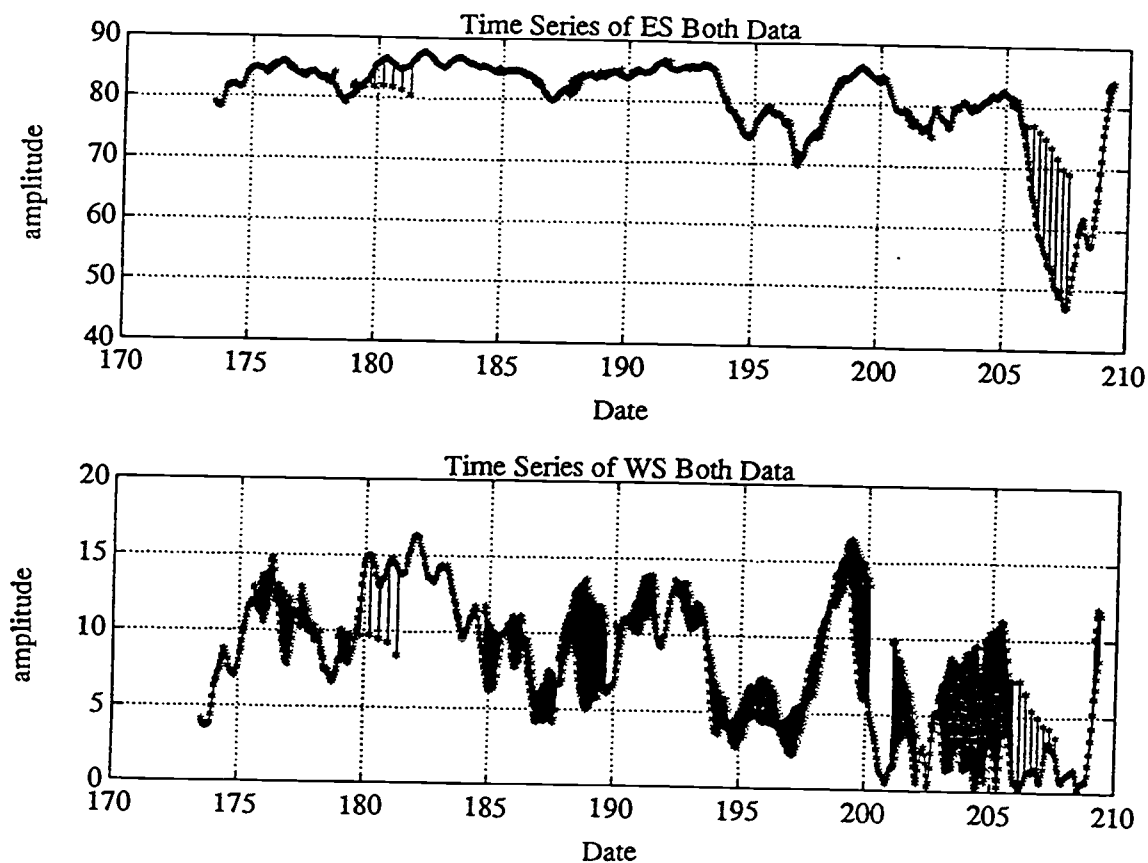
Figure 4.10 Station 201 time series of smoothed combined echo strength (ES) and wind speed (WS), where ES and WS have been smoothed with a 13 hr moving average. Notice the large off-set between both wind series, probably due to the great distance between ship and ADCP. Dates are in 1988 Julian days (late June and July).
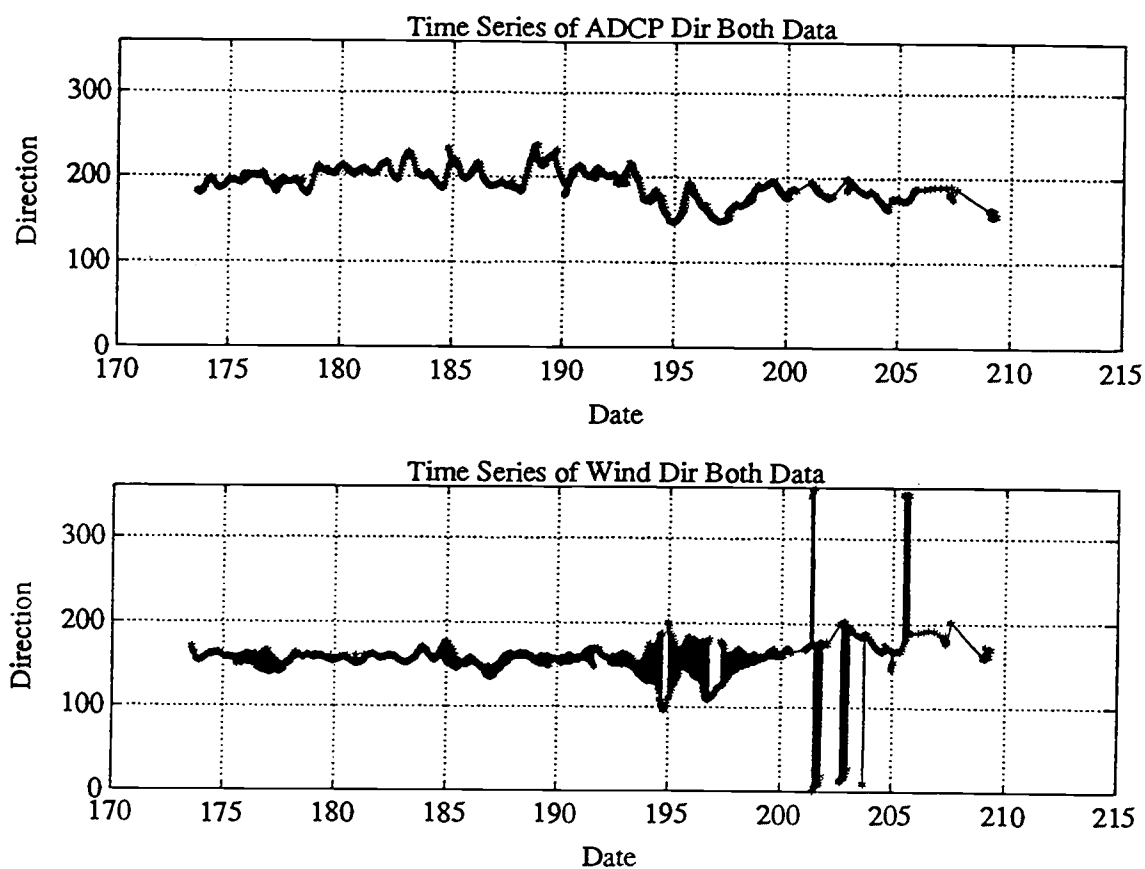
Figure 4.11 Station 201 time series of smoothed combined acoustical direction (AD) and wind direction (WD), where AD and WD have been smoothed with a 13 hr moving average. Notice the off-set between both wind series, probably due to the great distance between ship and ADCP. Dates are in 1988 Julian days (late June and July).
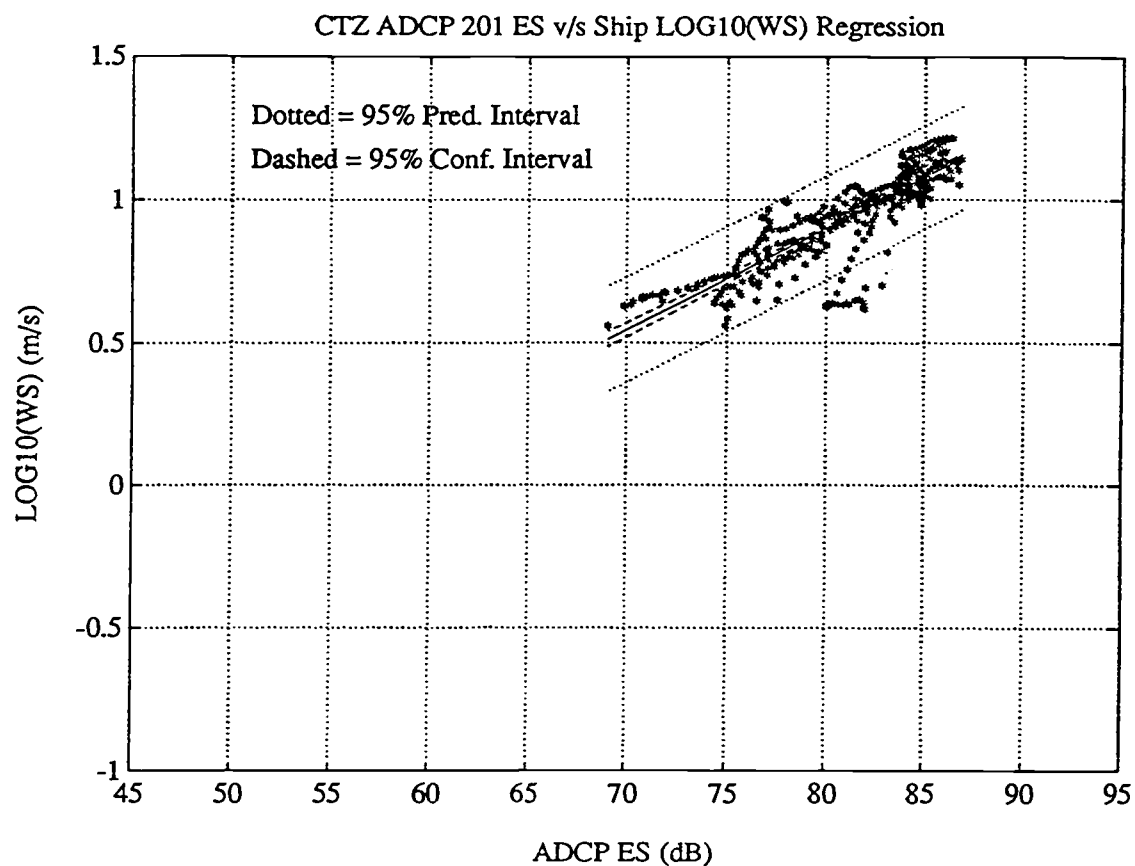
Figure 4.12 Station 201 ship data scatter plot of ES and LOG10(WS) with the ship-regression function, showing the 95% confidence and prediction intervals.
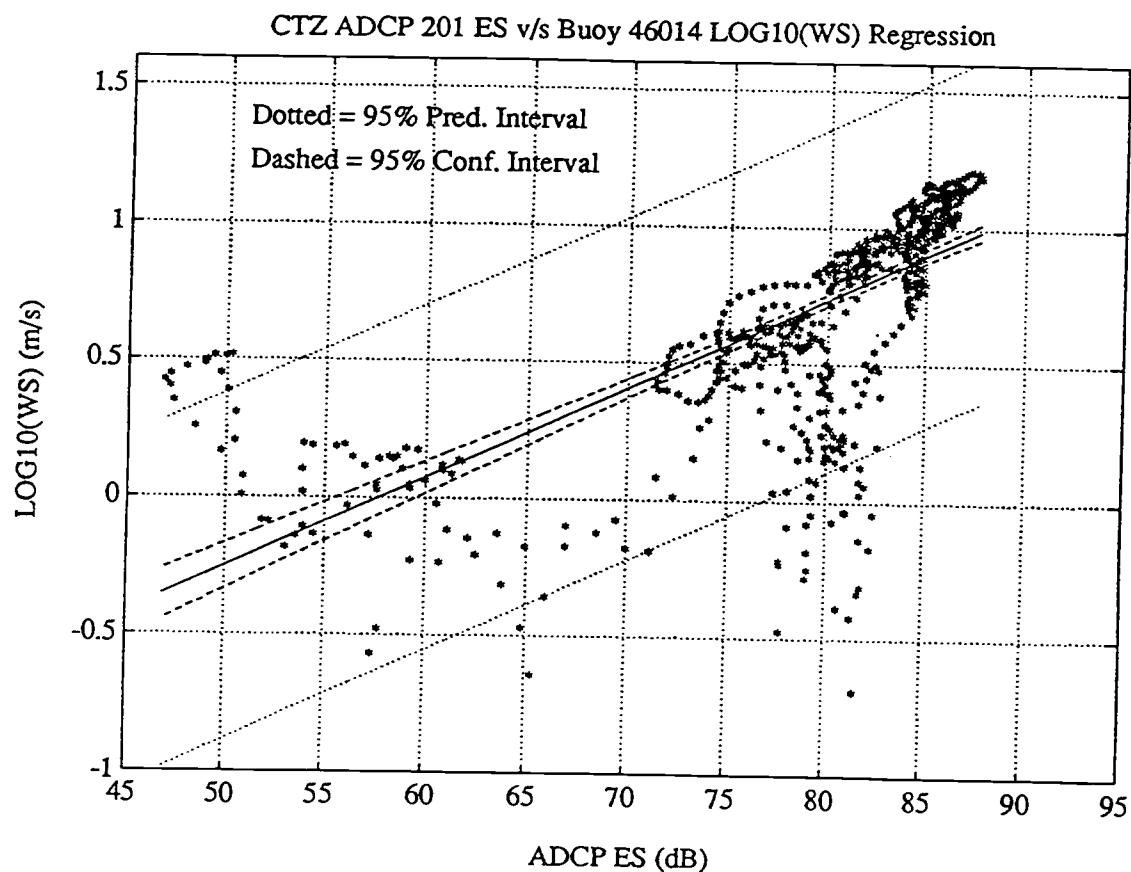
Figure 4.13   Station 201 buoy 46014 data scatter plot of ES and LOG10(WS) with the buoy-regression function, showing the 95% confidence and prediction intervals.
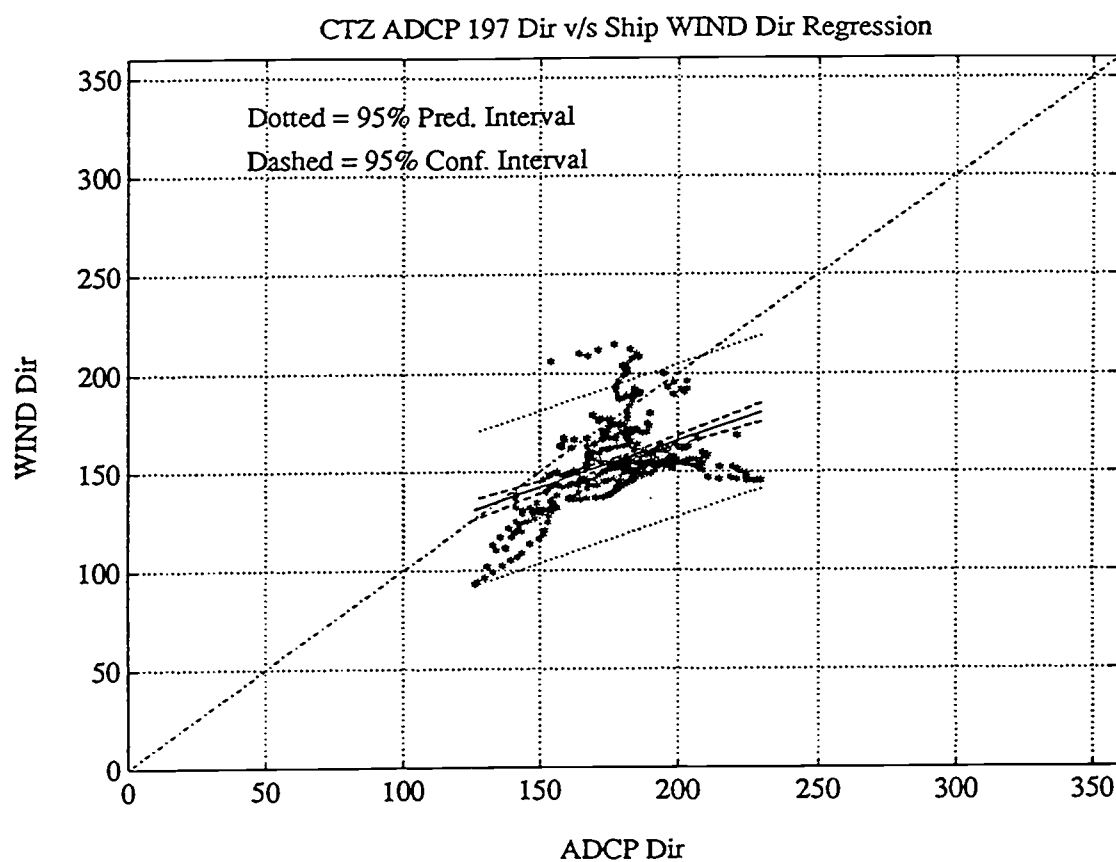
Figure 4.14 Station 197 ship direction scatter plot of AD and WD with the ship-regression function, showing very large 95% confidence and prediction intervals.
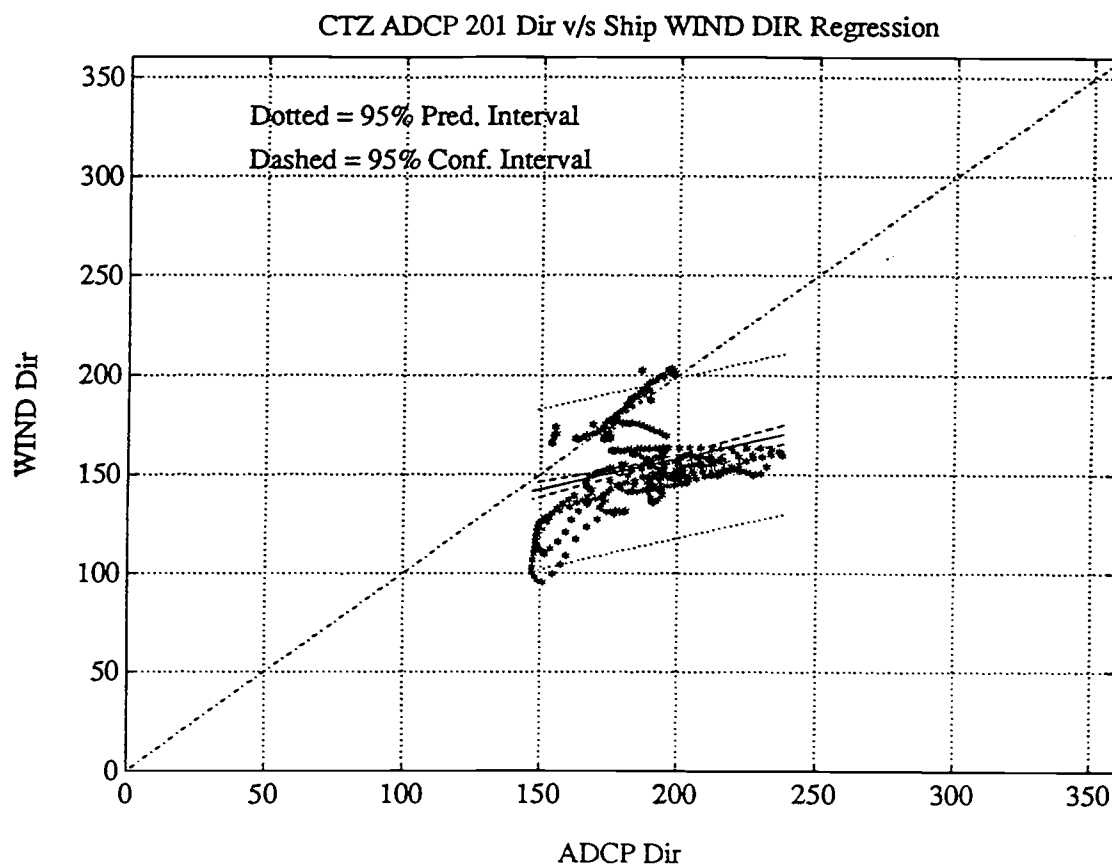
Figure 4.15 Station 201 ship direction scatter plot of AD and WD with the ship-regression function, showing very large 95% confidence and prediction intervals.

Chapter 5

Comparison, Discussion, and Conclusions

Comparison of the regression analysis results done at each site will be performed only to same instruments in different locations, since there were no *in situ* calibrations of any ADCP. The comparison will be made between results of ADCP 197 at Coos Bay and CTZ, and also between results of ADCP 201 at Mexico and CTZ. ADCP 209 was used only in the Mexico experiment, and gave a regression whose slope was considerably different from the other four cases, so only results for 197 and 201 are used for the following analysis.

The comparison of the regression results for Coos Bay and CTZ (done with ADCP 197) will be called the *197 results*. The comparison of the regression results for Mexico and CTZ (done with ADCP 201) will be called the *201 results*.

Comparison Criterion

It was necessary to define a procedure to test whether the two regressions under examination were similar or not. Since these regressions are simple, they have only two parameters that can be tested, namely the intercept and slope. From these two, the far most interesting is the slope, although both are required to get the correct wind prediction.

Recall that the intercept is defined as the value of the dependent variable when the independent variable reaches zero. From previous chapters it can be seen that the scope of the model almost never included the zero value (the *sole* exception was Coos Bay directions' time series). Hence, a zero value of the independent variable would imply a large extrapolation, where the predictability of the model is unknown. Also all acoustical data were corrected to 100 m reference depth by the transmission losses, which only account for spreading and absorption. There was no correction done for other processes that could change the backscatter energy, such as changes in biology density at each measurement site. Even more, there were no *in situ* calibration done to any ADCP. Therefore, based on the above, it will not be surprising that the intercepts were statistically different from each other.

As a summary of the regression results of previous chapters, table 5.1 shows a comparison of Coos Bay and CTZ intensities from the 197 results, table 5.2 shows the same comparison for directions. Table 5.3 shows a comparison of Mexico and CTZ intensities from the 201 results, and table 5.4 shows the same comparison for directions.

The slope coefficient at Mexico directions (Table 5.4) is attributed to casually (fortunate large outliers) relationship, rather than a true one to one acoustic direction to wind direction relationship.

Table 5.1 Comparison of intensity regression analysis results from Coos Bay and CTZ when ADCP 197 was used. Recall that all acoustic ES data were converted to a 100 m reference level. Where SL = significance level.

197 Intensities	Coos Bay (buoy data)	CTZ (ship data)
Corr. Coeff.	0.73	0.93
MSE	0.061	0.0045
Coeff b_1	0.031	0.029
Coeff b_0	-1.79	-1.47
95%$(SL)\beta_1$	0.0009	0.0034
95%$(SL)\beta_0$	0.063	0.088
Eff. deg. of freedom	142	17

Table 5.2 Comparison of direction regression analysis results from Coos Bay and CTZ when ADCP 197 was used. Where SL = significance level.

197 Directions	Coos Bay (buoy data)	CTZ (ship data)
Corr. Coeff.	0.92	0.45
MSE	1250.3	314.5
Coeff b_1	1.005	0.477
Coeff b_0	-7.5	70.6
95%$(SL)\beta_1$	0.0149	0.091
95%$(SL)\beta_0$	2.74	16.55
Eff. deg. of freedom	177	13

Figure 5.1 shows a scatter plot of the intensities of the 197 results. Notice how well the CTZ ship data (crosses) overlaps the Coos Bay buoy data (dots), and that both sets have similar shapes, though CTZ winds were higher than those at Coos Bay, hence they do not cover as large a dynamic range as Coos Bay does. A directions scatter plot of the 197 results is shown in Figure 5.2, notice the scope of each data set, *i.e.*, Coos Bay covers the whole 360° range, while CTZ goes roughly from 120 to 220, nevertheless there is still a fair overlap. CTZ acoustic data, though, are shifted slightly towards the right of Coos Bay observations, meaning that at CTZ (far from shore and deep waters) there is a

stronger tendency of the surface scatterers to move towards the right of the wind direction than it is at Coos Bay (close to shore and shallow waters). It seems that the large scope (dynamic range) of Coos Bay, gives the possibility to obtain a good slope coefficient ($b_1 = 1.005$, acoustic direction's standard deviation = 84.24°) in contrast to CTZ, where all measurements were confined to a 100° span around southern directions ($b_1 = 0.477$, acoustic direction's standard deviation = 18.8°). Making an analogy with the signal to noise ratio, used in engineering, this can be explained as the ratio of dynamic range (signal) to spreading of the wind direction at a given acoustic direction (noise), *i.e.*, the residuals' standard deviation. Thus there are two alternatives to increase the signal to noise ratio - either to lower the residuals' variance (which is not very likely to happen due to measurement errors, variability of the wind direction, variability of the acoustic direction, etc.), or to increase the dynamic range (what can be accomplish by selecting the right site to obtain measurements to develop the transfer function of the instrument). In order to quantify this, let us define the dynamic range (signal) of the independent variable as the mean plus minus one standard deviation, and the spreading of wind direction at a given acoustic direction (noise) as the standard deviation of the residuals. Then for Coos Bay 197 the signal to noise ratio is S/N = 4.77, for CTZ 197 ship S/N = 2.12, for CTZ 201 ship S/N = 2.14, and for Mexico 201 combined S/N = 0.79. A parabola was fitted to the first three S/N ratios against their respective slope coefficients, founding that in order to have slope coefficients greater than 0.95, the S/N ratio must be greater than 4.5. Mexico 201 was not included in the parabolic fitting, since it showed very strong outliers

Table 5.3 Comparison of Intensity regression analysis results from Mexico and CTZ when ADCP 201 was used. Recall that all acoustic ES data were converted to a 100 m reference level. Where SL = significance level.

201 Intensities	Mexico (combined)	CTZ (ship data)
Corr. Coeff.	0.94	0.85
MSE	0.017	0.007
Coeff b_1	0.03	0.035
Coeff b_0	-1.47	-1.94
95%(SL)β_1	0.003	0.002
95%(SL)β_0	0.21	0.164
Eff. deg. of freedom	10	18

Table 5.4 Comparison of Direction regression analysis results from Mexico and CTZ when ADCP 197 was used. Where SL = significance level.

201 Directions	Mexico (combined)	CTZ (ship data)
Corr. Coeff.	0.38	0.32
MSE	888.7	318.6
Coeff b_1	1.03	0.32
Coeff b_0	-19.5	94.8
$95\%(SL)\beta_1$	0.62	0.09
$95\%(SL)\beta_0$	127.8	16.5
Eff. deg. of freedom	18	14

Figure 5.3 shows a scatter plot of intensities of the 201 results. Notice that they overlap quite nicely. Again CTZ's winds were stronger than Mexico's (in average), on the other hand Mexico had a wider scope of the model (a desirable feature). Figure 5.4 shows a scatter plot of directions of the 201 results, notice that there is not an agreement of both data sets. However CTZ data again is shifted slightly toward the right of the Mexico's observations. It is very rare to have acoustic directions to the left of wind directions, on the contrary, acoustic direction measurements are usually larger than wind directions, meaning that they lay toward the right the wind direction. From Figures 5.2 and 5.4 a clear tendency is observed of the surface bin Doppler backscatter energy (from water particles or air bubbles) to move towards the right of the wind direction.

From an overlapping comparison of the sample parameter (b_0 and b_1) plus minus its significance level at a 95% confidence (table 5.5), it can be concluded that instrument 197 at Coos Bay produced statistically similar slope from the intensities' regression as CTZ ship data. However it produced statistically different intercepts. The directions' regressions were shown to have different slopes and intercepts (which was obvious from table 5.5). Instrument 201 at Mexico (combined data) produced almost statistically similar slope coefficients from the intensities' regression as CTZ ship data, and different intercepts with the same 95% confidence. The directions' regressions were shown to have different slopes and intercepts (which was obvious from table 5.5). A more sophisticated statistical test was applied (an hypothesis test procedure, via a partial F-test, using a multiple linear regression model to verify if the addition of new data from a second site changes the original parameters obtained from a first site data), which was found to be very sensitive to the confidence level chosen.

Table 5.5 Comparison of sample parameter (b_0 and b_1) plus minus its significance level at a 95% confidence from the 197 and 201 results for intensities and directions.

197 Intensities	Coos Bay	CTZ
Slope	0.031±0.0009	0.029±0.0034
Intercept	-1.79±0.063	-1.47±0.088
201 Intensities	**Mexico**	**CTZ**
Slope	0.030±0.003	0.035±0.002
Intercept	-1.47±0.21	-1.94±0.164
197 Directions	**Coos Bay**	**CTZ**
Slope	1.005±0.015	0.477±0.091
Intercept	-7.5±2.74	70.6±16.55
201 Directions	**Mexico**	**CTZ**
Slope	1.03±0.62	0.32±0.09
Intercept	-19.5±127.8	94.8±16.5

Discussion

The true coefficient β_1 from the regression analysis of intensities at Coos Bay, Mexico 201 and 209 (combined data), and CTZ 197 and 201 (ship data) was shown to be statistically different from zero with a 99% confidence. This also shows that the correlation coefficient is different from zero with the same confidence (only a 1% probability of making a type I error. See Appendix A). This result is important, since a correlation coefficient different from zero implies that a linear relationship between the independent and dependent variables of the regression equation explains some variability of the dependent variable. The amount explained is proportional to the coefficient of determination R^2. For the directions' time series, it was also shown that the true coefficients β_1 were statistically different from zero with a 99% confidence, at the same stations as for intensities (except at Mexico 209).

A common feature found in intensities' plots is the spreading of LOG10(WS) at low echo strengths, *i.e.*, at low wind speeds. This is clearly observable at Coos Bay (Figure 2.4), not very noticeable at Mexico 201 (Figure 3.8), and very clear at Mexico 209 (Figure 3.14). Since CTZ winds (from ship data) were strong, this feature is not observed

as clearly as above (Figures 4.6 and 4.12), but it is present when buoy data is used (Figures 4.7 and 4.13).

In this regard, it is not known what is the ADCP actually measuring at the surface bin (or in the whole shadow zone). Is it the backscatter energy of the bubbles' density, or is it the backscatter energy of the very ocean's surface?. Wu (1988) mentions that the bubble density in the ocean's surface is proportional to the wind speed at 10 m reference height to the power of 3.5. Hence at low wind speeds a very low density of bubbles is expected. Therefore in the situation of low wind speeds, it might be that the ADCP is being influenced by something other than bubbles, like by the surface wave pattern, as suggested by Schott (1989).

It is also noticeable that usually spreading occurs at echo strengths lower than about 75 dB which in Coos Bay implies wind speeds lower than 3.4 m/s (approximately 6.8 knots), and in Mexico 209 wind speeds lower than 3.5 m/s (approximately 7 knots). Notice the good agreement.

This study also found that the correlation of acoustic measurements with wind speed and with wind direction decreased rapidly away from the surface. Figure 5.5 (top) shows, for Coos Bay data, a graph of the correlation coefficient of wind speeds and counts at each bin as a function of bin number (which are proportional to depth, See Appendix B). Notice how fast the correlation decreases with depth, where bin 19 is the lower limit of the shadow zone, and bin 18 is the first bin outside it. The same quick decrease of correlation coefficient is found between acoustic direction and wind direction (Figure 5.5, bottom). To emphasize this point, Figure 5.6 shows, again for Coos Bay data, four scatter plots of wind direction versus acoustic direction of the surface bin 21; the bin at the lower limit of the shadow zone (bin 19); one bin below the shadow zone (bin 17); and a deeper bin 15. Clearly the surface bin represents the wind direction better than the rest of the deeper bins. The same conclusion applies to wind speed. Notice that the bin within the shadow zone still represents somewhat the wind direction, but as soon as it gets out of the shadow zone a wider spread is produced.

Piggott (1965) showed that there is a relationship between the wind speed and the ambient acoustic noise. He found that there was a 7.2 dB increase of ambient noise per wind speed double or that the ambient noise is approximately proportional to the square of the wind speed (actually to the power of 2.4). In light of this well-established relationship between the broad frequency band, passive acoustic noise and wind speed, it was postulated that a relationship between the backscatter energy of a strong active pulse - of narrow frequency band and limited duration - and the wind speed might exist. This study provides enough evidence to support the hypothesis that a relationship between active

backscatter energy and wind speed exists. In contrast to Piggott's study of passive ambient noise, the instruments used in this research, *i.e.*, ADCPs, generate strong active acoustic pulses of narrow frequency band and limited in duration, however a relationship between wind speed and the backscatter energy from these active pulses was found and it is presented as Table 5.6. This relationship between the active backscatter energy (BE) and the wind speed at 10 m height (U_{10}), has the form $BE \approx U_{10}^{\mu}$, where on average, at these ADCPs' operation frequency (300 kHz), $\mu \approx 3.23$, or the BE increases by 9.7 dB per wind speed doubling. However it was not possible to find a single relationship valid at every site. Notice that the exponent μ found in this study is higher than Piggott's value by 2.5 dB per wind speed doubling. Also notice the similarity of the relationship for Coos Bay and CTZ 197. Recall that these two sites were shown to have statistically similar slopes.

Table 5.6 Relationship between wind speed and backscatter energy produced by active acoustic short pulses of a narrow frequency band at 300 kHz, here "increase in dB" means the increase of active backscatter energy in decibels when the wind speed doubles, and "power exponent μ" is the exponent of the power law $BE \approx U_{10}^{\mu}$, where U_{10} is the wind speed in m/s at a 10 m reference level measured at each station, BE is the active backscatter energy from the surface bin, and μ is the power law's exponent.

Station	increase in dB	power exponent μ
Coos Bay (C-MAN)	9.7	3.24
CTZ 197 (ship data)	10.4	3.47
CTZ 201 (ship data)	8.6	2.87
Mexico 201 (combined)	10.0	3.34
Mean	9.68	3.23
Standard deviation	0.77	0.26

Schott (1989) found a strong agreement between wind direction and acoustic direction. Two ADCPs of different frequency were used (75 and 150 kHz); the intensities results from the 75 kHz ADCP are: intercept -0.08, slope 0.132, and correlation coefficient 0.85; and for the 150 kHz intercept -0.26, slope 0.076, and correlation coefficient 0.75. Notice that as the frequency is doubled, the slope coefficient is roughly

divided by two. It is remarkable that if the frequency is doubled once more and the slope coefficient reduced by half, we approximately get this study's intensities results, since here we only used 300 kHz ADCPs. This implies that the value of $\mu \approx 3.23$ would be valid only at a frequency of 300 kHz.

Brown *et al.* (1992) found a weaker relationship between the directions, in agreement, this study found that acoustic direction gave noisy estimates of wind direction.

To evaluate the wind speeds predicted by the regressions, wind speeds were computed from $WS = 10^{(b_0 + b_1 ES)}$ for Coos Bay 197, CTZ 197, CTZ 201, and Mexico 201, these values were plotted as Figures 5.7, 5.8, 5.9, and 5.10 respectively. Since the log-transformation produced relatively large outliers at low wind speeds, these outliers generated large standard deviations, which are responsible for the large prediction intervals in the Figures mentioned above. On the other hand, the method of least square estimates applied to the log model minimizes the mean square error of the LOG10(WS), not the wind speed's MSE.

In order to avoid the signal to noise ratio constraint, the slope coefficient of the directions' regression was forced to be one, and then the following model was computed: $WD = AD + \beta_0$, values of the sample intercept estimates for different locations are presented as table 5.7. This table shows that this model predicts wind direction with a rms error of 30 to 40 degrees.

By correcting for transmission losses and logarithmic wind profile, the data sets from different deployments (Figures 5.1 and 5.3) were made to overlap quite well.

Table 5.7: Values of the sample intercept estimate, b_0, for the model $WD = AD + \beta_0$, where the slope coefficient has been forced to the value of one, standard deviation of the intercept coefficient, and its root mean square (rms) error.

Experiment	b_0 rms error	Mean Value of b_0	b_0 standard deviation
Coos Bay 197	36.0	-6.6	35.4
CTZ 197	30.8	-23.2	20.3
CTZ 201	40.4	-33.9	22.1
Mexico 201	32.4	-13.8	29.5

Conclusions

As expected, a strong relationship was found between the active backscatter energy produced by the ADCP acoustic pulse and the wind speed at the surface bin. The relationship has the form $BE \approx U_{10}{}^{\mu}$, where, on average (at an ADCP frequency of 300 kHz), $\mu \approx 3.2$. However, this value is frequency dependent. Taking logarithms this can be expressed as an increase of active backscatter energy of about 9.7 dB per wind speed double. The mechanism that produces this process is not known.

ADCPs provide some skill in predicting wind speed. However it was not possible to find a single equation valid at every site.

A weak relationship was found between the acoustic direction and the wind direction. There is enough evidence to believe that a high signal to noise ratio (S/N) and a large record lengths are needed to obtain reliable relationships. With respect to record lengths, it was learned from Coos Bay that a six month record length produced a slope coefficient close to one, and from CTZ that a month of measurements with a low S/N still does not produce data with acceptable basic statistics. However, a wide dynamic range is perhaps even more important than the record length. Maybe a month of measurements at CTZ, but with a large S/N, would have produced a reliable predictor model.

There is a clear spreading of LOG10(WS) at wind speeds lower than 3.5 m/s (approximately 7 knots).

From the results of this study there is not enough evidence to identify what is the ADCP actually measuring at the surface bin. It is believed, though, that at high wind speeds the ADCP is measuring the backscatter energy from a high bubble density at the surface bin.

ADCP 197 produced statistically equivalent intensities' slope regression results at Coos Bay and Mexico. All other comparisons showed different intercepts and slopes. It is not clear if the lack of an *in situ* calibration produced this disagreement of results or if there are some other physical effects altering the results.

It was learned that wind measurements have to be measured close to the ADCP in order to build a prediction model and to use it. Also it was learned that coastal influences on meteorological data are strong enough to spoil the relationship with acoustic measurements, especially when instruments are apart from each other.

Figures 5.7 to 5.10 suggest that perhaps a non-linear regression analysis for intensities would produce a satisfactory fit. Recall that the assumption of equal residual's variance was violated with a simple linear regression model. However, notice that from

these Figures the residuals would be considerably more constant than those from the log model.

A multiple linear regression analysis with other predictors, like ocean currents should be tried for directions.

The model $WD = AD + \beta_0$, where the slope coefficient was forced to be one, predicts wind direction with a rms error of 30 to 40 degrees.

Future Work

Determine the mechanism that produces the active backscatter energy to increase with wind speed.

Validate the value of $\mu = 3.23 \pm 0.26$ from the relationship between active backscatter energy and wind speed, where 0.26 is a standard deviation.

Investigate the existence of an Ekman spiral (Ekman, 1905) using deeper bins at different stations. Mexico station may provide a good research area, since the onset of the northers is dramatic and then they persist for 3 to 5 days, providing a rough steady state, which is one of the assumption of Ekman's theory (Kundu, 1990).

Perform a non-linear regression analysis to the intensities' time series to verify if it produces a better fit. Perform a multiple linear regression including some other parameters like ocean currents, atmospheric pressure, sea water temperature, sea water density, and ADCP's pitch and roll.

Determine an *in situ* calibration procedure for ADCPs that would enable the possibility to make inter comparisons between different instruments at different locations.
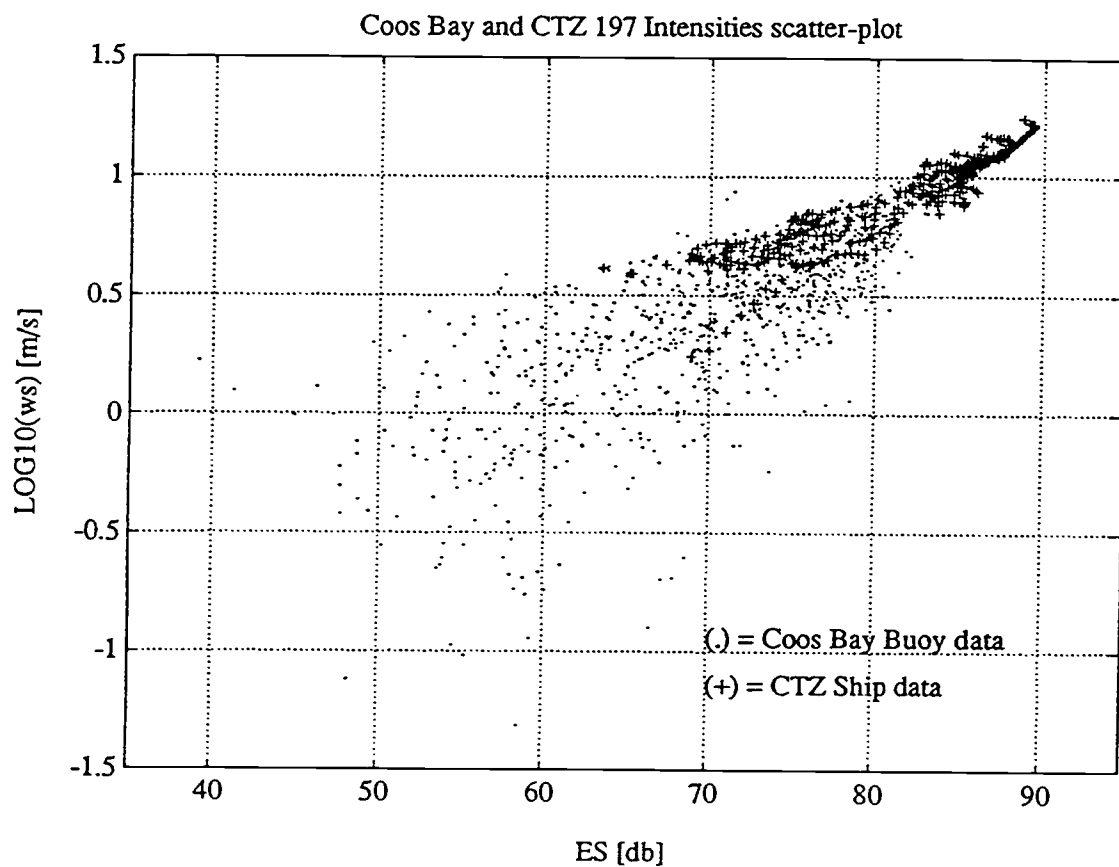
Figure 5.1   Scatter plot of CTZ ship data (crosses) and sampled Coos Bay (dots) intensities, when ADCP 197 was used. Coos Bay intensities were sampled every 5 hours, since its integral time scale was of 19.8 hours. Both ES were corrected to a 100 m reference depth.
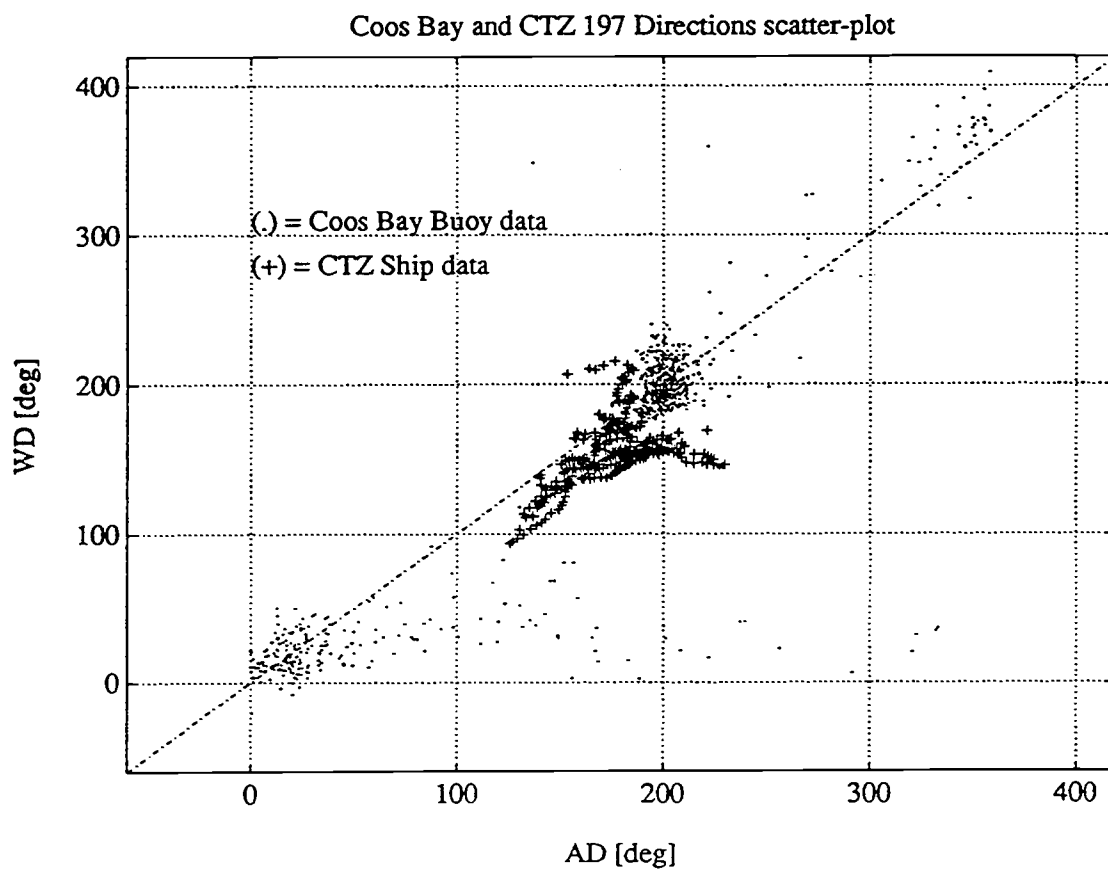
Figure 5.2   Scatter plot of CTZ ship data (crosses) and sampled Coos Bay
(dots) directions, when ADCP 197 was used. Coos Bay
directions were sampled every 4 hours, since its integral time
scale was of 12.1 hours.
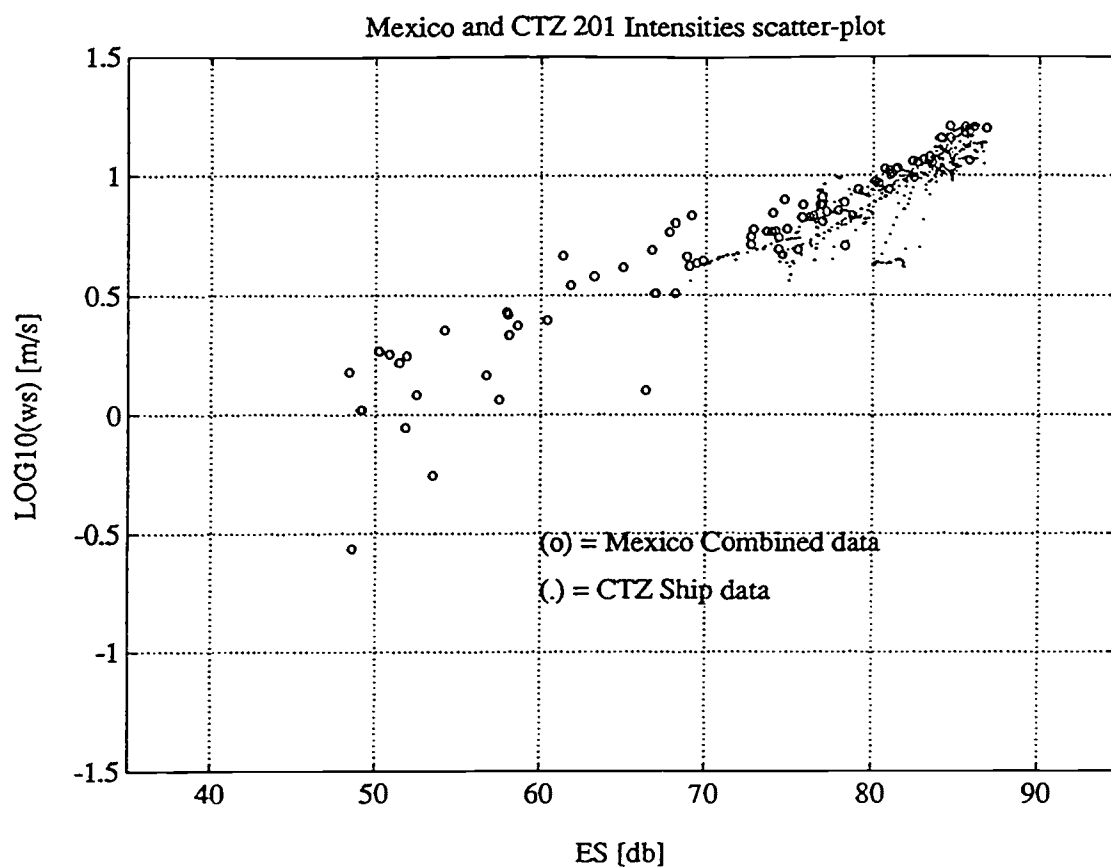
Figure 5.3   Scatter plot of CTZ ship data (dots) and Mexico combined data (circles) intensities, when ADCP 201 was used. Both ES were corrected to a 100 m reference depth.
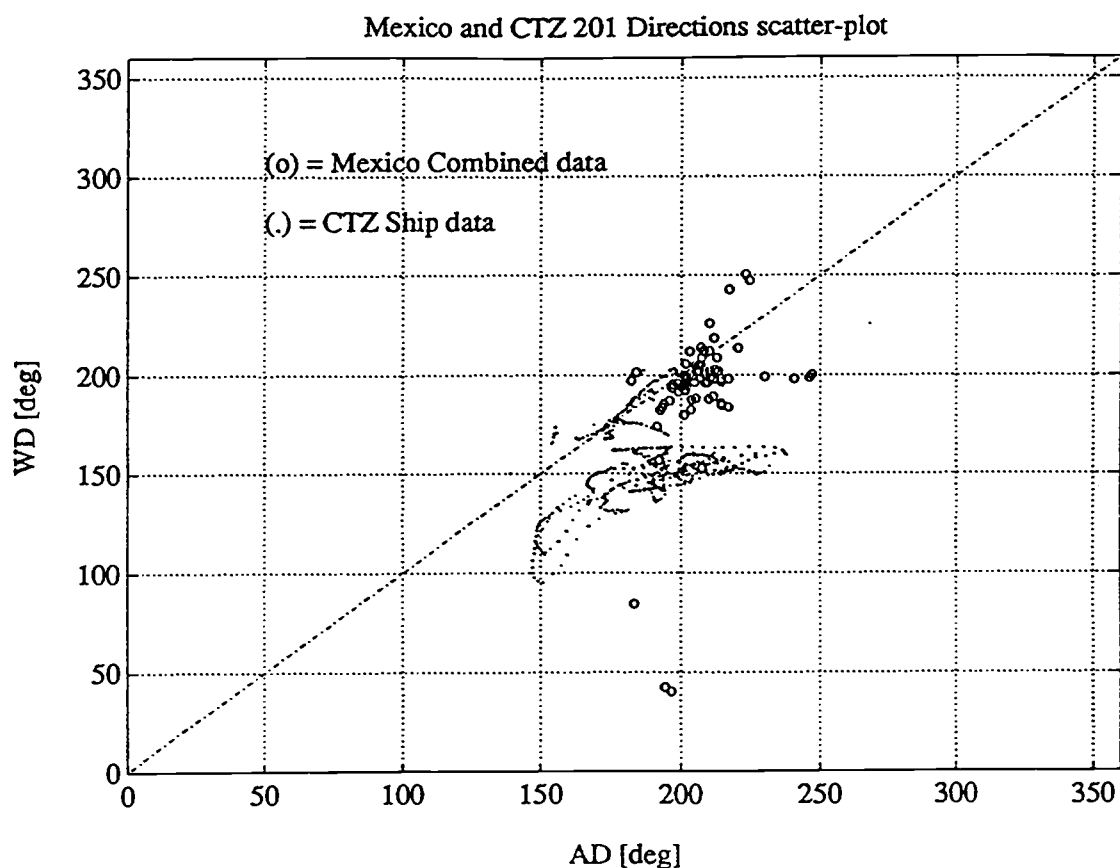
Figure 5.4   Scatter plot of CTZ ship data (dots) and Mexico combined data (circles) directions, when ADCP 201 was used. There is a tendency to observe acoustic directions larger than wind directions for a given observation, *i.e.*, water particles tend to move to the right of the wind.
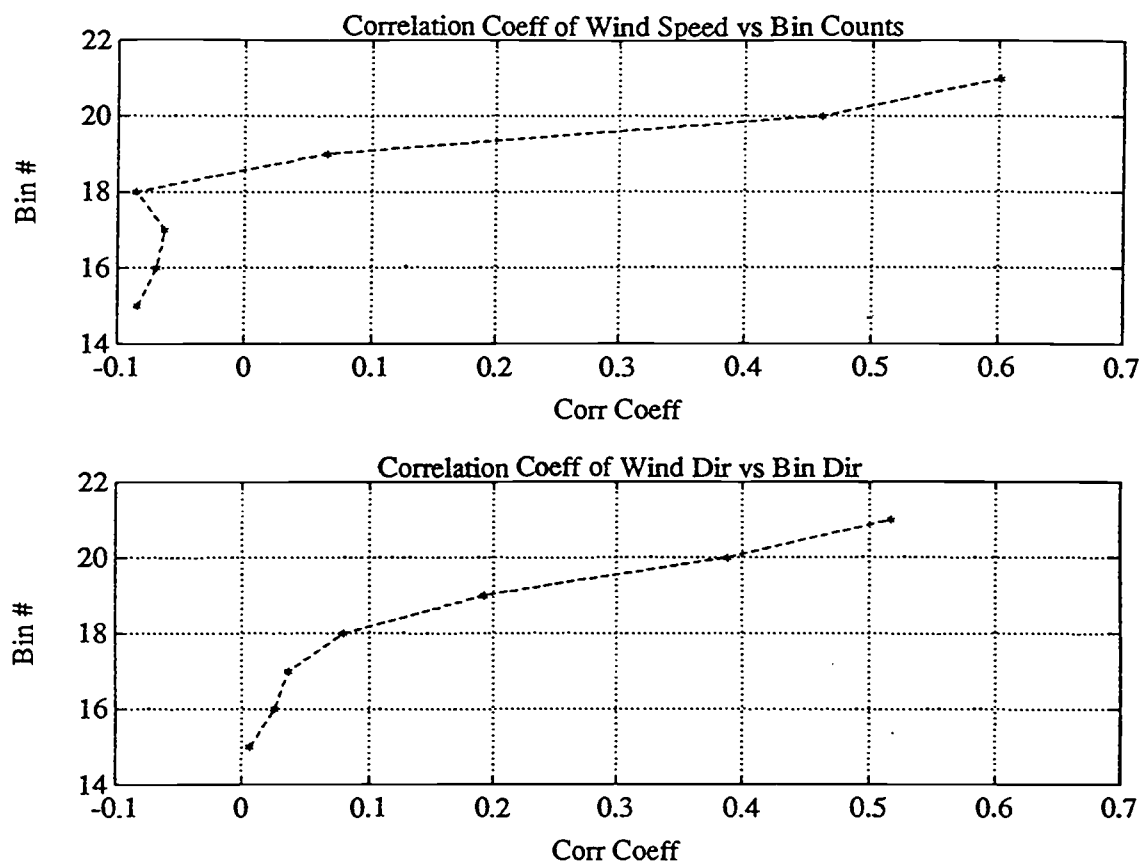
Figure 5.5 Plot of correlation coefficient of wind speed and ADCP bin counts versus bin number (top), and plot of correlation coefficient of wind direction versus bin number. Notice how quick the correlation decreases with depth. The shadow zone lower limit is at bin 19, bin 18 is the first bin outside the shadow zone.
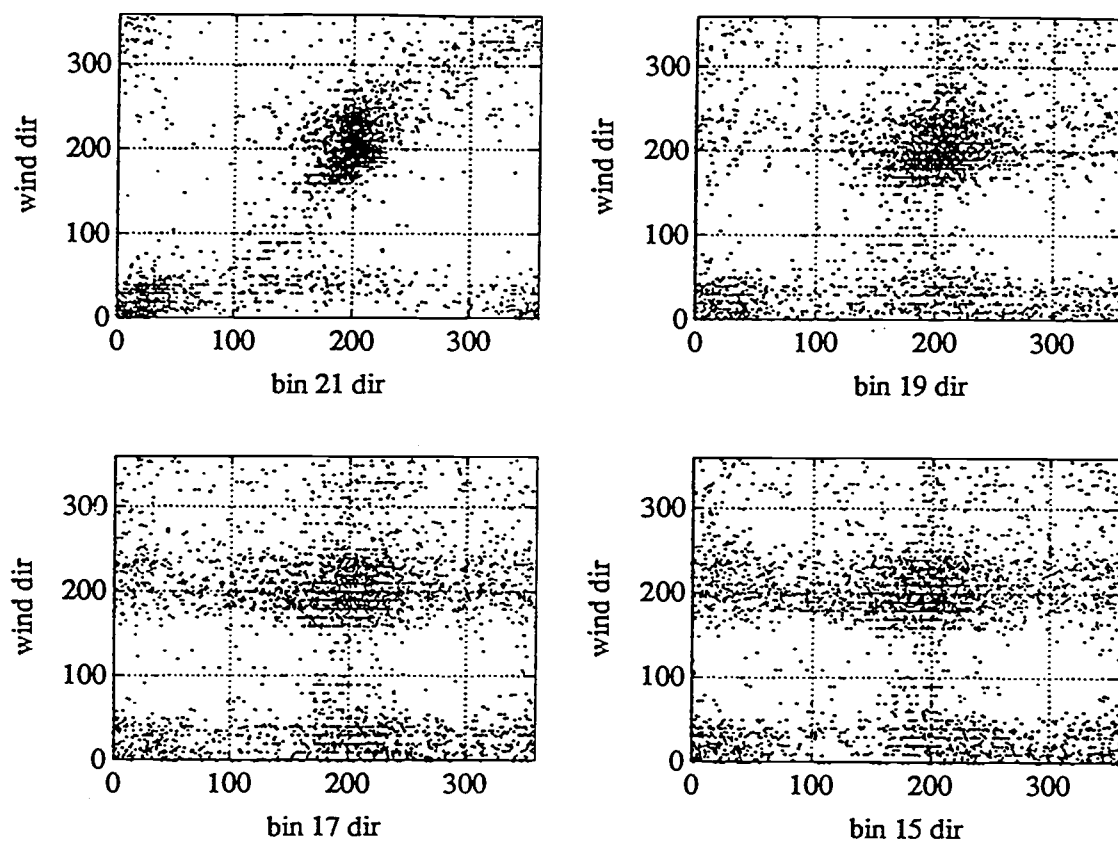
Figure 5.6   Scatter plots of wind direction versus bin 21 (at surface), bin 19 (lower limit of the shadow zone), bin 17 (one bin below the shadow zone), and a deeper bin 15. The surface bin explains the wind direction much better than the deeper bins.

Coos Bay ADCP 197 ES v/s C-MAN WS Regression

Dotted = 95% Pred. Interval
Dashed = 95% Conf. Interval
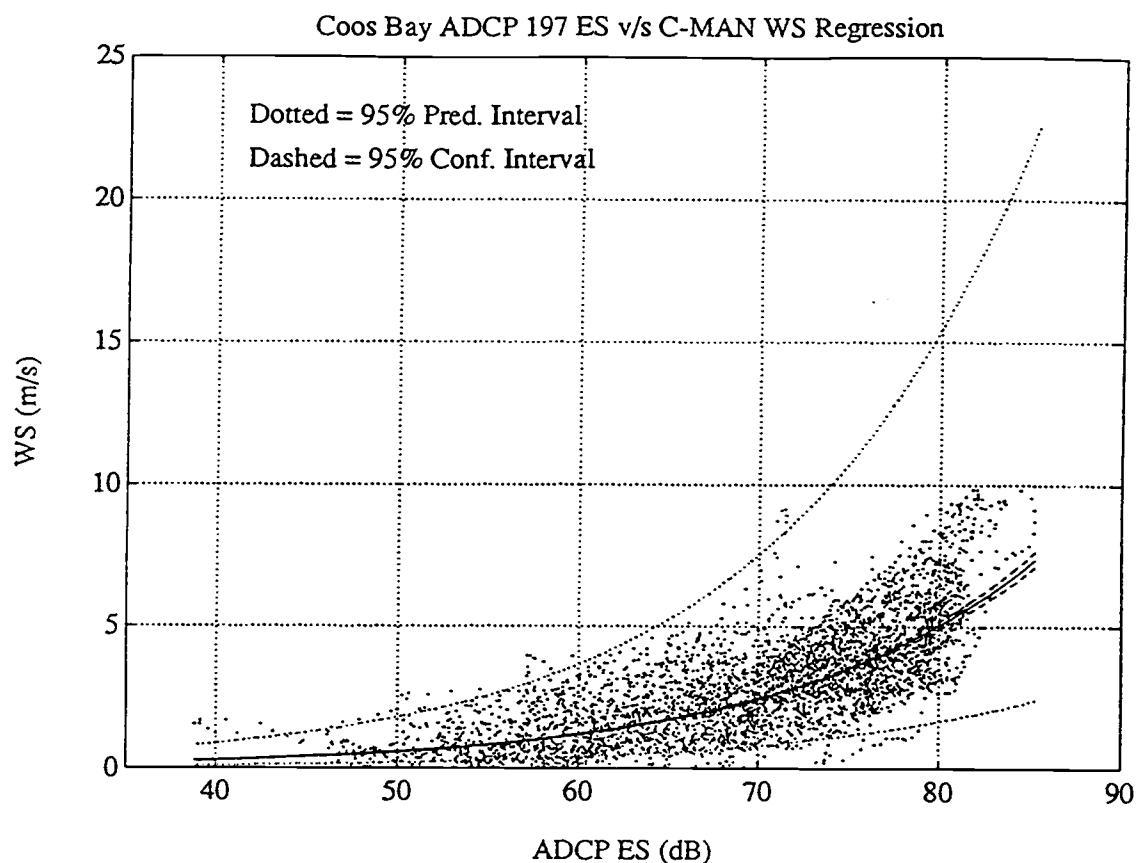
Figure 5.7   Scatter plot of wind speed (WS) and echo strength (ES) at Coos Bay 197, showing the anti-logarithmic transformation of the equation $LOG10(WS) = b_0 + b_1 ES$. The large prediction intervals are due to the large standard deviations produced by the log-model at low wind speeds.

CTZ ADCP 197 ES v/s Ship WS Regression
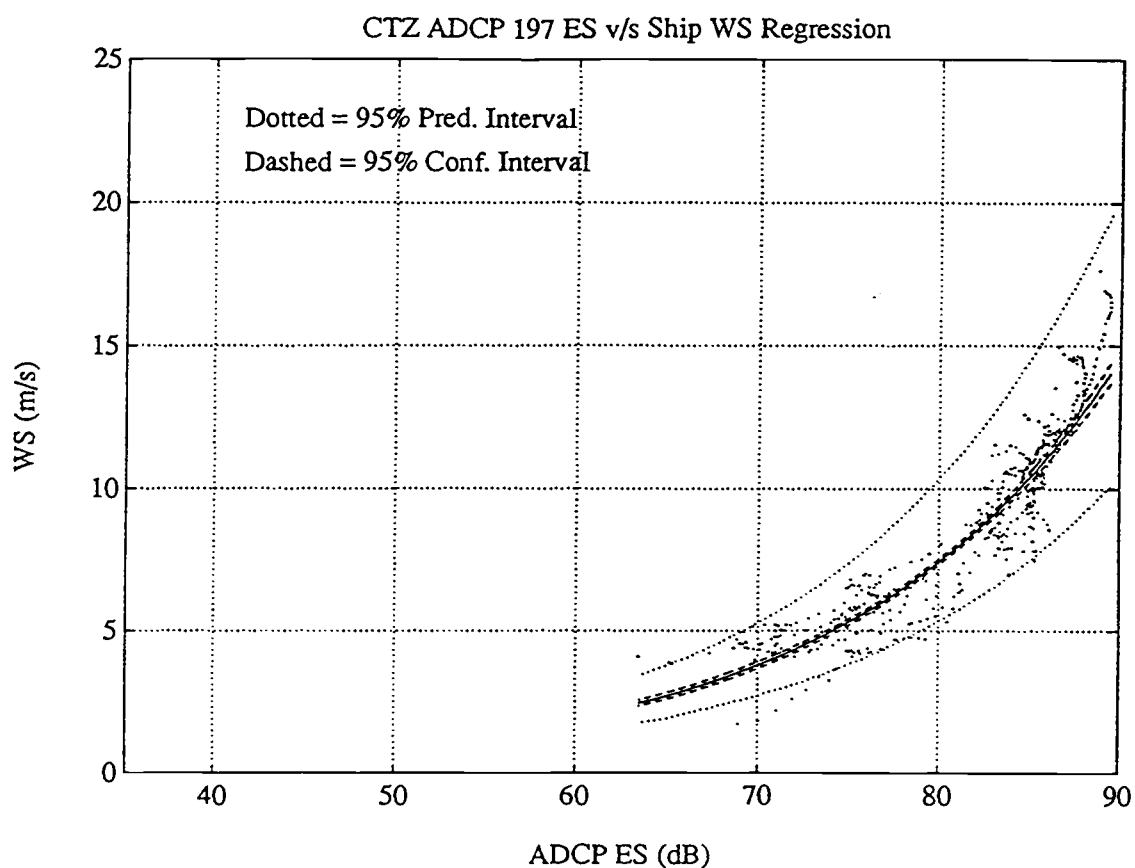
Figure 5.8   Scatter plot of wind speed (WS) and echo strength (ES) at CTZ 197, showing the anti-logarithmic transformation of the equation $LOG10(WS) = b_0 + b_1 ES$. The large prediction intervals are due to the large standard deviations produced by the log-model at low wind speeds.

CTZ ADCP 201 ES v/s Ship WS Regression
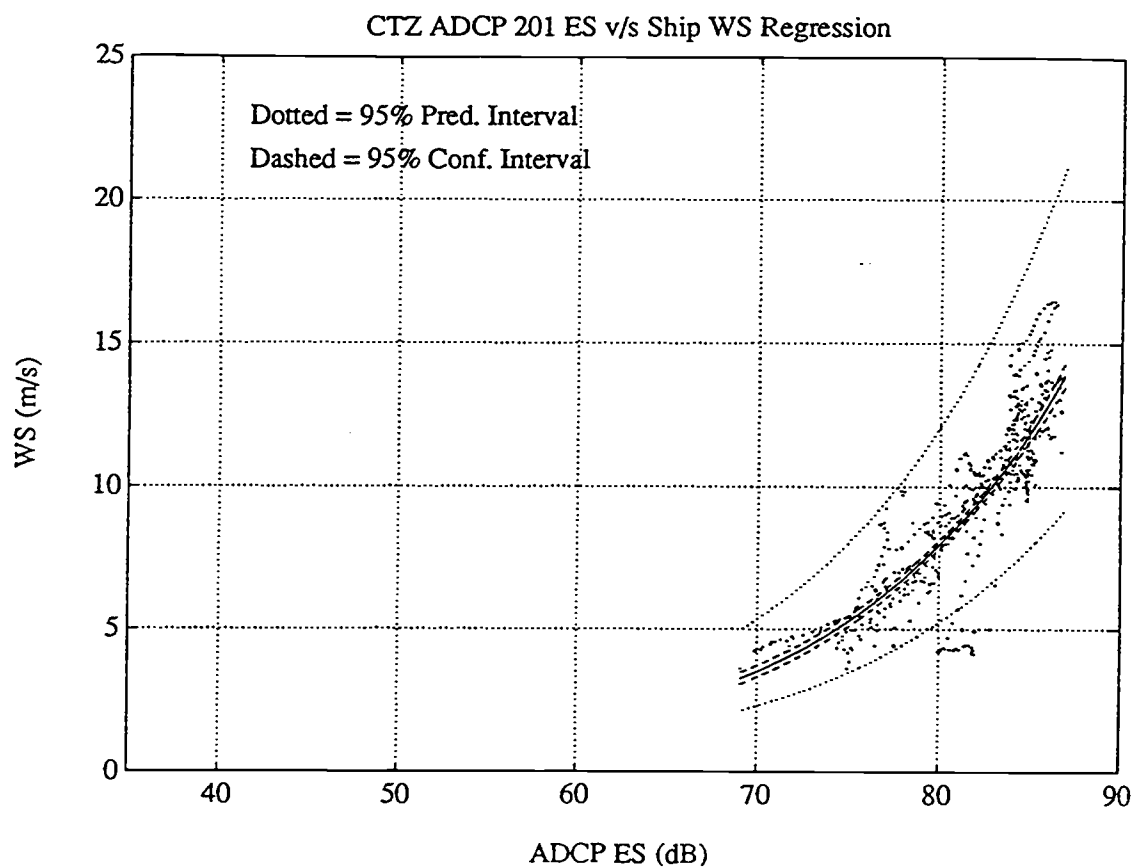
Figure 5.9 Scatter plot of wind speed (WS) and echo strength (ES) at CTZ 201, showing the anti-logarithmic transformation of the equation $LOG10(WS) = b_0 + b_1 ES$. The large prediction intervals are due to the large standard deviations produced by the log-model at low wind speeds.
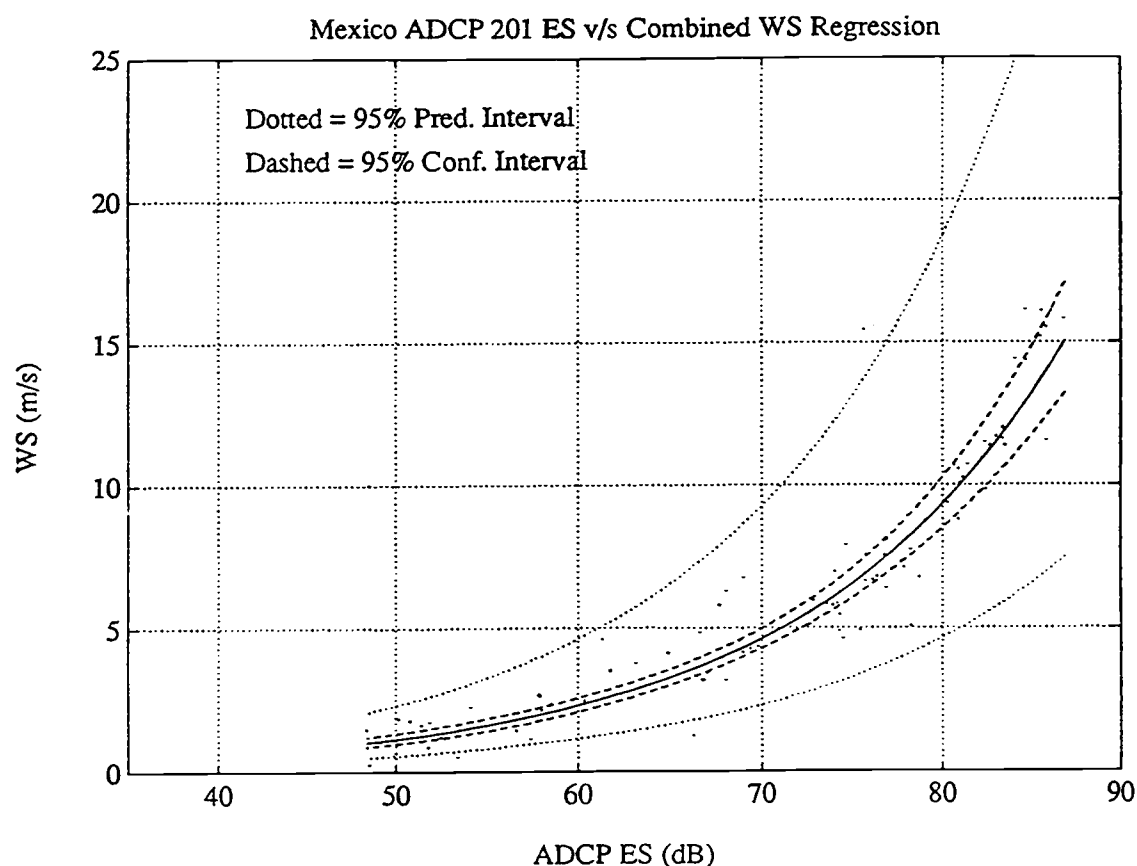
Figure 5.10 Scatter plot of wind speed (WS) and echo strength (ES) at Mexico 201, showing the anti-logarithmic transformation of the equation $LOG10(WS) = b_0 + b_1 ES$. The large prediction intervals are due to the large standard deviations produced by the log-model at low wind speeds.

Bibliography

Brown 1992:	Brown J., Barton E., Trasviña A., Velez H., Kosro P. & Smith R., Estimation of Surface Wind From Upward Looking Acoustic Doppler Current Profilers, Journal of Geophysical Research, Vol. 97 N° C11, pages 17925 to 17930
NDBC 1992:	National Data Buoy Center, Coastal-Marine Automated Network (C-MAN) User's Guide, U.S. Department of Commerce, National Oceanic and Atmospheric Administration, National Data Buoy Center, September 1992, 55 pages.
Chelton 1983:	Chelton D., Effects of sampling errors in statistical estimation, Deep-Sea Research, Vol. 30, pages 1083 to 1103.
Davis 1976:	Davis R., Predictability of Sea Surface Temperature and Sea Level Pressure Anomalies over the North Pacific Ocean, Journal of Physical Oceanography, Vol. 6, pages 249 to 266.
Ekman 1905:	Ekman Walfrid, On the Influence of the Earth's Rotation on Ocean-Currents, Arkiv for Matematik, Astronomi och Fysik, Band 2 N°11, pages 1 to 52.
Evans 1984:	Evans D., Watts D., Halpern D., & Bourassa S., Oceanic Winds Measured From the Seafloor, Journal of Geophysical Research, Vol. 89, pages 3457 to 3461.
Fofonoff 1969:	Fofonoff N. P., Spectral Characteristics of Internal Waves in the Ocean, Deep-Sea Research, Vol. 16, pages 58-71.
Heywood 1991:	Heywood Karen, Scrope-Howe S. & Barton E., Estimation of Zooplankton abundance from ship borne ADCP back-scatter, Deep-Sea Research, Vol. 38 N° 6, pages 667 to 691.
Huyer 1991:	Huyer A., Kosro M., Fleischbein J., Ramp S., Stanton T., Washburn L., Chavez F., Cowles T., Pierce S., and Smyth R., Currents and Water Masses of the Coastal Transition Zone off Northern California, June to August 1988, Journal of Geophysical Research, Vol. 96 C8, pages 14809 to 14831.
Hurd 1929:	Hurd W., Northers of the Gulf of Tehuantepec, Monthly Weather Review, Vol. 57, pages 192 to 194.
Kinsler 1962:	Kinsler Lawrence E. and Frey Austin R., Fundamentals of Acoustics 2nd Edition, John Wiley & Sons Inc., 524 pages.

Kinsman 1965:   Kinsman Blair, Wind Waves their generation and propagation on the ocean surface, Prentice-Hall Inc., 676 pages.

Kundu 1976:   Kundu Pijush & Allen John, Some Three-Dimensional Characteristics of Low-Frequency Current Fluctuations near the Oregon Coast, Journal of Physical Oceanography, Vol. 6 N° 2, pages 181-199.

Kundu 1990:   Kundu Pijush K., Fluid Mechanics, Academic press Inc., 638 pages.

Neter 1989:   Neter John, Wasserman William & Kutner Michael, Applied Linear Regression Models 2nd Edition, Richard Irwin Inc., 667 pages.

Ostle 1988:   Ostle Bernard & Malone Linda, Statistics in Research: Basic Concepts and Techniques for Research Workers 4th Edition, Iowa State University Press / Ames, 664 pages.

Parmenter 1985:   Parmenter Tish & Bailey Robert, The Oregon Oceanbook, Oregon Department of Land Conservation and Development, 85 pages.

Pettigrew 1983:   Pettigrew N. & Irish J., An evaluation of a bottom-mounted Doppler acoustic profiling current meter, IEEE proceedings of Oceans, Vol. 83, pages 182 to 186.

Piggott 1965:   Piggott C., Ambient Sea Noise at Low Frequencies in Shallow Waters of the Scocian Shelve, Journal of The Acoustical Society of America, Vol. 36, page 2152.

RD Instruments 1989: RD Instruments, Acoustic Doppler Current Profilers Principles of Operation: A Practical Primer, RD Instruments, 39 pages.

Schott 1989:   Schott F., Measuring Winds from Underneath the Ocean surface by Upward Looking ADCPs, Journal of Geophysical Research, Vol. 94 N° C6, pages 8313 to 8321.

Stull 1988:   Stull Roland B., An Introduction to Boundary Layer Meteorology, Kluwer Academic Publishers, 666 pages.

Urick 1983:   Urick Robert J., Principles of Underwater Sound 3dr Edition, McGraw-Hill Inc., 423 pages.

Vagle 1990:   Vagle S., Large W., & Farmer D., An Evaluation of the WOTAN Technique of Inferring Oceanic Winds from Underwater Ambient

Sound, Journal of Atmospheric and Oceanic Technology, Vol. 7, pages 576 to 595.

Wu 1988:   Wu J., Bubbles in the near-surface ocean: A general description. Journal of Geophysical Research, Vol. 93, pages 587 to 590.

APPENDICES

Appendix A

Statistics associated with
Simple Linear Regression

The purpose of this Appendix is to make a summary of the statistical principles used, mainly from Neter *et al.*, 1989 and Ostle and Malone, 1988, in order to facilitate the writing and understanding of the main chapters.

Regression analysis is a statistical tool that utilizes the relationship between two or more quantitative variables so that one variable can be predicted from the others. In the case of a simple regression, a single predictor is used for predicting the variable of interest, and linear regression means that the coefficients used in the regression are constant.

The Model

Consider the situation involving one independent variable and a linear regression relationship. The model can be stated as follows:

$$y_i = \beta_0 + \beta_1 x_i + \varepsilon_i$$

where:

y_i : value of the response in the i-th trial

β_0, β_1 : unknown parameters

x_i : value of predictor (independent variable) in the i-th trial

ε_i : random error terms, with:

    i) $E[\varepsilon_i] = 0$, *i.e.*, the expected value of the random error terms

    ii) $VAR[\varepsilon_i] = \sigma^2$, for all i, (i.e. same constant variance for all ε_i), and

    iii) ε_i are statistically uncorrelated, *i.e.*, $E[\varepsilon_i \varepsilon_j] = 0$ for $i \neq j$.

Let us define $\eta = E[y_i] = \beta_0 + \beta_1 x_i$, which is known as the regression function, so that it can be written:

$$y_i = \beta_0 + \beta_1 x_i + \varepsilon_i = E[y_i] + \varepsilon_i = \eta + \varepsilon_i$$

Least Squares Estimates

Using the method of least squares, b_0 and b_1 are the estimates of the parameters β_0 and β_1 respectively, which can be found as follows:

- Minimize $Q = \sum_i \varepsilon_i^2$, by solving the basic equations $\dfrac{\partial Q}{\partial \beta_0} = 0$ and $\dfrac{\partial Q}{\partial \beta_1} = 0$ for β_0 and β_1.

- Define:

$$Sxx = \sum (x_i - \bar{x})^2$$
$$Syy = \sum (y_i - \bar{y})^2$$
$$Sxy = \sum (x_i - \bar{x})(y_i - \bar{y})$$

where:
$\bar{x}$ = is the mean value of all x_i and $\bar{y}$ = is the mean value of all y_i.

- Then:

$$b_1 = \frac{Sxy}{Sxx} \qquad \text{and} \qquad b_0 = \bar{y} - b_1 \bar{x}$$

give the calculated sample parameter estimates of the regression function, $\eta = E[y] = \beta_0 + \beta_1 x$.

- The estimate of the regression equation (line) is given by:

$$\hat{y}_i = b_0 + b_1 x_i$$

- Define the **residuals** as:

$$e_i = y_i - (b_0 + b_1 x_i) = y_i - \hat{y}_i$$

In contrast to the random error terms that are defined as:

$$\varepsilon_i = y_i - (\beta_0 + \beta_1 x_i)$$

Analysis of Variance Applied to a Simple Linear Regression

Since the true error variance, σ^2, is unknown, the sample error variance must be used instead:

$$s_e^2 = \frac{\sum e_i^2}{n-2} = \frac{\sum (y_i - \hat{y}_i)^2}{n-2}$$

which is also known as the mean square error or MSE.

An additional assumption about the random error terms has to be added, to make inferences in simple linear regression, namely the random error terms ε_i's are assumed to have a normal distribution for all i. With this new assumption, uncorrelated variables became independent variables, which allows the following inferences:

Inferences for β_1

Variance of b_1: $\sigma^2[b_1] = \dfrac{\sigma_e^{\,2}}{Sxx}$ estimated by

Sample Variance of b_1: $s_{b_1}^{\,2} = \dfrac{s_e^{\,2}}{Sxx}$

Inferences for β_0

Variance of b_0: $\sigma^2[b_0] = \sigma_e^{\,2}(\dfrac{1}{n} + \dfrac{(\overline{x})^2}{Sxx})$ estimated by

Sample Variance of b_0: $s_{b_0} = s_e^{\,2}(\dfrac{1}{n} + \dfrac{(\overline{x})^2}{Sxx})$

Inferences for the model $y = \beta_0 + \beta_1 x + \varepsilon$ when used as a predictor of $\eta = E[y]$

Variance of $\hat{y}_\eta$: $\sigma^2[\hat{y}_\eta] = \sigma_e^{\,2}(\dfrac{1}{n} + \dfrac{(x_h - \overline{x})^2}{Sxx})$ estimated by

Sample Variance of $\hat{y}_\eta$: $s_{\hat{y}_\eta}^{\,2} = s_e^{\,2}(\dfrac{1}{n} + \dfrac{(x_h - \overline{x})^2}{Sxx})$

$s_{\hat{y}_\eta}^{\,2}$ is the sample variance of $\hat{y}$, when used as an estimate of $\eta = E[y] = \beta_0 + \beta_1 x$, the expected value of y at $x = x_h$. Notice that η at $x = x_h$ is a fixed number, not a random variable.

Prediction of a New Observation

In addition to use the regression (the value of $\hat{y}$) as an estimate of the mean of y at $x = x_h$, it is often used as an estimate of the predicted random variable y. In this situation - prediction of a random variable instead of a mean value - one must allow variability due to the unknown random error term ε. Notice that when estimating the mean value of y, this random error was canceled out by the assumption i), $E[\varepsilon_i] = 0$. The added variability shows up as an increase in the estimated variance of $\hat{y}$, which when used as an estimate of the predicted random variable of y at $x = x_h$, is:

$$s_{\hat{y}_h}^{\,2} = s_e^{\,2}(1 + \dfrac{1}{n} + \dfrac{(x_h - \overline{x})^2}{Sxx})$$

Let us consider the prediction of a new observation Y corresponding to a given level X of the independent variable: the new observation on Y is viewed as the result of a new trial, independent of the trials on which the regression analysis is based. The level of X for the new trial shall be denoted as x_h, and the new observation on Y as $y_{h(new)}$.

The distinction between the estimation of the mean response, $E[y_h]$, and the prediction of a new response, $y_{h(new)}$, is that in the former case, the mean of the distribution of Y is estimated. In the present case, an individual outcome drawn from the distribution of Y is predicted. Of course, the majority of individual outcomes deviate from the mean response, and this must be allowed for in the procedure of predicting $y_{h(new)}$.

There are two probability distributions of Y, corresponding to the upper and lower limits of a confidence interval for $E[y_h]$. In other words, the distribution of Y could be located as far left as the left-most boundary point of the confidence interval, as far right as the right-most boundary point of the same confidence interval, or anywhere in between. Since we do not know the true mean $E[y_h]$, and only estimate it by a confidence interval, the location of the distribution of Y is not certain, hence prediction limits for $y_{h(new)}$ clearly must take into account two elements:

i) Variation in possible location of the distribution of Y.
ii) Variation within the probability distribution of Y.

Estimation in Simple Linear Regression

As stated before, to provide more than just point estimates, the normality assumption of ε_i is needed. Hence ε_i's are assumed to be normal independent random variables with $E[\varepsilon] = 0$ and a constant variance. In other words, it is assumed that a given x_i, y_i is a normal random variable with $E[y_i] = \beta_0 + \beta_1 x_i$ and $VAR[y_i] = \sigma_e^2$. With the added assumption of the normality of the random error terms, b_0, b_1 and $\hat{y}$ are normal random variables with means β_0, β_1 and η respectively, and variances as given above.

In most linear regression problems the parameter of greatest importance the slope coefficient β_1. Of course, b_1 is a point estimate of the slope of the fitted line. Let us define $\gamma = 1 - \alpha$, where α is the probability of a Type I error. (See Appendix end for an explanation of Error Types). Then a 100γ % Confidence Interval for β_1 is given by the limits:

$$(L, U) = b_1 \pm t_{[(1+\gamma)/2], (n-2)} s_{b_1}$$

For the intercept β_0, b_0 provides a point estimate, and the 100γ% Confidence Interval for β_0 is given by the limits:

$$(L,U) = b_0 \pm t_{[(1+\gamma)/2],(n-2)} s_{b_0}$$

Another estimation problem in simple linear regression is the one associated with $\hat{y} = b_0 + b_1 x$, where $\hat{y}$ is the mean of a normal population. Thus a 100γ % Confidence Interval for $\hat{y}$ is provided by the limits:

$$(L,U) = \hat{y}_h \pm t_{[(1+\gamma)/2],(n-2)} s_{\hat{y}_h}$$

Note that, as stated before, $\hat{y} = b_0 + b_1 x_i$ is also a predictor of the true regression $y_i = \beta_0 + \beta_1 x_i + \varepsilon_i$. That is, $\hat{y}$ can also be used to predict an individual random variable value associated with a known fix value x_h. This is in contrast to the preceding paragraph where $\hat{y}$ was used to estimate the mean of a normal population (a fix quantity). When $\hat{y}$ is used to predict an individual value rather than a mean value, a 100γ % *Prediction Interval* is provided by the limits:

$$(L',U') = \hat{y}_h \pm t_{[(1+\gamma)/2],(n-2)} s_{\hat{y}_h}$$

The most noticeable feature of the prediction and confidence intervals, is the curvature of these limits. That is, estimates are most precise at the mean value of X and may be almost useless at values of X far removed from the mean.

Effective Number of Independent Sample Observation

Up to now, the discussion has followed the classical approach where it is assumed that all sample observations are normally distributed and independent. The assumption of normality is rather elastic in Oceanography (Sciremammano, *et al.* 1979). However the assumption of independence is rarely justified in geophysical applications where the sample observations are nearly always serially correlated. This serial correlation reflects an over-sampling in the data records.

The results of the previous section can be generalized in terms of the effective number of independent sample observation, also known as the effective degrees of freedom, *n*, which can be estimated from the sample data record (Davis *et al.*, 1976)
Procedure:

The computed time-lagged autocorrelation is defined as:

$$Cxx = \frac{\sum_{i=1}^{N} [X(i\Delta t) - \overline{X}]^2}{(NS_x^2)}$$

where $X(t)$ is the input time series sampled at N discrete time intervals Δt. The total length of time of the record, is therefore $T = N\Delta t$, and Sx is the standard deviation and $\overline{X}$ the mean of $X(t)$.

The effective degrees of freedom, n, can be calculated by computing the *integral time scale* τ as:

$$\tau = \sum_{i=-\infty}^{\infty} Cxx(i\Delta t)Cyy(i\Delta t)\Delta t$$

where $Cxx(t)$, $Cyy(t)$ are the discrete auto-correlation functions of $X(t)$ and $Y(t)$, respectively. The integral time scale determines the time period required to gain a new degree of freedom. In practice, the summation is carried out to values $i = \pm M$, where M is large compared to the lag number at which both $Cxx(t)$ and $Cxx(t)$ are statistically zero.

Then τ is used to get the number of effective degrees of freedom as:

$$n = \frac{N\Delta t}{\tau}$$

This n is then entered into standard table of probabilities to obtain the critical values. Note that n depends on T, the total record length, and not only on N, the number of observations.

Error Types

When a decision to accept or reject a hypothesis based on the result of an experiment is made, it is possible to make one of two types of wrong decisions.
These wrong decisions or errors are called:
i)   Type I Error: Rejection of a hypothesis that is true.
ii)   Type II Error: acceptance of a hypothesis that is false.

The relationship between the decision made, the true situation, and the error type are summarized as follows:

Table A1:   Types of errors associated with tests of hypotheses.

	True Situation	
Decision	Hypothesis is True	Hypothesis if False
Accept the Hypothesis	No Error	*Type II Error*
Reject the Hypothesis	*Type I error*	No Error

Let α denote the probability of a Type I error (α means the "long-run" relative frequency of making a Type I error when the experiment is repeated many times under identical conditions with the same decision rule.) That is, α is the probability that a true null hypothesis is rejected using the test selected (100α % is commonly referred to as the significance level.). Similarly, let β denote the probability of a Type II error; β is the probability of accepting the hypothesis when in fact it is false. It is important to mention that when a Type I error is committed, the hypothesis is rejected with a known probability α. However when a Type II error is committed, the hypothesis is accepted with an unknown probability β. The former is due to the fact that the value of β is determined by the distribution of the alternative hypothesis, which is unknown.

A hypothesis is defined as a tentative theory or supposition provisionally adopted to explain certain facts and to guide in the investigation of others. A statistical hypothesis is a statement about the statistical population and usually is a statement about the values of one or more parameters of the population. It is frequently desirable to test the validity of a hypothesis, which is called the Null Hypothesis. To do this an experiment is conducted and the null hypothesis is rejected if the results obtained are improbable under this null hypothesis. When a null hypothesis is rejected it is in favor of what is known as the Alternative Hypothesis, which is the opposite to the null.

Procedure to Run an Hypothesis Test

1. A null hypothesis, denoted by Ho, is specified.
2. An alternative hypothesis, denoted by Ha, is specified.
3. A test statistic is identified, *e.g.*, a t-test, or an F-test.
4. A decision rule must be stated, *i.e.*, a rejection and acceptance criterion for the null hypothesis Ho.
5. Calculations: calculate the observed t-value; obtain from table the critical t-value.
6. Conclusions: reject the null hypothesis and conclude Ha with a known α probability of making a type I error, or reject the alternative hypothesis and conclude Ho with an uncertain β probability of making a type II error.

Appendix B

Acoustic Doppler Current Profiler ADCP,
Underwater Acoustics, and
Log Wind Profile

The purpose of this appendix is to make a collection of existing information on the Acoustic Doppler Current Profiler principles of operation (RD Instruments *et al.*, 1989), review some basics of underwater acoustics (Urick, 1983 and Kinsler and Austin, 1962), and the Log Wind Profile (Kinsman, 1965 and Stull, 1988) in order to facilitate the writing and understanding of the main chapters. This chapter is not a personal creation of the author, instead, a compilation of explanations from the authors cited above.

Acoustic Doppler Current Profilers (ADCP), are instruments that measure current velocity profiles. They can do this measurement in three dimensions, *i.e.*, North-South, East-West, and vertical. They could be of the upward looking type, mounted in a mooring or downward looking, ship mounted type.

The Doppler Effect and Radial Current Velocity

The Doppler effect is a change in the observed sound pitch that results from relative motion. Therefore if the pitch is measured, and how much it changes, then the speed of the sound source can be calculated.

The Doppler shift is the difference between the frequency one hears when moving at the same velocity as the source and what one hears when moving relative to the source. The equation for the Doppler shift, in this situation, is:

$$F_D = F_S(V/C)$$

where :

F_D : is the Doppler frequency shift

F_S : is the frequency of the sound when everything is still

V : is the relative velocity between the sound source and receiver in m/s

C : is the speed of sound m/s

ADCP use the Doppler effect by transmitting sound at a fixed frequency and listening to echoes returning from sound scatterers in the water. These sound scatterers are small particles or plankton that reflect the sound back to the ADCP. Scatterers are everywhere in the ocean. They float in the water and on average they are assumed to move at the same velocity as the water.

When sound scatterers move toward the ADCP, the sound heard by the scatterers is Doppler-shifted to a higher frequency. This shift is proportional to the relative velocity between the ADCP and the scatterers. Part of this Doppler-shifted sound reflects backward or is "backscattered" to the ADCP. The backscattered sound appears to the ADCP as if the scatterers were the sound source. The ADCP hears the backscattered sound Doppler shifted a second time; therefore, the Doppler shift is doubled, changing the frequency received at the ADCP to:

$$F_D = 2F_S(V/C)$$

Only radial motion, which changes the distance between the source and receiver, will cause a Doppler shift. Mathematically, this means that the Doppler shift results from the velocity component in the direction of the line between the source and receiver. This adds a new term, $\cos(\theta)$, to the equation for Doppler shift :

$$F_D = 2F_S(V/C)\cos(\theta)$$

where θ is the angle between the relative velocity vector and the line between the ADCP and scatterers.

Three-Dimensional Current Velocity Vectors

When an ADCP uses multiple beams pointed in different directions, it senses different velocity components. A key point is that one beam is required for each current component. Therefore, to measure three velocity components (*e.g.* East, North and vertical), it is necessary to have at least three acoustic beams.

The three velocity components are calculated using the standard four acoustic beams of an ADCP, in the following manner. One pair of beams produces the horizontal component and the vertical velocity component. The second pair of beams produces a second, perpendicular horizontal component as well as a second vertical velocity component. Thus there are two horizontal velocities and two estimates of vertical velocity for the three dimensions of the flow. This redundancy provides a means to estimate data quality.

Velocity Profile

The most important feature of ADCPs is their ability to measure current profiles. ADCPs break up the velocity profile into uniform segments called depth cells (depth cells are often called bins).

Each depth cell is comparable to a single current meter. Therefore an ADCP velocity profile is like a string of current meters uniformly spaced on a mooring. Thus, by analogy, the following definition can be made:

Depth cell size is like distance between current meters

The number of depth cells is like the number of currents meters

There are two important differences between a string of current meters and an ADCP velocity profile. The first difference is that the depth cells in an ADCP profile are always uniformly spaced while current meters can be spaced at irregular intervals. The second is that the ADCP measures average velocity over the depth range of each depth cell while the current meter measures current only at the current meter depth. Unlike conventional current meters, ADCPs do not measure currents in small, localized volumes of water, instead they average the velocity over the full range of a depth cell.

Profiles are produced by range-gating the echo signal. This method breaks the signal into successive segments and processes each segment independently of the others.

ADCP Data and The Echo Spectrum

A frequency spectrum describes the statistical frequency content of a signal. The ADCP controls the transmit frequency with an accurate crystal oscillator; before transmission this signal is a line spectrum, theoretically. In contrast, the spectrum of the returning signal covers a wide frequency band. This spectral broadening is a bell-shaped curve. In most situations, spectral broadening primarily occurs during transmission as a result of the short duration of the transmit pulse. Spectral broadening is measured by the ADCP as spectral width; this spectral width is directly related to the uncertainty of the mean Doppler frequency estimate.

The dominant source for spectral broadening is the short duration of transmit pulses. There is a direct inverse relationship between the two: reducing the transmit pulse by half doubles the spectral width. Other sources of spectral broadening include turbulence and the acoustic beam width.

Turbulence: broadens the spectrum because scatterers within the scattering volume will reflect sound back with different Doppler shifts.

The acoustic beam width: can cause the spectrum to broaden in two ways, both depending directly on the velocity. The first is a result of the angular spread of the beam, *i.e.*, the relative angles of the velocity vector and the beam are different from one side of the beam to the other, and the second is a result of the beam being very narrow. When

scatterers move across the scattering volume with a short residence time compared to the transmit pulse duration, the spectral width will increase.

Turbulence and acoustic beam width are usually secondary sources of spectral broadening when compared with the transmit pulse length.

As the signal-to-noise ratio decreases, the spectral width increases. This increase is directly related to the velocity uncertainty, particularly in the last 1/3 of the profiling range *i.e.* near the surface or bottom, depending on the ADCP type in use. ADCPs measure: scatterers' velocity, and echo amplitude.

The Velocity: is an average of the echo spectrum, or the mean value of the Doppler shift. Velocity data are recorded in Hz, corresponding to the Doppler shift.

The Echo Amplitude: is the area under the spectrum bell, which is a measure of the energy in the echo. The echo amplitude varies with a dynamic range of many orders of magnitude, so it is converted to dB.

Ensemble Averaging

The velocity measurement uncertainty of single-ping ADCP data is too large to meet most measurement requirements, therefore, data are averaged to reduce the measurement uncertainty to acceptable levels.

Two kinds of errors contribute to velocity uncertainty: random error and bias. Averaging reduces the random error but not the bias error. Because the random error is uncorrelated from ping to ping, averaging reduces the standard deviation of the velocity error by the square root of the number of pings, or :

$$\sigma \propto N^{-\frac{1}{2}}$$

where N is the number of pings averaged together.

An important point is that averaging can reduce the relatively large random error present in single-ping data, but after a certain amount of averaging, the random error becomes smaller than the bias. At this point, further averaging will do little to reduce the overall error.

Short term uncertainty is defined as the error in single-ping ADCP data. Short term uncertainty is dominated by random error, long term uncertainty is defined to be the error present after enough averaging has been done to essentially eliminate random error. Thus, long term error is the same as bias.

The size of the random error depends on factors such as the ADCP frequency, depth cell size , the number of pings averaged together, and the beam geometry.

For standard ADCPs using 30° transducers, the random error of horizontal velocity components is approximately :

$$\sigma = (1.6x10^5) / (FDN^{\frac{1}{2}})$$

where :

σ : is the standard deviation in m/s

F : is the ADCP's frequency in Hz

D : is the depth cell size in m

N : is the number of pings averaged together to get the velocity estimate

If the ADCP has 20° beams, the random error is greater by about 1.5 times the random error for a standard 30° beam instrument.

Bias is typically on the order of 0.5-1.0 cm/s. This bias depends on a variety of factors including temperature, mean current speed, signal-to-noise ratio, and beam geometry errors.

Echo Amplitude and Profiling Range

Echo amplitude is a measure of the signal strength of the returning echo, and is related to the following factors :

sound absorption

beam spreading

transmitted power

backscatter coefficient

An approximate equation for echo amplitude is the following :

$$EA = SL + SV + const - 20\log(R) - 2eR$$

where :

EA : is the echo amplitude in dB

SL : is the source level or transmitted power in dB

SV : is the water mass volume backscattering strength in dB

e : is the absorption coefficient in dB/m

R : is the distance from the transducer to the depth cell in m

The constant (const) is included because the measurement is relative rather than absolute. This means that the ADCP is able to see variations in echo amplitude, but that it is not able to make absolute measurements that can be compared with other ADCPs. The term $2eR$ accounts for absorption and $20\log(R)$ accounts for beam spreading.

i)   Sound Absorption, the 2eR term

Absorption reduces the strength of echoes as a result of physical and chemical processes in the ocean. Absorption in the ocean is more rapid than in fresh water, primarily because of the chemical reactions. Absorption causes a linear reduction, when measured in dB, proportional to $2eR$ above, of echo amplitude within the range $R = r_2 - r_1$, where r_1 and r_2 are distances from the apparent center of origin of the acoustical wave, which can also be stated as: absorption causes an exponential reduction in returned energy with range.

Sound absorption coefficient (in dB/m) increases roughly in proportion with frequency in the frequency range in which ADCPs operate (75-1200 kHz; see Table B1). This produces an inverse relationship between frequency and range.

Table B1:   Sound absorption coefficient (at 4°C, 35 ppt, and at sea level) and ADCP acoustic range. From RD Instruments *et al.*, 1989.

Acoustic frequency kHz	e dB/m	Nominal range low m	Nominal range high m
76.8	0.025	400	700
153.6	0.039	240	400
307.2	0.062	120	240
614.4	0.139	60	60
1228.8	0.440	25	25

For the purpose of this research, the computation of the Absorption coefficient will be done by the following equation (Urick, 1983):

$$e' = A \frac{S f_T f^2}{f_T^2 + f^2} + B \frac{f^2}{f_T^2}$$

$$f_T = 21.9 x 10^{6-1520/(T+273)}$$

where:

e'	:	absorption coefficient at sea level in dB/m
S	:	salinity in ppt
A	:	constant equal to $1.86 x 10^{-2}$
B	:	constant equal to $2.68 x 10^{-2}$
f	:	frequency in kHz
f_T	:	temperature-dependent relaxation frequency in kHz
T	:	water temperature in °C

The effect of pressure on the absorption coefficient has been investigated theoretically and experimentally, founding that it reduces the coefficient by the following formula:

$$e = e'\,(1 - 1.93x10^{-5}d) \ \ dB/m$$

where:

e : absorption coefficient at depth d

e' : absorption coefficient at sea level in dB/m

d : depth in ft

ii) Beam Spreading, the $20\log(R)$ term

Beam spreading is a purely geometric cause for echo attenuation as a function of range R, where in this case $R = \frac{r_2}{r_1}$, with r_1 and r_2 defined the same manner as in "Sound Absorption, the $2eR$ term". The beam spreading is represented as a logarithmic loss in echo amplitude with increasing range, when echo amplitude is measured in dB. In linear units, the echo amplitude decreases proportional to the range squared.

For the purpose of this research, the computation of the beam spreading and absorption coefficient, were combined in one term known as **Transmission Losses (TL)** which are defined as: (Kinsler and Austin, 1962)

$$TL = 20\log(\tfrac{r_2}{r_1}) + e(r_2 - r_1) \ \ dB$$

where:

TL : transmission losses between r_1 and r_2

r_1 and r_2 : distances from the apparent center of origin of the acoustical wave in m

e : absorption coefficient in dB/m

iii) Source Level and Transmitted Power, the *SL* term

The source level depends on the power transmitted and the efficiency of the transducer. The power transmitted depends only on whether the ADCP is powered by 110 VAC, which is transformed and rectified to 160 VDC, or battery-powered with only 35 VDC.

In the 600 and 1200 kHz ADCP, the transducer is smaller, and its efficiency is limited by shock formation (non-linear acoustics), this is the cause of the same nominal range low and high in Table B1.

The pulse length also has an effect on ADCP range. Doubling the pulse length causes twice the energy to radiate into the water, which increases the range by a small amount (perhaps 10%).

iv)   Backscattering Strength, the *SV* term

The concentration of scatterers affects range in a way that more scatterers radiate more sound.   The dominant oceanic sound scatterers at ADCP frequencies are zooplankton with sizes on the order of a millimeter.   Other scatterers can include suspended sediment and density gradients (though density gradients are relatively weak scatterers).   On occasion, the lack of scatterers in the water could reduce the range relative to the nominal range.

Bubbles

In rough seas, breaking waves generate bubbles near the ocean surface, which can act as scatterers, increasing the backscatter energy of the upper bins.   It has been also detected that as wind speed decreases, the backscatter energy does the same.   This may be related to the bubble density in the upper ocean.

ADCP Signal Processing

Echo amplitude as measured by the ADCP is a byproduct of the Automatic Gain Control (AGC) circuit.   Echo signal strength typically varies over a range of 70 to 100 dB, therefore an ADCP must use automatic gain control to keep the signal level approximately constant in spite of large input signal strength variations.   An indicator of the AGC circuit performance is the feedback signal into the AGC, a sample of that signal is taken and used to compute the digitized output, measured in *counts*.

There is a conversion factor of 0.46 dB/count at 22° C, to get echo strength (ES) from the counts.   This conversion factor is dependent on the ADCP electronics temperature mounted in the mooring (or in the ship's hull), this variation is 0.34% per °C (Heywood *et al.* 1991).   A computational formula for the conversion, temperature corrected, is the following:

$$ES = 0.46(counts(0.9966)^{(22°-T°)})$$

where

ES   :   echo strength measured in dB

0.46   :   conversion factor in dB/counts

counts   :   as explained above, output of the AGC circuit

$(0.9966)^{(22°-T°)}$:   temperature correction factor from 1-0.34/100

T°   :   ADCP electronics temperature in °C

Transducers

The transducer is a key factor for data quality, the active elements in transducers are piezoelectric ceramic disks that expand or contract under the influence of an electric field.

ADCPs require narrow and directional acoustic beam. Two aspects are important: the beamwidth and the sidelobe level.

The beamwidth: is the width of the beam in degrees at the -3 dB level (-3 dB corresponds to half the signal strength).

The sidelobe level and its suppression: the radiation diagram has a main lobe that is at the center of the pattern, and it contains most of the power, the sidelobes consist of the remaining power. The sidelobes that most strongly affect the ADCP measurement quality are the ones more than 15° away from the main lobe. RDI's target design specification is that these sidelobes should be at least 40 dB below the main lobe. If the transducer is larger (at a given frequency), the beam becomes narrower, and sidelobes are suppressed.

Measurement Near The Surface or Bottom

The echo from a hard surface such as the sea surface or bottom is so much stronger than the echo from scatterers in the water that it can overcome the sidelobe suppression of the transducer. Data from distances too close to the surface (when looking up) or bottom (when looking down) should normally be rejected. Figure B1 shows a transducer oriented 30° from vertical. The echo from the sidelobe facing the surface will return to the ADCP at the same time as the echo from the main lobe at 85% of the distance to the surface. This means that data from the last 15% of the range to the surface will usually be contaminated by sidelobe noise. The effect would be the same for a vessel-mounted ADCP looking down to the bottom.

The equation that governs this is :
$$R_{max} = D\cos(\phi)$$
where :

R_{max} : is the range for acceptable data in m

D   : is the distance in m from the ADCP to the surface or bottom (as appropriate)

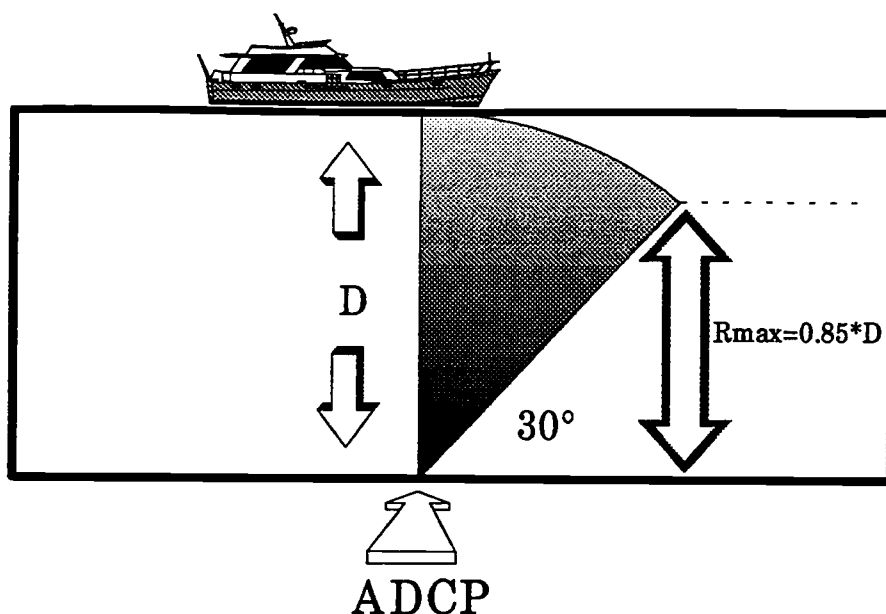ϕ : is the angle of the beam relative to vertical in degrees

Figure B1: ADCP transducer oriented 30° from vertical, showing that the sidelobe facing the surface will return energy to the ADCP at the same time as the echo from the main lobe at 85% of the distance to the surface.

Note that $\cos(30°) = 0.866$, which is approximately equal to 85%. If the angle is reduced to 20°, then because $\cos(20°) = 0.94$, data may be obtained to within about 6% of the ocean surface. However, the ability to get data closer to the surface comes at a cost. The 20° beam increases the standard deviation by a factor of about 1.5 times the standard deviation of the 30° beam.

Sound Speed Variation with Depth

Variation of sound speed with depth will not affect the estimate of the horizontal current. In simple terms, sound speed variation has two effects that exactly counteract one another. The effect of changing sound speed is to refract or bend the sound beams, but the bend is exactly the right amount to preserve the accuracy of the horizontal current. That is necessary to obtain horizontal current at any depth, is the sound speed at the transducer.

The theoretical basis for this result is Snell's law that says that horizontal wavenumber ($k = 2\pi / \lambda$, where λ is the wavelength) is conserved when sound passes through horizontal interfaces.

Because the frequency remains constant, sound speed variation does not affect the horizontal component of sound velocity. And because measurement of the horizontal

current depends directly on the horizontal sound speed, the horizontal current measurement is not affected. In contrast, the vertical current component variations are proportional to variations in sound speed.

The Log Wind Profile

The wind speed usually varies approximately logarithmically with height in the surface layer (Kinsman, 1965). Frictional drag causes the wind speed to become zero close to the ground, while the pressure gradient forces cause the wind to increase with height.

The following variables are potentially relevant to estimate the mean wind speed, $\overline{M}$, as a function of height, z, above the ground: surface stress (represented by the friction velocity, u_*), and surface roughness (represented by the aerodynamic roughness length, z_0). Stull (1988), postulates that the following equation represents this situation:

$$\frac{\overline{M}}{u_*} = (\frac{1}{k})\ln(\frac{z}{z_0})$$

Where $(1/k)$ is a constant of proportionality. The von Karman constant, k, is supposedly a universal constant that is not a function of the flow nor of the surface. The precise value of this constant has yet to be agreed on, but most investigators feel that it is either near $k = 0.35$ or $k = 0.4$.

For simplicity, meteorologists often pick a coordinate system aligned with the mean wind direction near the surface, leaving $\overline{V} = 0$ and $\overline{U} = \overline{M}$. This gives the form of the log wind profile most often seen in the literature :

$$\overline{U} = (\frac{u_*}{k})\ln(\frac{z}{z_0})$$

By setting $z = z_r$, the wind reference level, $\overline{U_r}$ is obtained. Doing the same with $z = z_b$, the buoy wind sensor height, $\overline{U_b}$ is now obtained. Then applying some basic algebra to $\overline{U_r}$ and $\overline{U_b}$, it can be shown that:

$$\overline{U_r} = \overline{U_b}\{\frac{\ln(\frac{z_r}{z_0})}{\ln(\frac{z_b}{z_0})}\}$$

Which means that the wind speed at the buoy height can be transported to a reference height by the factor $\frac{\ln(\frac{z_r}{z_0})}{\ln(\frac{z_b}{z_0})}$. For this research the reference height was chosen as 10 m, the usual wind reference height used in Oceanography.

Appendix C

List of Symbols

ES	:	Echo strength in dB
WS	:	Wind speed in m/s
AD	:	Acoustic direction in degrees
WD	:	Wind direction in degrees
b_1	:	Estimate of the true slope coefficient β_1
b_0	:	Estimate of the true intercept coefficient β_0
MSE	:	Mean square error, Appendix A
s_e^2	:	Sample error variance or mean square error, MSE
$s_{b_1}^2$	:	Sample variance of the slope b_1
$s_{b_0}^2$	:	Sample variance of the intercept b_0
U_{10}	:	Wind speed in m/s at a reference height of 10 m
BE	:	Active backscatter energy from the surface bin
μ	:	Exponent of the power law $U_{10} = BE^\mu$
S/N	:	Signal (independent variable's dynamic range) to noise (residuals' standard deviation) ratio.
rms	:	Root mean square
dB	:	decibel equals $10\log(a/b)$
nm	:	Nautical mile (1856 m)
ppt	:	Parts per thousand